STUDY OF COMPACT AND EFFICIENT DIODE PUMPED SOLID STATE GREEN LASERS FOR DISPLAY APPLICATION

BY

BIN ZHANG

M. Sc

STUDY OF COMPACT AND EFFICIENT DIODE PUMPED SOLID STATE GREEN LASERS FOR DISPLAY APPLICATION

By BIN ZHANG, M. Sc

A Thesis Submitted to the School of Graduate Studies in Partial Fulfillment of the Requirement for the Degree Doctor of Philosophy

McMaster University Hamilton, Ontario, Canada

DOCTOR OF PHILOSOPHY (2020) (Engineering Physics)

Title: Study of Compact and Efficient Diode Pumped Solid State Green Lasers for Display Application

Author: BIN ZHANG
M. Sc (Ningbo University, Ningbo, Zhejiang, P. R. China)
B. Sc (Ningbo University, Ningbo, Zhejiang, P. R. China)

Supervisor: Dr. Chang-Qing Xu

Number of pages: xvii, 138

Abstract

Due to the long lifetime, high directionality, and narrow spectral linewidth, laser-based displays have several advantages over other display technologies, such as high brightness, low maintenance cost and vivid color. In recent years, laser displays have attracted a lot of attention from academia and industrial community, but a number of difficulties prevent further commercialization of laser displays. The main obstacle is the speckle noise caused by the high coherence of lasers, especially in the green region, because the wavelength of commercial watt-class LD is still too short, > 530 nm DPSS green laser need to be employed to improve the image's color quality and further speckle reduction. Since DPSS green lasers are still essential for display application, their miniaturization is necessary for pico-projection system and the field sequential modulation is needed as well. However, the modulation properties of the compact DPSS green module have not been studied yet.

In this dissertation, the field sequential modulation properties of a compact Nd:YVO_4/MgO:PPLN green laser module was investigated. Its output performance under a modulation condition were studied and analyzed. Furthermore, a number of single-(dual-) wavelength continuous wave green DPSS lasers are proposed and demonstrated for the purpose of speckle reduction and color improvement. An intra-cavity frequency doubling configuration was used to achieve efficient nonlinear conversion and smaller dimensions. Specifically, a 531.5 nm was built based on Nd:$GdVO_4$ and MgO:PPLN crystals, it has a output power of 1.9 W with an O-O efficiency of 37%. A compact 540 nm laser was

achieved by using Nd:YAP and LBO, in which a 0.8 W output power was achieve with an O-O efficiency of 20%. Watt-class 542 nm / 543 nm Nd:YVO_4/MgO:PPLN green lasers was achieved by customized cavity coating design since weaker fluorescence peaks are used as fundamental light. An O-O efficiency of 22% and 35% was obtained, which are the highest O-O efficiencies achieved so far to the best of our knowledge. In addition, an orthogonally polarized dual-wavelength (542 & 543 nm) was realized by using a conventional Nd:YVO_4 crystal and two MgO:PPLN crystals. An optical-to-optical (O-O) efficiency as high as 15.3% was achieved when the powers of the two emission wavelengths were equal. This is the first time that a dual-wavelength orthogonally polarized visible solid state laser is achieved. Moreover, the speckle reduction performance of the proposed lasers was studied as well. It shows that the SCR value is effectively reduced by blending different green wavelengths together, which agree well with the theoretical expectation. Generally, those lasers have features of efficient, compact, and low cost which are suitable for laser display application.

At last, a tri-wavelength wavelength blending method was proposed and studied. A 523 nm green LD, 532 nm and 543 nm green DPSS lasers are employed for wavelength blending purpose. It shows that lower SCR was achieved where all three wavelengths are involved, which agrees well with the theory. Moreover, optimal color performance was maintained as a result of the employment of 543 nm laser, which was the purpose for developing long wavelength green laser.

Acknowledgements

I would like to express my sincerest gratitude and appreciation to my supervisors Dr. Chang-qing Xu for his expert guidance, enormous support and patience through this project. Dr. Xu's profound knowledge and professional attitude always inspire me during the course of this work and have placed enormous influences on my life.

I would like to thank my supervisory committee members, Dr. Qiyin Fang and Dr. Adrian Kitai for their help, guidance, and advice through my study. I benefited greatly by their constructive suggestions and support.

I would like to thank Dr. Yi Gan and Dr. Qianli Ma for their generously help on research. I also would like to thank Dr. Yang Lu, Dr. Tianyi Guo, Dr. Zaijin Li and Dr. Jian Sun for their professional opinions and beneficial discussion. I would like to thank my colleagues, Joshua Kneller, Tyler Kashak, Liam Flannigan, Rong Zha, Mahmoud Khalil Mahmoud, Fangfang Zhang, Linkun Cheng, Jianxi Qu, Yushan Zhang, and Ying Zhao, it is a great experience for me to work with them, and I have also learnt a lot from them.

Thanks all the faculty members and staff in the Department of Engineering Physics for them. Their continuous supports help me to complete my study. I also like to thank Dr. Wei-dong Tao from Ningbo University for his encouragement and help.

Finally, I would like to express my sincere gratitude to my parents, I cannot image I can complete the work without their understanding and support.

Declaration of Academic Achievements

This dissertation was used to fulfill the requirements of Ph.D. degree. All the research was conducted from September 2015 to March 2020. The majority of the written work described within the written thesis was conceived, conducted, analyzed, and written by the author of the thesis, in consultation from Dr. Chang-Qing Xu, with the exception to the following:

Chapter 2: Dr. Yi Gan assisted experiments preparation.

Chapter 4, 5, 6, and 7: Dr. Qianli Ma assisted speckle measurement.

Chapter 6 and 7: Dr. Qianli Ma assisted theoretical simulation for speckle measurement.

This thesis has resulted in three peer-reviewed journal articles, two conference presentations, and one unsubmitted article. I am the first author and main contributor on all the works. These publications are listed below:

1. ***Bin Zhang***, Yi Gan, and Chang-Qing Xu. "Study of the field-sequential modulation of Nd:YVO_4/MgO: PPLN based intra-cavity frequency doubling green laser." Optics & Laser Technology 102 (2018): 174-179. (Journal article)
2. ***Bin Zhang***, and Chang-qing Xu. "Compact, and efficient continues wave intra-cavity frequency doubling Nd:YVO_4/MgO: PPLN 542/543 nm green lasers." Optics & Laser Technology 122 (2020): 105885. (Journal article)

3. ***Bin Zhang***, Qianli Ma, and Chang-Qing Xu. "Orthogonally polarized dual-wavelength Nd:YVO_4/MgO: PPLN intra-cavity frequency doubling green laser." Optics & Laser Technology 125 (2020): 106005. (Journal article)
4. ***Bin Zhang***, Qianli Ma, and Chang-Qing Xu. "High Efficiency Nd:$GdVO_4$/MgO:PPLNs 531.5 nm green laser." Photonic North, May 2019, Québec City, QC, Canada. (Conference)
5. ***Bin Zhang***, Qianli Ma, and Chang-Qing Xu. "Intra-cavity frequency doubling Nd:YAP/LBO 540 nm green laser for laser display." Photonic North, May 2019, Québec City, QC, Canada. (Conference)
6. ***Bin Zhang***, Qianli Ma, and Chang-Qing Xu. "Study of multi-wavelength blending for speckle reduction and color improvement." (Pending for submission)

Contents

List of Figures

List of Tables

List of Abbreviations and Symbols

3-D	3 dimension
AR	Anti-reflection
APLN	Aperiodically poled lithium niobate
CCD	Charge-coupled device
CMOS	Complementary metal–oxide–semiconductor
CW	Continuous wave
DLP	Digital light processing
DPSS	Diode pumped solid state
E-O	Electrical-to-optical
FAC	Fast axis collimator
FWHM	Full width half maximum
FSC	Field-sequential color
HR	High reflectivity
HT	High Transmission
HVPE	Hydride vapor phase epitaxy

ICFD	Intra-cavity frequency doubling
LCoS	Liquid crystal on silicon
LD	Laser diode
MOPA	Master oscillator-power amplifier
ND	Neutral density
NECESEL	Novalux Extended Cavity Surface-Emitting Laser
O-O	Optical-to-optical
OC	Output coupler
OSA	Optical spectrum analyzer
PPLN	Periodically poled lithium niobate
QPM	Quasi-phase match
QW	Quantum well
SCR	Speckle contrast ratio
SHG	Second harmonic generation
TEC	Thermo-electric cooler
THz	Terahertz
TPLN	Tandem-poled lithium niobate

UHD	Ultra-high definition
VCM	Voice coil motor
VCSEL	Vertical-cavity surface-emitting laser

Chapter 1

Introduction

1.1 Laser based video display

Since the 1st laser display system was demonstrated by Baker, Charles E. and Anthony D. Rugari in 1965 [1], a lot of experimental and commercial laser display systems have been reported. Before 2000s, the laser-based illumination technology was remained too costly because of the lack of efficient, compact and low cost RGB laser sources. However, as a result of the rapid developments of Laser diode (LD) and diode pumped solid state (DPSS) laser, a number of consumer grade laser display systems start to be introduced to the market. Currently, a lot of the laser projectors on the market are using single blue laser sources, the red and green color are split from white light which are combined from blue and yellow light, while the yellow light is created by shining the blue laser beam on a phosphor wheel. However, a 'true' laser display system should include separate red, green, and blue laser sources to maximize its color gamut.

The pure RGB laser displays are considered as the most promising display technology in the new century. Due to the long lifetime and high wavelength purity of illuminating

laser sources, laser displays have a large color range, long-term stability, long lifetime, low maintenance cost, and high brightness, which provides an advantage over other projection technologies. The longer lifetime of laser sources leads to laser-based projectors having lower maintenance costs when compared to lamp-based projectors.

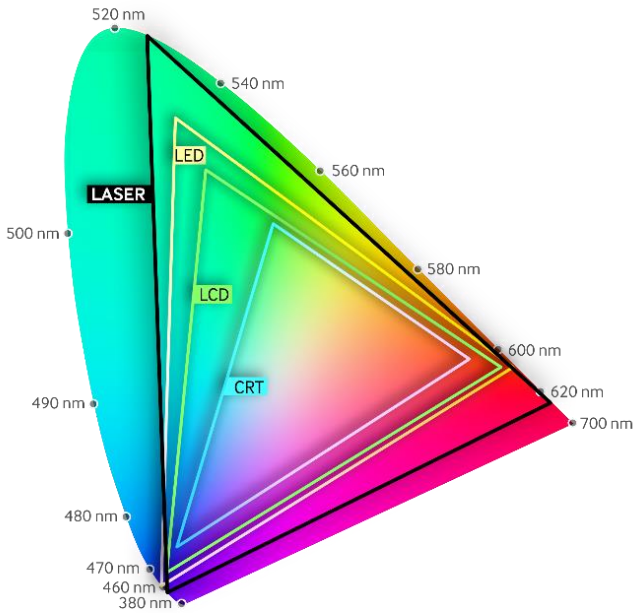

Fig. 1.1 A comparison of the color gamut for different light sources in display systems, which clearly shows that the laser light engine can provide the largest color range over any other display sources/techniques. [2]

Though laser displays can provide superior picture quality and longer lifetimes, laser speckle noise is still a significant obstacle for broad commercialization of laser-based display systems.

1.1.1 The origin of laser speckle noise

The laser speckle noise results from the high coherence of laser sources, as it is a random interference pattern generated from laser light reflected by a rough surface (i.e. projection screen). The speckle noise could blur the displayed image and reduce the image quality with the result that speckle noise becomes a serious problem for laser-based display systems like laser projectors.

The laser speckle noise is quantified by a quantity known as the speckle contrast ratio (SCR). Presently, research has shown that the SCR value should typically be smaller than 5% [3][4], which is the point where the audience would hardly notice the existence of laser speckle noise. An SCR value less than 4% is also recommended for 3-D projection display, since a polarized projection screen is typically used for presenting the image.

1.1.2 Conventional methods for speckle reduction

For a projection system, there are three parameters that contribute to the speckle noise: the angle, polarization, and wavelength of the laser source. Therefore, the SCR can be reduced by increasing the diversity of these three parameters.

For example, angular diversity could be increased by employing a diffuser inside the light path [5], and a depolarized screen can increase the polarization diversity when the laser beam is projected on to it. In the case that multiple single wavelength lasers are used as illuminating light sources and we take the number of single wavelength lasers as N_λ, then the corresponding reduction factor is $R_\lambda = \sqrt{N_\lambda}$ [6]. Therefore, it is possible to further

reduce the SCR of a laser projection system by increasing the wavelength diversity of the illuminating light sources.

1.1.3 Wavelength diversity techniques for speckle reduction

In modern display systems, a broad array of colors is reproduced by mixing three different primary colors, i.e. blue, green and red. Currently, red, green and blue LDs are commercially available, and their large spectral linewidth make them ideal for display applications due to the relatively low SCR value. However, the output wavelengths of high power commercial green LDs are around 510~520 nm and so the LD cannot provide the appropriate green color for the Rec. 2020 color gamut. (Rec. 2020 is a new color space standard posted in 2012, and it is widely used in UHD (4K UHD and 8K UHD) display systems (TVs and projectors, etc.). In Rec. 2020 standard, the wavelengths of the three primary colors are 630 nm, 532 nm and 467 nm). Moreover, human eyes are more sensitive to green light than blue and red colors, so much of the study of speckle reduction has been focused on green lasers [3,6,7-9].

For a laser-based projection system, three main methods can be used to increase the wavelength diversity of the illuminating laser sources: First, increasing the spectral width of single wavelength lasers; second, using a combination of multiple lasers with different wavelengths; third, achieving multi-wavelength emission from a single laser.

1.1.3.1 Speckle reduction via the use of broadband lasers

The spectral linewidths of lasers mainly depend on the gain media of lasers. For example, laser diodes (LDs) usually have larger linewidths (around several nm), especially when

compared to diode pumped solid state (DPSS) lasers. Additionally, the operation modes of lasers also influence the output spectral linewidth. A femtosecond laser typically has a spectral linewidth larger than 10 nm, but they are not appropriate to be used in display applications due to their large size and extremely high cost.

Since there is significant technical difficulty in manufacturing stable and powerful >530 nm green LDs, researchers have been attempting to find alternate methods for broadband green laser sources. For example, in 2014, Nan Ei Yu et al. [9] reported a wide spectral linewidth green laser (center wavelength: ~531 nm) by using tandem-poled lithium niobate (TPLN) as a nonlinear crystal. The effectiveness of the speckle reduction was also demonstrated by using their broadband green light source, which shows significantly lower SCR values than using normal periodically poled lithium niobate (PPLN) crystals. To make the full use of wavelength tolerance of the PTLN crystal, a Q-switch 1064 nm laser was employed as fundamental light, which significantly increase the cost and size of the green laser system. Moreover, the conversion efficiency of the developed TPLN crystal was too low, so that it is not suitable for practical laser display application.

1.1.3.2 Wavelength blending by multiple lasers with different wavelengths

Among the reported green lasers, DPSS lasers can provide compact, powerful, and cost-effective 532 nm light [10], but the spectral linewidth of DPSS 532 nm lasers are around 0.1~0.2 nm which causes higher speckle noise.

As a result, the wavelength blending technique becomes a popular solution to increase the wavelength diversity [3,11,12]. To minimize the speckle noise, the wavelength

difference between each mixed laser should be greater than or equal to 1 nm [3]. In the meantime, these wavelengths must be uniformly distributed around 532 nm to keep the center wavelength as close as possible to 532 nm.

In 2015, Takayuki Yanagisawa et. al [11] from Mitsubishi Electric Corporation demonstrated lower speckle noise by blending multiple green wavelengths together. Their results also showed that the SCR value will decrease by increasing the number of mixing wavelengths, which agrees with the theoretical model. In 2017, a study from McMaster University [12] also showed a lower SCR value via mixing of a 532 nm DPSS laser and a 520 nm LD. That literature proposed a detailed theoretical model for calculating the SCR value with the wavelength blending method and proved that better color gamut (than using single 520 nm light) can be achieved by blending 520 nm and 532 nm together.

The wavelength blending technique is the most straightforward method to realize speckle reduction through increased the wavelength diversity. It provides a simple and low-cost method for speckle reduction. Current challenges for wavelength blending techniques involve building an efficient and compact green laser which has emission wavelengths distributed around 532 nm.

1.1.3.3 Multi-wavelength laser for speckle reduction

In wavelength blending techniques, when a couple of single wavelength lasers are combined, it increases the overall size of the laser system. Thus, lasers with simultaneous multi-wavelength emission have attracted a lot of attention recently. In 2011, Dmitri V. Kuksenkov et. al [13] developed an external cavity frequency doubling multi-wavelength green laser by using a quantum-well laser as the pumping source and a specialized quasi-

periodically poled MgO-doped lithium niobate waveguide as the nonlinear crystal. Output powers as high as 62 mW were obtained for multi-wavelength green lasers, with a frequency doubling conversion efficiency of 33 %. However, the complicated configuration significantly increases the cost and the size of the system. In 2014, Wang et. al [14] from Shandong University developed a tri-wavelength green laser based on a new gain medium material which has a wide spectral linewidth around 1080 nm. A multi-period MgO:PPLN crystal was used as the nonlinear crystal for converting the broadband fundamental light into three separate green wavelengths: 538 nm, 542 nm and 546 nm. Due to the use of a mature 808 nm LD and the z-type cavity configuration, this multi-wavelength green laser had advantages of compact size and simplicity, and its speckle test showed an obvious advantage on the SCR value when compared to a single wavelength 532 nm, 538 nm and 546 nm laser. However, the optical-to-optical (O-O) efficiency was too low (less than 2 %), and the use of an uncommercialized gain medium could increase the overall cost.

Compared to a typical single wavelength green DPSS laser with an O-O efficiency of 30%-40%, the multi-wavelength green laser is still underdeveloped. In a practical application scenario, approximately 20% O-O efficiency is necessary. Therefore, energy efficiency and cost are the main obstacles for multi-wavelength green lasers.

1.2 Compact green lasers for laser display

For laser display application, the development of compact and efficient green laser has attracted more attention than other colors due to the lack of commercial ~530 nm green LD.

In this section, we introduce the development of green laser and discuss the common technologies for achieving green radiation.

1.2.1 The development of compact green lasers

The laser was considered as a remarkable tool for a lot of applications after its invention in 1960 [15]. However, due to the lack of suitable lasers, the implementation of a variety applications was limited. The need for a compact, robust, cost-effective and powerful green laser sources is one common requirements for many applications.

The initial green lasers were gas lasers in which the ionized gas – such as argon-ion and helium-neon was used as the gain medium [16][17]. The argon laser typically can emit a green wavelength at 514 nm and had been applied to many applications such as laser surgery, pumping titanium–sapphire lasers, and laser light show. However, the gas laser usually has a number of deficiencies, such as low electrical-to-optical efficiency, limited lifetime, and relatively larger size. Furthermore, some applications require a wavelength that can not be offered by a gas laser because the available lasing wavelengths are fixed by the atomic transition of the species of gas.

At about the same time, researchers started to use the nonlinear effect to generate green (532 nm) radiation. For example, in 1968, Bell Telephone Laboratories, Inc reported a 532 nm laser that generated 1.1 W of green power [18]. The laser was based on an intra-cavity frequency doubling configuration in which the Neodymium-doped yttrium aluminum garnet (Nd:$Y_3Al_5O_{12}$, Nd:YAG) was used as the gain medium to produce the fundamental 1064 nm radiation. However, pumping with lamps is inherently inefficient in which only

several percentages of the electrical power was converted into laser radiation and the most the power being wasted as heat [19]. This problem had not been well solved until the ~810 nm semiconductor diode lasers was successfully developed in 1970s - 1980s [20][21][22][23]. At present, the ~810 nm gallium aluminium arsenide (GaAlAs) laser diodes (LDs) typically has an electrical-to-optical efficiency around 50% and more compact size. The invention of the high efficiency, powerful, long lifetime and inexpensive infrared pumping LDs considerably changed the rule for solid state lasers. It provides a competitive option for green radiation generation and significantly increase the practicability of DPSS lasers.

In the beginning, the green DPSS lasers were mostly operated in pulse mode [24], and the power and efficiency of the continuous wave (CW) green DPSS lasers are limited by inappropriate laser gain media and low efficiency nonlinear materials. Not long after, the new and improved laser materials [25] and nonlinear crystals [26] opened up the possibility of powerful, efficient and compact DPSS green lasers. Currently, the CW operation DPSS green laser can reach up to 40 % -50 % [10,27] optical-to-optical (O-O) efficiency with a corresponding electrical-to-optical efficiency of 20% - 25%. Furthermore, the use of high effective nonlinear coefficient materials made it practical to miniaturize the green DPSS laser into an extremely small dimension [10].

On the other hand, using a LD to generate the green radiation is always a more direct and attractive way. Currently, InGaN and AlGalnP LDs are well developed which can cover a wide range of visible wavelength for both blue and red. However, it is still rather difficult to achieve ‘real green’ radiation through semiconductor lasers. Since the first

commercialized green LD (510-515 nm) was demonstrated by Nichia Corp. [28] by improving the growth quality and LD's structure. The wavelength of commercial green LD kept stayed at 510-520 nm due to the limitation of the fundamental material and device designs. However, a number of applications like display and fluorescence excitation need the green wavelength at ~532 nm.

1.2.2 Direct-emitting semiconductor green laser diodes

Despite the semiconductor laser became well-know from 1980s when the first commercial high-power LD was put into market by Spectra Diode Labs, the first LD was made by a team from MIT Lincoln Laboratory only a year after Maiman operated the first laser. However, all the initial LDs were wide-area homojunction devices [29]. As a result, the LDs were required to be cooled in cryogenic temperature [30,31,32]. The room temperature operation of LD remained elusive until Alferov [33] made the first protype room-temperature CW GaAlAs LD by using heterostructures to improve current and light confinement. On the other hand, the development of visible LDs had not fallen behind the pace of infrared LDs. The first visible semiconductor laser was made by Nick Holonyak [34] in 1962 which has red radiation at 710 nm. Decades later, researchers from Sony Corp. reported their achievement of 671 nm radiation at room temperature by using AlGaInP [35]. And in 1996, Shuji Nakamura et al firstly reported a ~400 nm semiconductor laser based on InGaN. In the next decades, the fabrication technologies for blue and red semiconductor laser were developing quickly and more powerful and efficient blue and red LDs were put into the market.

Despite the success in blue and red semiconductor laser, it is still challenging in achieving lasing longer than 500 nm. The 1st green semiconductor laser was demonstrated by J. M. Gaines et. al [36] and M. A. Haase et al [37]. in 1993. But they were unable to be commercialized because of the poor reliability caused by high drive current needed for achieving lasing operation. Then in 2009, a number of groups (Nichia Corp., Osram, Sumitomo, Corning, Soraa, and UCSB) achieved reliable green LDs by using c-plane or semi-polar GaN substrate. Currently, the commercial green LD can achieve watt-level output power with lasing wavelength near 515 nm. However, the wavelength is still too short to meet the wavelength requirement of Rec. 2020. The main reasons are linked to the physical and material properties of the InGaN QW of the green LD. In order to push the radiation wavelength further into the green region, the concentration of the of the indium in the quantum walls (QWs) need to be increased. Due to the piezoelectric effect of the material, strain is caused by the piezoelectric field with MV/cm strength for only ~0.1 eV energy drops across the QW [38]. Therefore, the electrons and holes are pushed to the different interfaces of the QW, reducing their spatial overlap and causing the radiative recombination rate to decrease. The second problem is that the spontaneous emission spectrum broadening and gain spectrum broadening of the InGaN QW caused by the increase of Indium concentration. It results in decreasing of the peak optical gain for overcoming the loss in the laser cavity [39]. Another problem is relating to the lack of industry grade freestanding nonpolar and semi-polar substrates. Conventional c-plane (polar) orientation GaN epitaxial cystal lasers still have piezoelectric interface charges,

which would cause further reduction in optical gain and luminous efficiency in the highly strained green QW [39,40].

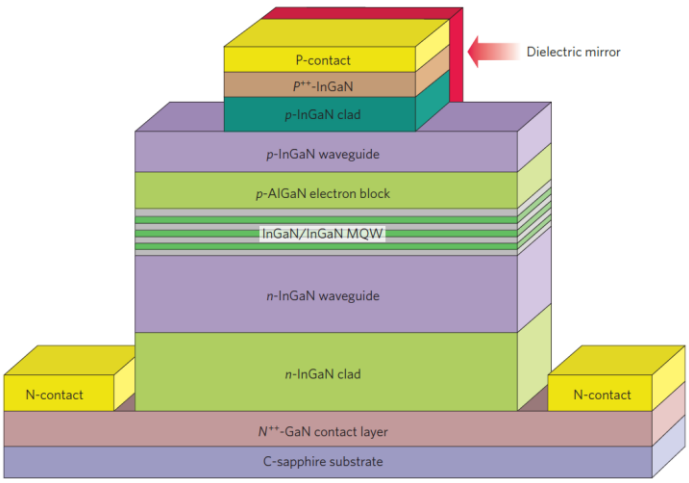

Fig. 1.2 Epilayer structure of an InGaN green laser diode on a c-sapphire substrate. Reprinted from Ref. [41] with permission from Springer Nature.

Inspiring news came out in 2018, in which a research group from Sony Corp. successfully demonstrate a watt-class 530 nm green LD based on GaN and achieved a wall-plug efficiency of 17.5% at a current of 1.2 A [42]. However, its commercialization is still limited due to use of semi-polar GaN substrate. Though semi-polar orientation substrate shows excellent performance in the green region, some semi-polar planes do not naturally exist in the GaN crystal structure, so a series of complicate methods must be taken to grow them artificially. Especially, the use of hydride vapor phase epitaxy (HVPE) method limits the size of these semi-polar substrate when growing a specific thickness of GaN layer.

Therefore, though the report of the ~530 nm LD by Sony was very encouraging, the high cost and small size of semi-polar and nonpolar substrates make these LDs have not been made suitable for industry yet.

1.2.3 Green lasers via second harmonic generation

1.2.3.1 Single-pass SHG

Second harmonic generation (also called frequency doubling) is a nonlinear process in which a new photon with frequency 2ν is generated by combing two photons with frequency ν after passing through a nonlinear material. Second harmonic generation (SHG) was first demonstrated by P. A. Franken in 1961 [43]. Since then, it becomes a very powerful method for generation of a variety of wavelengths across UV and visible range. The simplest approach for SHG green generation is single-pass SHG in which a focused infrared laser beam incident on a suitable nonlinear crystal directly.

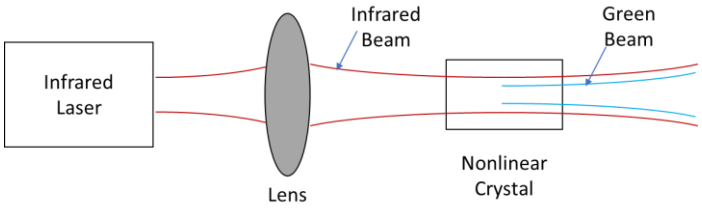

Fig. 1.3 Typical configuration for single-pass SHG

For achieving efficient SHG conversion, a powerful infrared laser with spectral and spatial mode properties is required. Moreover, a material with suitable nonlinear

characteristics is needed to work with the fundamental laser. So far, a lot of approaches have been developed for achieving efficient single pass SHG, such as single-pass SHG by multiple-stripes laser arrays [44], master oscillator-power amplifier (MOPA) [45], and single-pass SHG of DPSS lasers [46]. However, those methods typically need complicated focusing system for modifying the shape of the fundamental beam, which could dramatically increase the size and complicity of the green lasers.

1.2.3.2 Extra-cavity SHG

While the single-pass method is most straightforward approach to achieve green radiation, the main disadvantage of this method is the need of very powerful infrared lasers. Furthermore, the use of high-power infrared lasers would result in high electrical power consumption, increase the manufacturing cost and resulting in difficulty for heat management which are not acceptable for a lot of practical applications. For that matter, a number of methods has been developed to overcome the disadvantages of the use of high-power infrared lasers. One approach is the extra-cavity SHG in which the remaining infrared light energy is repeatedly redirected into the nonlinear material by mirrors. Figure 1.4 shows a typical configuration of a resonator enhancement of SHG. Since a nonlinear crystal is placed inside a resonator, the infrared energy could successively pass through the crystal and it can interact with the crystal many times. Therefore, the SHG conversion efficiency is increased due to the high circulating infrared light density.

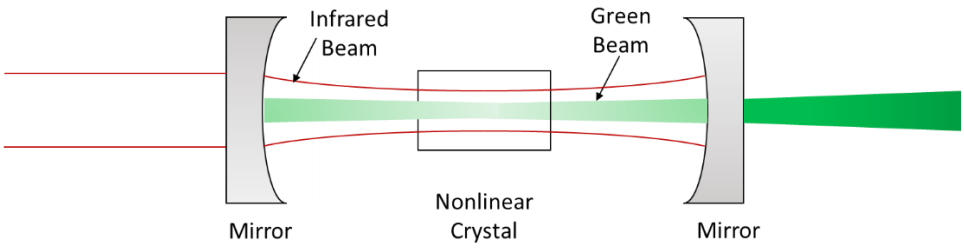

Fig. 1.4 Typical configuration for extra-cavity configuration

1.2.3.3 Intra-cavity SHG

Despite the use of the extra-cavity configuration to increase the SHG efficiency and lower the requirement of the infrared laser in which a conventional cw laser is able to achieve sufficient green power. There is still possibility to further simplify the structure to put the nonlinear material inside the cavity of the infrared DPSS laser. The intra-cavity SHG laser was first demonstrated by J.K. Wright in 1963 [47]. However, this configuration had not attracted a lot of attention until 1980s when high-power infrared LD are commercially available to efficiently pumping the solid state laser[48]. Then research focus was transferred to the invention of novel laser materials, nonlinear crystals, and cavity configuration optimization. Currently, this configuration has been widely used for building a compact DPSS visible lasers, and a lot of research work have been reported for achieving the efficient and compact green DPSS laser by the intra-cavity configuration. In 1998, Deyuan Shen et. al demonstrated a compact intra-cavity Nd:YVO_4/KTP 532 nm laser with an O-O efficiency of 32.5% [49]. In 2009, Spectralus Corp. [50] reported a monolithic microchip 532 nm green laser based on Nd:YVO_4 and MgO:PPLN crystals. They claimed

that 250 mW output green power and an O-O efficiency > 13 % was achieved where the overall volume of the green laser was only 0.33 cm^3. Same year, Gan et al [10] demonstrated a watt-class 532 nm green laser module which can achieve 39% O-O efficiency by pumping with a 5 W 808 nm LD. That integrated packing green module was also based on Nd:YVO_4 and MgO:PPLN crystals, its overall volume was only 0.09 cm^3.

Figure 1.5 shows a basic configuration for an intra-cavity DPSS green laser. Because the nonlinear crystal is placed inside the cavity, both the input and output mirror need high reflective coating for the fundamental light for confining the fundamental energy inside the cavity. In the meantime, a high reflective coating for the visible wavelength should be put on any interface before the nonlinear crystal. The main advantage of intra-cavity SHG is the utilization of the high-power density of the fundamental light within the laser cavity. Unlike other extra-cavity SHG, less optical components are needed, because the gain medium and nonlinear crystal share the same cavity mirrors.

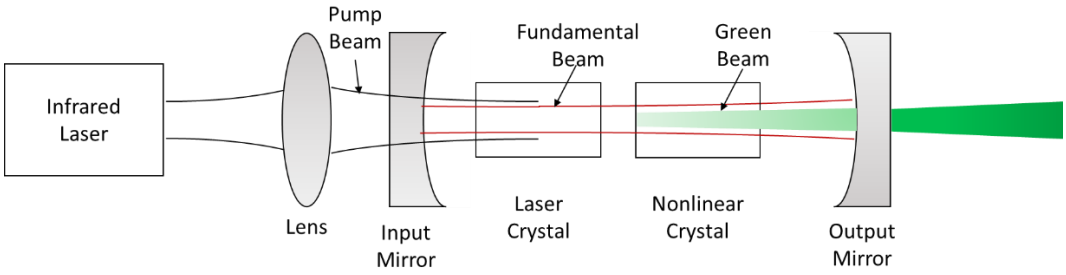

Fig. 1.5 Typical configuration for intra-cavity SHG configuration

1.2.3.4 Intra-cavity SHG based on VCSEL laser

Attribute to the invention of vertical-cavity surface-emitting laser (VCSEL), it becomes possible to further reduce the size of intra-cavity structure to put the nonlinear material inside the cavity of the pump laser. The VCSEL is a type of semiconductor laser in which the laser beam directly come out from the top surface of the diode junction instead of the edge-emitting for conventional LDs. In 2004, Novalux Inc [51] first introduce an intra-cavity frequency doubling VCSEL 532 nm green laser, which they called "NECESEL" (Novalux Extended Cavity Surface-Emitting Laser). By placing the nonlinear crystal inside the VCSEL's cavity, the SHG conversion of the circulating infrared energy is enhanced, and it also allowed for a more flat and compact architecture. Current issues for the NECESEL green laser are the relatively low electrical-to-optical efficiency (~5 % according to the specification of NECSEL-532-3000) and the pulsed mode operation which are designed for increase the SHG conversion efficiency.

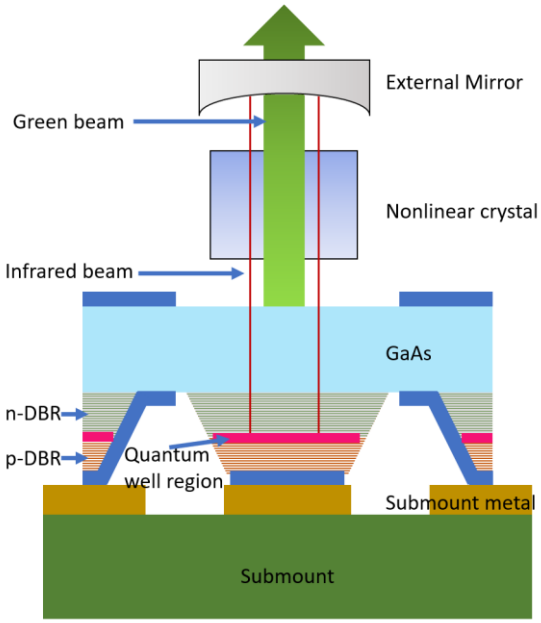

Fig. 1.6 Basic structure of the NECSEL visible surface emitting laser.

1.2.4 Compact green laser for laser display and speckle reduction

Generally, for display application, the illuminating laser source should have features of high power, small divergence angle, compact size, high electrical-to-optical (E-O) efficiency, and certain wavelength diversity for lowering the speckle noise. In this thesis, we are going to use the intra-cavity SHG configuration to build the green lasers which are designed for laser display applications. Though the ICFD is not the newest technique, it possesses several advantages than other approaches, especially for achieving green radiation > 530 nm which is beneficial for improving the color in the laser display system. For example, the ICFD DPSS laser can offer rich selection on the wavelength range of 530-

550 nm by changing the laser crystal and cavity coating. In the meantime, the overall cost can keep low since the DPSS laser is a mature technology. Furthermore, it is able to achieve efficient green output under low pump power by improving the laser design and using efficient laser host material and nonlinear crystals. Therefore, the heat management can be effectively improved, and the energy consumption of the whole laser system can be significantly lowered.

1.2.4.1 Laser host materials and nonlinear crystals

As discussed in the previous section, for the wavelength blending technique, the main challenge is to develop high power, high efficiency and compact green lasers with appropriate output wavelengths. Since the output green wavelength is ultimately determined by the gain medium, it is necessary to choose a suitable gain medium with proper emission peaks. For example, in the case of two wavelength blending, the wavelengths of both green lasers need to be close to 532 nm to maintain a good color performance. In a scenario where three different wavelengths are used, these three wavelengths should be located close to 532 nm with reasonable wavelength differences. In detail, if a 532 nm DPSS laser and ~515 nm LD are chosen, the third green laser should have emitting wavelength around 540 nm to balance the wavelength distribution.

Based on the mechanical properties, spectral characteristic, gain performance, and production cost, a lot of laser host materials are able to achieve sufficient power in the green range. Among them, neodymium-doped gain media is the most widely used gain medium in diode pumped laser technology. Table 1. lists several Nd^{3+} doped gain media which we are going to explore in this dissertation, the selection was based on the cost, gain

performance, spectrum properties and accessibility. There are also other Nd^{3+} doped gain materials like Nd:YLF and Nd:glass, etc., which are also widely used in modern laser systems. However, the Nd:YLF is vulnerable to water vapour and the Nd:glass based lasers typically have higher threshold pump powers which may cause difficulties with heat dissipation.

Table 1.1 A list of suitable gain media have emission peaks around 1064 nm.

Laser Crystal	Available wavelengths around 1064 nm / nm
Nd:YVO_4 (Neodymium-doped Yttrium Orthovanadate)	1062 [52],1064 [52,53], 1066 [52], 1073 [54], 1084 [55], 1086 [55]
Nd:$GdVO_4$ Neodymium-doped Gadolinium Vanadate	1063 [56], 1065 [56], 1071 [56], 1083 [57]
Nd:YAP Neodymium-doped Yttrium Aluminium Perovskite	1073 [58], 1080 [58], 1084 [58]

The nonlinear crystal function to convert the infrared laser light to visible wavelengths. This significantly extend the spectral coverage of laser light sources. At present, a lot of nonlinear crystals have been developed to obtain efficient SHG conversion. Beta Barium Borate (BaB_2O_4, BBO), Potassium Titanium Oxide Phosphate ($KTiOPO_4$, KTP), Lithium Triborate (LiB_3O_5, LBO) and Magnesium doped periodic-poled lithium Niobate (MgO:PPLN) are the most common nonlinear crystal that have been widely used to generate visible and UV radiation in many commercial products and research experiments.

Among them, the MgO:PPLN typically has the highest nonlinear coefficient (17pm/V). In contrast, the nonlinear coefficients of KTP, BBO and LBO are 3.4 pm/V, 2.5 pm/V and 0.85 pm/V, respectively. In PPLN crystal, because the axis of the $LiNbO_3$ crystal is periodically reversed, the strength of the SHG light can be enhanced after constructive interference through propagation. Moreover, the PPLN crystal is an alignment-free component since the use of the quasi-phase match (QPM) allows for a small phase mismatch over the light propagation direction. Furthermore, the 5 mol% MgO doping drastically increase the photoconductivity of $LiNbO_3$. Therefor the photorefraction effect is significantly minimized due to the decrease of the ratio of photovoltaic current to the photoconductivity. Those advantages make the MgO:PPLN become an ideal nonlinear crystal for achieving compact and efficient green radiation.

1.2.4.2 Single wavelength green DPSS laser for wavelength blending purposes

As shown in Table. 1.1, Nd:YVO_4 is the most common host material for generating continuous wave (CW) 1064 nm and 532 nm via LD end pumping. It has been studied for several decades [53], so the crystal growth technology is well developed and available at very low prices. Nd:YVO_4 has a large absorption coefficient over a wide spectral range around 808 nm, and it also has a high emission cross-section at the main lasing wavelength (1064 nm). By incorporating nonlinear crystals, the near infrared light from Nd:YVO_4 crystals can be converted to green, blue or even ultra-violet light.

There are three main transitions for Nd^{3+} doped host material: ${}^4F_{3/2}\rightarrow{}^4I_{9/2}$, ${}^4F_{3/2}\rightarrow{}^4I_{11/2}$, and ${}^4F_{3/2}\rightarrow{}^4I_{13/2}$. In Nd:$YVO_4$, The ${}^4F_{3/2}\rightarrow{}^4I_{11/2}$ transition corresponds to laser emission at 1064 nm and the ${}^4F_{3/2}\rightarrow{}^4I_{11/2}$ transition line can be further split into several closely stacked

stark levels. The fine spectroscopic study of the $^4F_{3/2}\rightarrow{}^4I_{11/2}$ transition reveals that there are several emitting wavelengths around the 1064 nm main peak [59]. In detail, for σ-polarization, it has emitting wavelengths at 1063 nm, 1065 nm, 1066 nm and 1084 nm. For π-polarization, there are emission peaks at 1064 nm, 1073 nm and 1086 nm. Since the 1064 nm has highest emission cross-section, the 1064 nm transition usually dominates stimulated emission in a laser system. However, by inserting wavelength selection elements or using specialized coating designs, the other wavelengths are able to achieve higher gain than 1064 nm and dominate the whole stimulated emission process.

To date, much of the literature [60-67] has focused on the study of Nd:YVO_4 near-infrared lasers, which were based on the weaker emission lines of Nd:YVO_4, i.e. $^4F_{3/2}\rightarrow{}^4I_{9/2}$ (914 nm) and $^4F_{3/2}\rightarrow{}^4I_{13/2}$ (1342 nm). For speckle reduction, $^4F_{3/2}\rightarrow{}^4I_{11/2}$ transition line is more interesting because it can provide infrared light near 1064 nm. But for the 1063 nm, 1065 nm and 1073 nm from the $^4F_{3/2}\rightarrow{}^4I_{11/2}$ transition, difficulties could arise for laser cavity coating design and manufacturing because those wavelengths are too close to 1064 nm. Therefore, the 1084 nm and 1086 nm emission lines are more appropriate than the other wavelengths from the $^4F_{3/2}\rightarrow{}^4I_{11/2}$ transition. Unfortunately, only a few of reports had discussed visible light generation through a frequency doubling process from 1084 nm or 1086 nm. Table 2 lists all of the literature we have found which are related to 542 nm and 543 nm visible green lasers based on the $^4F_{3/2}\rightarrow{}^4I_{11/2}$ transition.

Table 1.2 A list of published results for 542 nm and 543 nm Nd:YVO_4 intra-cavity SHG DPSS lasers.

Wavelength	Year	O-O Efficiency	Output Power / Pump Power	Nonlinear Crystal	Cavity Configuration
542 nm	2012 [68]	9.2%	1.33W/14.5W	KTP	V-type
	2006 [69]	3.22%	19mW/590mW	BBO	Linear
543 nm	2015 [11]	28%	7.5W/27W	Chirped PPLN	Linear
	2013 [70]	25.4%	4.5W/17.3W	LBO	V-type
	2013 [71]	21.3%	2.13W/10W	LBO	V-type
	2009 [72]	15.7%	2.35W/14.5W	LBO	V-type

As shown in Table 1.2, multi-watt output power of 542 nm and 543 nm has been demonstrated by using a Nd:YVO_4 crystal as a gain medium. However, the reported pumping power threshold was too high and overall O-O efficiency was low. The high pump power leads to issues with thermal management, so water cooling systems are typically required.

According to Table 1.2, the highest O-O efficiency of 542 nm and 543 nm are 9.2% and 28%, respectively. The highest efficiency record for 543 nm was achieved by a research group from Mitsubishi Electric Corp. by using a planar waveguide of magnesium oxide-

doped periodically poled lithium niobate (MgO:PPLN) to convert the fundamental light from a Nd:YVO_4 planar waveguide. However, the planar waveguide configuration significantly increased manufacturing cost and complexity. Therefore, it is desirable to developed efficient, compact and cost-effective Nd:YVO_4 542/543 nm green lasers by using bulk crystal components. Furthermore, the use of the inefficient nonlinear crystals (LBO, BBO, and KTP) also limited the SHG conversion efficiency.

As indicated in Table 1.1, Nd:YAP is another option which can provide infrared light near 1080 nm. Nd:YAP (also named as Nd:$YAlO_3$) is a well know Nd-doped laser material, other than Nd:YAG and Nd:YVO_4, which have been widely used. Nd:YAP possesses similar physical properties to Nd:YAG as both of their crystal structures are Y_2O_3-Al_2O_3 system [73]. The key difference between these two materials is that the YAG crystal is an isotropic crystal while the YAP is anisotropic in structure. The anisotropic crystal is beneficial for second harmonic generation since the frequency doubling mechanism is polarization sensitive. Additionally, the thermally induced birefringence effect can be significantly reduced because of the anisotropic property of Nd:YAP material. Nd:YAP has better thermal conductivity than Nd:YVO_4, and its emission cross-section is larger than a Nd:YVO_4 crystal at ~1085 nm. Another important feature of Nd:YAP is that the strong Stark level splitting causes multiple sharp fluorescence peaks for the ${}^4F_{3/2} \rightarrow {}^4I_{11/2}$ transition [74, 75]. As a results, simultaneous multi-wavelength emission can be achieved.

Current study of Nd:YAP has mostly focused on medical applications by using Nd:YAP as a 1.3 um infrared laser [76], creating a ~1080 nm tunable laser for helium optical pumping [58, 77], and simultaneous multi-wavelength lasers [78]. Only a few of research

reports [79, 80] have studied visible light generation by using Nd:YAP crystals, and the literature has focused on the power and mode stability improvement for quantum optics applications.

There is another strategy to maintain proper color gamut with low speckle noise via the wavelength blending method in which one or more near 532 nm lasers must be employed. Nd:$GdVO_4$ is an appropriate choice as its 1063 nm transition has the highest emission cross-section according to spectroscopic studies. Nd:$GdVO_4$ possess the same space group $I4_1/amd$ as Nd:YVO_4 [81]. The main difference is that the Y^{3+} ions in Nd:YVO_4 are replaced by larger Gd^{3+} ions in Nd:$GdVO_4$, thus Nd:$GdVO_4$ has very similar emission and absorption spectrums as Nd:YVO_4. The fluorescence lifetime, absorption and stimulated emission cross sections of Nd:$GdVO_4$ are only slightly smaller than those of Nd:YVO_4 [82]. Since the Nd:$GdVO_4$ was first introduced by Zagumennyi et. al in 1992 [83], most of the research papers focused on the crystal growth, spectroscopic characterisation, and infrared light generation. Only a few papers have explored continuous-wave (CW) green light generation [11, 84-86]. In contrast, for a 531.5 nm diode pumped Nd:$GdVO_4$ frequency doubling green laser, approximately 40% O-O efficiency should be expected due to similar gain characteristics shared with Nd:YVO_4 [10]. However, the best O-O efficiency of a 531.5 nm frequency doubled laser created with bulk laser material and nonlinear material was 26% [86], and more than 35 % O-O efficiency was also achieved with a waveguide configuration [11] because of the better optical energy confinement and higher optical power density. Unfortunately, the waveguide configuration can also increase the manufacturing cost and alignment difficulty.

1.2.4.3 Single wavelength green laser module for pico-projector

As discussed above, green DPSS lasers are necessary for laser projection systems to overcome the shortage of commercial green LDs that provide a poor color gamut. However, laser system dimensions are still a significant advantage of green LDs compared to normal green DPSS laser. Fortunately, in 2012, our research group had successfully demonstrated a very compact and high efficiency watt-level green DPSS laser module by integrating Nd:YVO_4 and MgO:PPLN on a piece of silicon substrate [10]. The length of the green laser module (mGreen) is less than 10 mm, which has comparable dimensions to its pumping 808 LD. This impressive design provides a practical solution for miniaturization of a variety of intra-cavity SHG DPSS green lasers. A micro green laser chip is in high demand for pico-projection systems, and field sequential modulation on illuminating laser sources is typically needed in pico-projectors in which digital light processing (DLP) or liquid crystal on silicon (LCoS) is used as an imaging panel. The refresh rate for a standard video system is 60 Hz, so a field-sequential color pico-projector needs a minimum frame rate of 180 frames/s for each color component. However, to avoid color breakup (the rainbow effect), modulation frequencies greater than 540 Hz are necessary [87]. It is well known that the LD intrinsically has modulation speeds as high as several MHz, while the modulation speed of a DPSS laser is limited by the fluorescence lifetime of the gain material. In the proposed mGreen module, since both the active and passive laser components (laser material and nonlinear crystal) are installed on the same silicon substrate and their top is covered by an Aluminum or Copper shell, the heat dissipation capabilities are significantly different than other green DPSS lasers with a separated configuration. It

is meaningful to investigate the lasing performance of the mGreen module under field-sequential modulation operation, which can provide valuable information for the utilization of micro green modules in pico-projector applications.

1.2.4.4 Multi-wavelength DPSS green laser

Compared to the wavelength blending method, multi-wavelength lasers have advantages in terms of compactness and manufacturing cost. Several methods have been used to achieve simultaneous multi-wavelength emission in a single laser. The most straightforward method is placing multiple laser crystals in a single cavity [88], where each crystal is responsible for generating one fundamental wavelength and afterwards one or more nonlinear crystals are used to convert the fundamental wavelengths to visible light. The underlying problem is that the more optical components inside the cavity can considerably increase the difficulty of alignment during the production packaging process. In contrast, the superiority of using multiple gain media is also noticeable, in which multiple gain media DPSS lasers generally possess the same level of power stability as single gain medium DPSS lasers.

The other popular method to realize simultaneous multi-wavelength emission is based on the utilization of different transition lines of a laser material. Those transition lines typically share the same upper energy level, and some of them even have the same lower energy level in which multiple optical transitions can occur on the sub-energy states of the Stark level manifolds of the upper energy state. Therefore, strong mode competition arises since electron transitions originate from the same upper energy state. The output power stability of each wavelength component can seriously deteriorate due to the strong mode

competition. As a result, in order to balance the gain and loss of each wavelength components, some special treatments need to be carried out. Currently, methods such as wavelength selection elements (i.e. etalons) [89], specialized coating design of the resonator [90] and the external stress induced birefringent effect [91] were used to achieve simultaneous multi-wavelength emission.

Until now, the primary motivations for studying the multi-wavelength emission laser is for the potential applications in terahertz generation and laser interferometers. It follows that a lot of research articles regarding the multi-wavelength lasers settle on the infrared spectral region, and comparatively little of the literature further investigated the feasibility of multi-wavelength visible lasers [14, 92, 93]. Consequently, multi-wavelength visible lasers were poorly developed, and the performance of the reported lasers was too poor for practical applications. For example, in 2008 [92], dual-wavelength green lasing was achieved by using Nd^{3+} doped aperiodically poled lithium niobate (APLN) crystals as the nonlinear crystal and 814 nm Ti:sapphire laser as the pumping source with 1.2 mW total green output power. Ye et. al [94] demonstrated watt-level output power for dual-wavelength green emission, but it was achieved under Q-switched operation and its output power and O-O efficiency at the balance point (the case where each wavelength component has the same power level) were still poor (the total output green power at the balance point was ~300 mW with an O-O efficiency of approximately 6%).

As mentioned earlier, terahertz generation and heterodyne laser interferometry are two main applications for dual/multi-wavelength lasers. Unlike the terahertz generation application in which dual-wavelength laser based THz generation was only achieved in the

laboratory, the dual-wavelength laser already has practical applications in industry for heterodyne laser interferometry. Heterodyne interferometry requires that the dual-wavelength laser has orthogonal polarization where the polarization of each output wavelength component is perpendicular with each other. Most current laser interferometry is based on the traditional Zeeman He-Ne laser [95] or using a Bragg cell [96] to separate out a new frequency component. The bottle neck of current commercial orthogonally polarized dual-wavelength light sources is that the wavelength difference (frequency difference) was still too small. The typical frequency difference of commercial techniques ranges from several megahertz (MHz) to several gigahertz (GHz) [97]. For a heterodyne interferometer, the measurement speed [97] and displacement measurement resolution [98] are normally restricted by the frequency difference of the dual-wavelength sources used in the system. Current development of orthogonally polarized dual-wavelength lasers concentrates on the infrared region [89, 91, 99, 100]. However, visible light lasers are more convenient to align when performing in-field measurements.

1.2.5 Numerical modal for intra-cavity SHG DPSS laser

The general form of the Maxwell equations may be written [101]

$$\nabla \cdot \vec{E} = -\frac{\rho}{\varepsilon_0} \tag{1.1}$$

$$\nabla \cdot \vec{B} = 0 \tag{1.2}$$

$$\nabla \times \vec{E} = -\frac{\partial \vec{B}}{\partial t} \tag{1.3}$$

$$\nabla \times \vec{H} = \frac{\partial \vec{D}}{\partial t} + \vec{J} \tag{1.4}$$

where $\vec{E}$ is the electric field, $\vec{H}$ is the magnetic field, $\vec{B}$ is the magnetic flux density, $\vec{D}$ is the electric flux density, ρ is the charge density, which includes both free charge density ρ_f and the bound charge density ρ_b. In a nonmagnetic dielectric medium, $\vec{B} = \mu\vec{H} = \mu_0\vec{H}$, $\vec{D} = \varepsilon_0\vec{E} + \vec{P}$, $\rho_f = 0$, and $\vec{J} = 0$. The relationship between bound charge density and polarization density ($\vec{P}$) is $\rho_b = -\nabla \cdot \vec{P}$. Therefore, the four Maxwell equations for a dielectric medium can be written

$$\nabla \cdot \vec{E} = -\frac{\nabla \cdot \vec{P}}{\varepsilon_0} \tag{1.5}$$

$$\nabla \cdot \vec{B} = 0 \tag{1.6}$$

$$\nabla \times \vec{E} = -\frac{\partial \vec{B}}{\partial t} \tag{1.7}$$

$$c^2 \nabla \times \vec{B} = \frac{\partial \vec{E}}{\partial t} + \frac{1}{\varepsilon_0}\frac{\partial \vec{P}}{\partial t} \tag{1.8}$$

In a homogeneous dielectric, a net surface charge density is produced by the effect of polarization. However, the internal charge density is kept unchanged ($\rho_b = 0$). Therefore, we can conclude $\nabla \cdot \vec{E} = 0$ in the medium. Take the curl of both sides of Eq. (1.7) and using the identity $\nabla \times \left(\nabla \times \vec{E}\right) \equiv \nabla\left(\nabla \cdot \vec{E}\right) - \nabla^2\vec{E}$, giving

$$\nabla^2 \vec{E} = \frac{\partial}{\partial t}\left(\nabla \times \vec{B}\right) \tag{1.9}$$

Substitute the Eq. (1.8) into Eq. (1.9), giving

$$c^2\nabla^2\vec{E} = \frac{\partial^2\vec{E}}{\partial t^2} + \frac{1}{\varepsilon_0}\frac{\partial^2\vec{P}}{\partial t^2} \tag{1.10}$$

where $\vec{E}$ is the electric field, $\vec{P}$ is the polarization density.

In the intra-cavity SHG configuration, the fundamental and second harmonic electric fields exist in the resonator all the time. Their time varying polarized electric field vectors can be expressed as [102]: (for convenience, cylindrical coordinate system with rotationally symmetric (along z-axis) is used, z is axial coordinate, and *r* is distance from the z-axis to the point P)

$$\vec{E}_1(\vec{r},t) = \frac{1}{2}\left[A_1^+(r,z)e^{jk_1z} + A_1^-(r,z)e^{-jk_1z}\right]e^{-j\omega_1 t} + c.c. \tag{1.11}$$

$$\vec{E}_2(\vec{r},t) = \frac{1}{2}\left[A_2^+(r,z)e^{jk_2z} + A_2^-(r,z)e^{-jk_2z}\right]e^{-j\omega_2 t} + c.c. \tag{1.12}$$

Where $A_1^+(r,z)$ and $A_1^-(r,z)$ is amplitude of the forward and backward fundamental wave, and $A_2^+(r,z)$ and $A_2^-(r,z)$ is the amplitude of the forward and backward second harmonic wave. k_1 and k_2 are the wave vector of the fundamental and second harmonic wave. ω_1 and ω_2 are the angular frequency of the fundamental and second harmonic waves. $\vec{r}$ is the position vector.

In laser gain medium, the interaction of electric field $\vec{E}$ and polarization density $\vec{P}$ can be given by [103]:

$$\vec{P} = \varepsilon_0 \kappa \vec{E} = \varepsilon_0 (\kappa' + j\kappa'')\vec{E} \tag{1.13}$$

$$\kappa' = \frac{\sigma_0}{k} \Delta N \frac{\nu - \nu_0}{\Delta \nu} \frac{(\Delta \nu/2)^2}{(\nu - \nu_0)^2 + (\Delta \nu/2)^2} \tag{1.14}$$

$$\kappa'' = \frac{\sigma_0}{k} \Delta N \frac{(\Delta \nu/2)^2}{(\nu - \nu_0)^2 + (\Delta \nu/2)^2} \tag{1.15}$$

where σ_0 is the cross section for stimulated emission at $\nu = \nu_0$, $\Delta\nu$ is the gain bandwidth of the Lorentzian lineshape function, ν_0 is the resonance frequency, and ΔN is the population inversion density. For a four-level laser system (such as Nd:YVO_4 and Nd:$GdVO_4$.), the spatial dependence rate equation of the population inversion density $\Delta N(r,z)$ is written as [104]

$$\frac{d\Delta N(r,z)}{dt} = R_P(r,z) - \frac{\Delta N(r,z)}{\tau} - c\sigma \Delta N(\phi_1^+ + \phi_1^-) \tag{1.16}$$

where R_p is the pump rate ($cm^{-3}s^{-1}$), and for end pump configuration $R_P(r,z) = \frac{\eta P_{in}}{h\nu_P} \frac{2\alpha e^{-\alpha z}}{\pi \omega_P^2(z)[1-e^{-\alpha l_1}]} e^{-2\frac{r^2}{\omega_P^2(z)}}$, P_{in} is the incident pump power, α is the absorption coefficient of gain material at the wavelength of the pump light, and ν_P is the frequency of the pump wave.

$\omega_P^2(z)$ is the pump beam waist inside the cavity under the paraxial approximation, which can be given by: $\omega_P(z) = \omega_{P0}\left\{1 + \left[\frac{M^2\lambda_P(z-z_0)}{\pi\omega_{P0}}\right]^2\right\}^{\frac{1}{2}}$, where ω_{P0} is the initial pump beam waist, λ_P is the pump beam waist, and M^2 is the beam quality factor of the pump light. ϕ_1

is the photon density of the fundamental wave inside the cavity [105], $\phi_1^{\pm} = \frac{I_1^{\pm}}{ch\nu_1} = \frac{1}{2}\frac{\varepsilon_0 c n_1 |A_1^{\pm}|^2}{ch\nu_1}$, where h is the Plank constant, ν_1 is the frequency of the fundamental wave, n_1 is the refractive index of the gain material.

Substitute the Eq. (1.11-13) into Eq. (1.10) leads to

$$c^2 e^{jk_1 z}\left[\nabla^2 A_1^+ + 2jk_1\frac{\partial A_1^+}{\partial z} - k_1^2 A_1^+\right] + c^2 e^{-jk_1 z}\left[\nabla^2 A_1^- - 2jk_1\frac{\partial A_1^-}{\partial z} - k_1^2 A_1^-\right] \quad (1.17)$$
$$= -\omega_1^2\left[A_1^+ e^{jk_1 z} + A_1^- e^{-jk_1 z}\right] - \omega_1^2(\kappa' + j\kappa'')\left[A_1^+ e^{jk_1 z} + A_1^- e^{-jk_1 z}\right]$$

$$c^2 e^{jk_2 z}\left[\nabla^2 A_2^+ + 2jk_2\frac{\partial A_2^+}{\partial z} - k_2^2 A_2^+\right] + c^2 e^{-jk_2 z}\left[\nabla^2 A_2^- - 2jk_2\frac{\partial A_2^-}{\partial z} - k_2^2 A_2^-\right] \quad (1.18)$$
$$= -\omega_2^2\left[A_2^+ e^{jk_2 z} + A_1^- e^{-jk_2 z}\right] - \omega_2^2(\kappa' + j\kappa'')\left[A_2^+ e^{jk_2 z} + A_2^- e^{-jk_2 z}\right]$$

In the nonlinear medium for second harmonic generation, the relationship between electric field and polarization density is written as

$$\vec{P} = \varepsilon_0\left(\chi^{(1)}\vec{E} + \chi^{(2)}\vec{E}^2\right) = \varepsilon_0\chi^{(1)}\vec{E} + \varepsilon_0\chi^{(2)}\vec{E}^2 \quad (1.19)$$

where $\chi^{(n)}$ is the n^{th} order susceptibilities of the medium.

Substitute the Eq. (1.11-12) into Eq. (1.16) leads to

$$\vec{P} = \varepsilon_0\chi^{(1)}\left[\vec{E}_1(\vec{r},t) + \vec{E}_2(\vec{r},t)\right] + \varepsilon_0\chi^{(2)}\left[\vec{E}_1(\vec{r},t) + \vec{E}_2(\vec{r},t)\right]^2 \quad (1.20)$$

Substitute the Eq. 1.11, 1.12, and 1.20 into Eq. 1.10, the nonlinear interactions of the forward and backward second harmonic wave and fundamental wave in a nonlinear material can be written as

$$c^2 e^{jk_1 z}\left[\nabla^2 A_1^+ + 2jk_1\frac{\partial A_1^+}{\partial z}\right] + c^2 e^{-jk_1 z}\left[\nabla^2 A_1^- - 2jk_1\frac{\partial A_1^-}{\partial z}\right] \tag{1.21}$$

$$= -\omega_1^2\chi^{(2)}\left[A_1^+ e^{jk_1 z} + A_1^- e^{-jk_1 z}\right]^*\left[A_2^+ e^{jk_2 z} + A_2^- e^{-jk_2 z}\right]$$

$$c^2 e^{jk_2 z}\left[\nabla^2 A_2^+ + 2jk_2\frac{\partial A_2^+}{\partial z}\right] + c^2 e^{-jk_2 z}\left[\nabla^2 A_2^- - 2jk_2\frac{\partial A_2^-}{\partial z}\right] \tag{1.22}$$

$$= -2{\omega_1}^2\chi^{(2)}\left[A_1^+ e^{jk_1 z} + A_1^- e^{-jk_1 z}\right]^2$$

Most of the intra-cavity SHG lasers use plano-concave configuration, in which the output coupler is a curved mirror and the input mirror is planar facet. Therefore, the boundary condition of the input side and output side can be given by [106]

$$E_1^-(r,0) = E_1^+(r,0)\sqrt{R_I} \tag{1.23}$$

$$E_2^-(r,0) = E_2^+(r,0)\sqrt{R_I} \tag{1.24}$$

$$E_1^-(r,L) = E_1^+(r,L)\sqrt{R_o^1}exp\left(\frac{jk_1 r^2}{2f}\right) \tag{1.25}$$

$$E_2^-(r,L) = E_2^+(r,L)\sqrt{R_o^2}exp\left(\frac{jk_2 r^2}{2f}\right) \tag{1.26}$$

Where R_I is the reflectivity of the input mirror, R_o^1 and R_o^2 are reflectivity of the output mirror at ω_1 and ω_2, and f is the curvature of the concave side of the output mirror.

A difference method can be used to solve the above coupled mode equations and the rate equation of population inversion. It was found that the higher output power would be expected if laser host material with larger emission cross-section and nonlinear material with higher nonlinear coefficient are employed. Furthermore, appropriate cavity design is also beneficial for improving the lasing performance. Good quality high reflective coating at the fundamental light is essential to provide high intensity fundamental light.

1.3 Research motivations

Given the developments of green DPSS laser and their various limitations in applications for laser display systems and other application scenarios which were discussed in the previous section, the main motivation is to overcome the limitations of conventional green LD and 532 nm DPSS lasers as light sources in projection systems.

The commercial green LDs still cannot provide the correct green wavelength recommended by the Rec. 2020 standard. Though the green DPSS lasers typically have an emission wavelength at 532 nm as recommended by Rec. 2020, the speckle performance is too poor due to its narrow linewidth. One main technique to improve the speckle performance of DPSS lasers is increasing the wavelength diversity of the illuminating light source. However, the proposed DPSS laser systems still cannot meet all of the requirements of green DPSS lasers for practical projection applications, and so there is plenty of space

for further improvement. For example, to maintain an appropriate color gamut and reduce the speckle noise, a green DPSS laser near 540 nm is necessary. However, efficient, compact and cost effective ~540 nm green DPSS lasers are still unavailable. Moreover, simultaneous multi-wavelength green lasers also have the benefit of reducing the speckle noise, but they were poorly developed and so have not attracted a lot of attention.

Furthermore, miniaturization of green DPSS lasers is also an important research interest because it is beneficial for the application of pico-projection systems. There is already a successful demonstration of a micro DPSS green module (i.e. mGreen) by using Nd:YVO_4 and MgO:PPLN crystals. This innovative design can also be applied to other types of intra-cavity SHG green lasers. One important deficiency of this micro chip green module is insufficient study of its modulation properties. The pico-projectors typically use DLP or LCoS panels for image generation, so a field sequential color operation is normally needed. However, there is a lack of research in regards to the modulation characteristics of the mGreen module.

1.4 Research objectives

The objectives of this research dissertation can be enumerated as follows:

1) Study the modulation properties of the compact watt-level Nd:YVO_4/MgO:PPLN intra-cavity SHG green module (mGreen).

   The aim of this study is to investigate the modulation properties of our proposed mGreen module. Since the laser material and nonlinear crystal are integrated into a

small chip, it is interesting to know the thermal effect on such a small DPSS laser when it is modulated with a high frequency signal, and some important parameters such as the conversion efficiency and the quasi-phase matching (QPM) condition are going to be studied.

2) Developing new green DPSS laser for wavelength blending.

   i) A ~540 nm DPSS laser is needed for reducing the speckle noise while maintaining a good color gamut. Our aim here is to develop a ~540 nm laser by using Nd:YVO_4/MgO:PPLN crystals. The laser should have stable watt-level power output by using a 5-6 W pumping LD, and it should also have comparable O-O efficiency to conventional 532 nm green DPSS lasers.

   ii) Developing a high-efficiency watt-level 531.5 nm Nd:$GdVO_4$/MgO:PPLN green laser for wavelength blending

   Nd:$GdVO_4$ has a main emission peak located at 1063 nm which can be used to generated 531.5 nm green laser by frequency doubling process. The Nd:$GdVO_4$ possesses very similar properties to Nd:YVO_4, so our target is to achieve comparable lasing performance to a Nd:YVO_4/MgO:PPLN intra-cavity SHG green laser by using Nd:$GdVO_4$ crystal.

   iii) Developing a compact and efficient 540 nm green laser based on a Nd:YAP crystal

   The Nd:YAP has a strong emission peak at 1080 nm, which is suitable for generating the 540 nm wavelength via frequency doubling techniques. The aims

of this section is to demonstrate a compact Nd:YAP based 540 nm green laser with small laser dimensions.

3) Developing an orthogonally polarized dual-wavelength green laser by using a single Nd:YVO_4 crystal.

   Orthogonally polarized dual-wavelength lasers have high demand in speckle reduction, THz generation and laser interferometry. Our aim here is to demonstrate the possibility of a high power, efficient, and stable dual-wavelength green DPSS laser by using a single gain medium. Specifically, the laser should have hundreds of milli-watt output with more than 10 % O-O efficiency. Moreover, it also should have comparable power stability to a normal DPSS laser so it can be used in similar practical applications.

4) Experimental demonstration of multi-wavelength blending for speckle reduction and color gamut optimization.

   One aim of this section is to study the speckle reduction performance by wavelength blending techniques in which three green laser sources with different output wavelengths are going to be used. We are going to find the optimal power ratio of each wavelength component for achieving the best speckle reduction performance and better color gamut.

Chapter 2 Modulation characteristics of a compact green laser module*

Chapter abstract

The field sequential modulation of a Nd:YVO_4/MgO:PPLN intra-cavity frequency doubling green laser was studied. The modulation frequency was set at 1 kHz and the duty cycle was changed from 20% to CW operation. It was shown that the quasi-phase matched (QPM) temperature decreases with an increase of the modulation duty cycle, and in turn causing the peak efficiency to rise. It was found that the temperature change in MgO:PPLN and the thermal lens effect in Nd:YVO_4 crystal were the respective origins of these observed experimental phenomena.

---

* *This chapter is reproduced from a journal article "**Bin Zhang**, Yi Gan, and Chang-Qing Xu. Study of the field-sequential modulation of Nd:YVO_4/MgO:PPLN based intra-cavity frequency doubling green laser. Optics & Laser Technology 102 (2018): 174-179.", doi: https://doi.org/10.1016/j.optlastec.2017.12.035. Reproduced with permission from Opt. Laser Technol., Copyright © 2017 Elsevier Ltd.*

The author of this thesis is the first author and the main contributor of this publication.

2.1 Introduction

Compact, low cost diode pumped solid state (DPSS) lasers operating in a modulation mode are required in many applications, such as optogenetic [107, 108], laser display [109] and surface treatment [110]. For instance, in a multipoint optogenetic application, laser sources with a narrow spectral linewidth and high beam quality are essential, and the light must be delivered in a sequence of short pulses (pulse durations on the order of 5-10 ms) with various duty cycles. In a laser projector employing liquid crystal on silicon (LCoS) or digital light processing (DLP), field-sequential color (FSC) modulation is necessary [111, 112]. In this scenario, the laser sources are modulated under a specific frequency (the interested modulation frequency range for DLP and LCoS being 0.06 kHz ~ 2 kHz) with various duty cycles. In these applications, the lasers should be operated at the maximum efficiency, and ideally the peak power is independent or nearly independent on the modulation duty cycle. Although DPSS lasers have been used in these applications, their modulation properties have not been studied in detail. Results on duty cycle dependence of a microchip DPSS green laser at a low power level (~100 mW) and low efficiency (about 10%) have been reported where thermal effect is negligible [113, 114]. Wang et al. [115] presented the frequency and duty cycle dependence of a blue DPSS laser without considering the wavelength shift of the pump laser diode at various modulation operations, which makes the conclusion become questionable. To date, none of the reported works [113-116] had studied the temperature dependence of the laser performance (such as efficiency, optimal operation temperature) under modulation operation, which is critically important to the frequency doubling based DPSS lasers.

In 2012, an intra-cavity frequency doubling DPSS green laser module, named mGreen was reported [10]. This module was formed by integrating a Nd:YVO_4 crystal and a MgO doped periodically poled lithium niobate (MgO:PPLN) crystal. Its maximum power was higher than 1.5 W with over 30% Optical-to-Optical (O-O) efficiency. Due to the utilization of the MgO:PPLN crystal, it can achieve a smaller size and lower cost as compared to the conventional KTP and LBO-based DPSS lasers. Like the conventional DPSS lasers, the modulation properties of the mGreen module based lasers have yet to be investigated. Properties such as the modulation frequency dependence, quasi-phase-matched (QPM) temperature dependence and duty cycle dependence of the mGreen module based lasers are unclear, thus providing the impetus for this research.

In this paper, the modulation characteristics of mGreen based green lasers were investigated, and the O-O conversion efficiency and the QPM temperature under a modulation mode with different duty cycles were studied. Physical origins of the experimental results are discussed and analyzed.

2.2 Experimental Setup and Procedure

2.2.1 Structure of the mGreen module

The mGreen module used in the experiments consists of 4 components: a silicon substrate, a Nd:YVO_4 crystal, a MgO: PPLN crystal, and an aluminum cover. The Nd:YVO_4 crystal is the laser medium, and the MgO: PPLN crystal is the frequency

doubling crystal. The output facet of the mGreen module was carefully aligned to the input facet, and both crystals were set on top of the silicon substrate to form a plane-parallel cavity. The spacing between these two crystals was 4.5 mm. The coating film on the input facet of the Nd:YVO_4 was antireflective (AR) at 808 nm and high reflective (HR) at 1064 nm and 532 nm. The coating film of the output facet of the MgO: PPLN crystal was AR at 1064 nm & 532 nm. The structure of the module is shown in Fig. 2.1 with dimensions of 7.0 (L) × 4.6 (W) × 2.0 (H) mm^3, (Nd:YVO_4: 3mm (L) x 3mm (W) x 0.5mm (H), MgO:PPLN: 1.5mm (L) x 2mm (W) x 0.5mm (H), QPM period: ~7 μm).

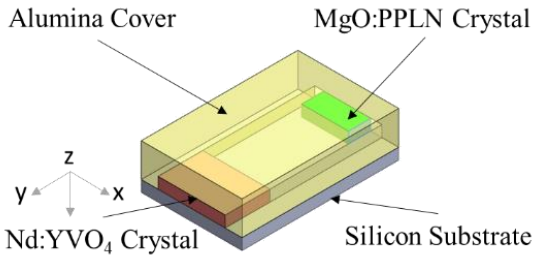

Fig. 2.1 3D scenography of an mGreen module.

2.2.2 Experimental setup and method

Since the QPM technique employed in the MgO:PPLN crystal is temperature sensitive, it's important to analyze the temperature dependence of the mGreen module. The experimental setup is shown in Fig. 2.2. An 808 nm laser diode (LD) with a fast axis collimated (FAC) lens was used as a pump source and was placed ~0.3 mm away from the

input surface of the mGreen module. A function generator that was used to produce a square waveform signal was connected to an LD driver, which was used to turn the LD on and off periodically at a specific frequency and duty cycle. A plane-concave mirror was placed 30mm from the output facet of the mGreen, which was employed as the output coupler. The mirror had HR coating at 1064 nm on its input surface and AR coating at 532 nm on both sides. A notch filter (@ 808 nm & 1064 nm) was employed to remove the fundamental light from the output green laser light. The mGreen module and LD were placed on top of two thermo-electric coolers (TECs), respectively.

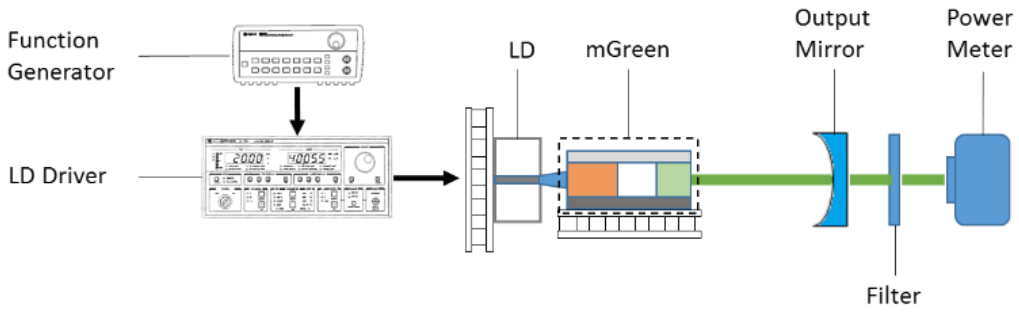

Fig. 2.2 Experimental setup for mGreen modulation property test.

To eliminate the rainbow effect in an FSC technique-based laser projector, the frame rate of the projector should be >180 Hz (or >540 Hz for color field rate) [87, 117]. Thus, the modulation frequency used in this experiment was set at 1 kHz, and the duty cycle was varied from 20% to CW (100%) with a 10% incremental step. Since the output wavelength of the LD depends on the duty cycle, the operating temperature of the LD was carefully

adjusted by the TEC module. The LD output power LD spectrum can be kept the same if the temperature compensation is applied properly. Table 2.1 shows the average power of the pumping LD at different duty cycles. It shows that the peak powers of the LD were kept within a 2% range in the measurements for each different duty cycle. For each duty cycle, the temperature tuning curve of the mGreen module was measured between 10 to 45℃ (with a 1℃ incremental step).

Table 2.1 Average power, peak power, and temperature of LD at different duty cycles

Duty Cycle	**20%**	**30%**	**40%**	**50%**	**60%**	**70%**	**80%**	**90%**	**CW**
Average Power/W	0.57	0.86	1.15	1.43	1.73	2.00	2.30	2.60	2.90
Peak Power/W	2.85	2.86	2.88	2.86	2.88	2.86	2.88	2.89	2.90
Temperature/℃	49	47.4	46	44.6	43.1	41.9	40.3	38.5	37
Center Wavelength	~ 808.6 nm								

2.3 Results and Discussion

2.3.1 Experimental results

Figure 2.3 shows the measured and fitting temperature tuning curves of the mGreen module at 30%, 60%, and 90% duty cycle respectively. The Y-axis is the O-O efficiency

of the mGreen module, which is the output power of the green laser divided by the LD pumping power. Since the operation of the MgO:PPLN crystal is based on the QPM technique, its temperature dependence should follow a sinc-squared waveform. By using the nonlinear regression method, the experimental results (dots, squares and triangles) can be fitted to the sinc-squared fitting curves (dashed lines), as shown in Fig. 2.3. One can observe that the duty cycle dependence of O-O efficiency strongly depends on the operation temperature. For example, at 25 ℃, the efficiency at 30% duty cycle is 30% lower than that at 90% duty cycle, but they are almost the same at 40 ℃.

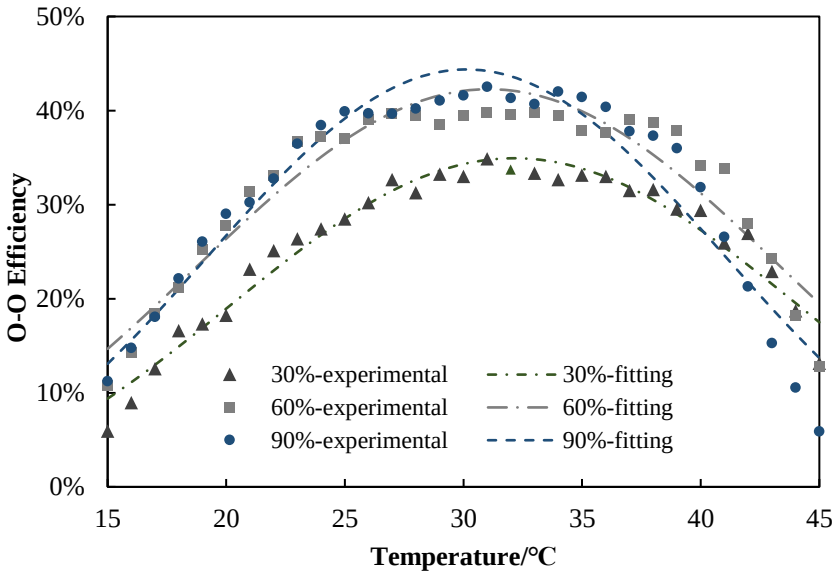

Fig. 2.3 The measured & fitting temperature tuning curves of the mGreen module based lasers under modulation modes with different duty cycles.

In each fitting temperature tuning curve, there is a peak efficiency which corresponds to a QPM temperature. Figure 2.4 shows the shifts in QPM temperature with changes in the duty cycle. The dots are the QPM temperature (i.e. the temperature corresponding to the peak of the temperature tuning curve) obtained from the fitting temperature tuning curves, while the dashed line is a linear fitting curve. As shown in Fig. 2.4, the QPM temperature declines linearly with an increase of the duty cycle, and overall the QPM temperature variation can be as large as 2.5℃ when the duty cycle changes from 20% to 100% (i.e. CW mode).

Figure 2.5 shows the peak efficiency shift with changes in the duty cycle. The dots are the peak O-O efficiency (i.e. the peak of the temperature tuning curve) obtained from the fitting temperature tuning curves which are partially shown in Fig. 2.3, while the dashed line is another fitting curve. As shown in Fig. 2.5, the peak O-O efficiency increases notably at first, and then becomes saturated around 80% duty cycle. The slightly decrease of the peak O-O efficiency beyond 80% duty cycle may be resulted from the uncertainty of the temperature tuning curve fitting with a small ripple (shown in Fig.2.3). One may observe that the efficiency varies from 30% to 45% when the duty cycle changes from 20% to 100%.

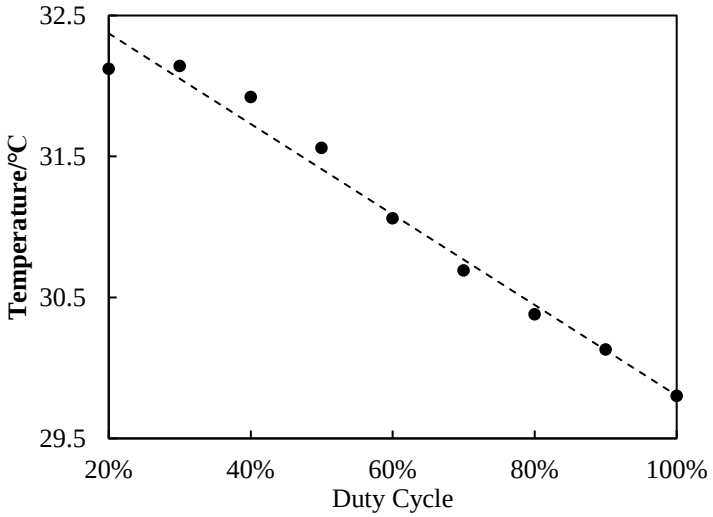

Fig. 2.4 QPM temperature of mGreen versus duty cycle.

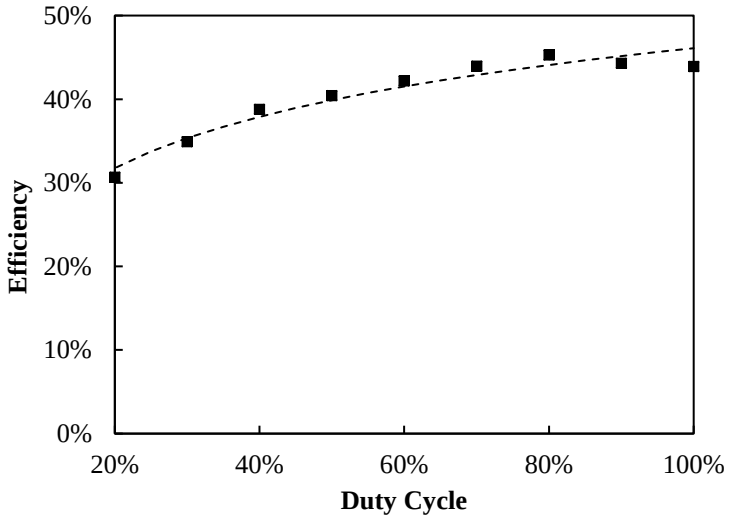

Fig. 2.5 The peak efficiency of mGreen versus duty cycle.

Experiments were also conducted to measure the size of the output green laser beam spot. A CMOS camera (Sony IMX071 16.2 megapixel, 23.6 x 15.6 mm) was used to

acquire the measurements. The CMOS camera was used to replace the power meter in Fig. 2.2, and it was placed 55 cm away from the mGreen module. Several ND filters were placed between the CMOS and the mGreen module to reduce the power of the green laser beam.

The captured beam spots under CW and modulation modes are shown in Fig. 2.6. The interference patterns observed in the beam profile were caused by Fabry-Perot interference between the ND filters. As shown in Fig. 2.6, the output beam is multimode, and most of the power concentrates in the centre spot. An elliptical fitting was employed to outline the shape of the output beam spot, which was obtained by measuring the light intensity drop to $1/e^2$ of the maximum value at the beam centre. It is more reasonable to consider that the minor axis length of the elliptically shaped beam corresponds to the beam diameter of the fundamental transverse mode of the green laser. Figure 2.7 shows the minor axis length changes as a function of the modulation duty cycle. It can be observed that the minor axis length becomes larger with an increase of duty cycle.

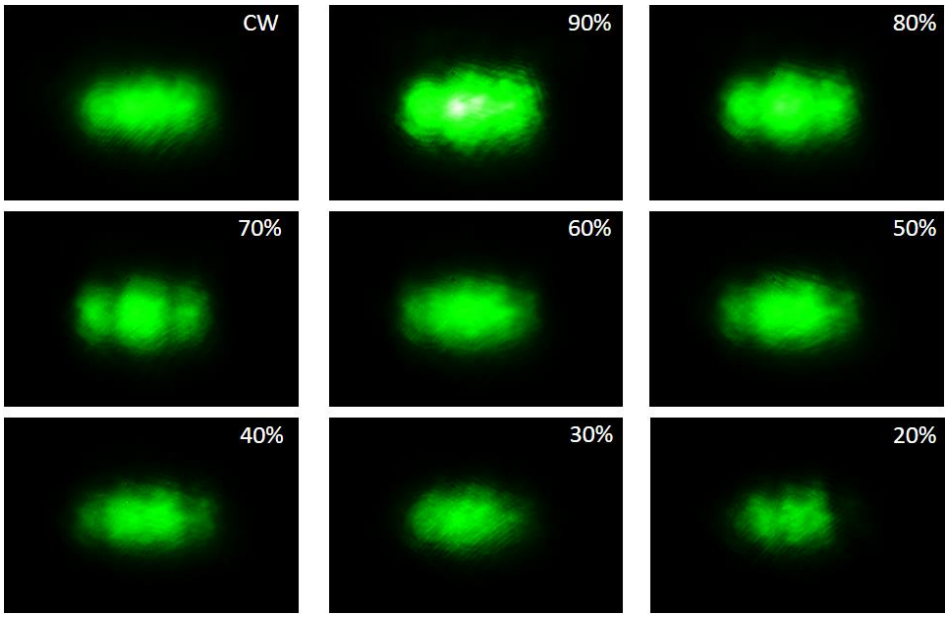

Fig. 2.6 The green laser beam profile under CW and modulation modes as captured by CMOS sensor.

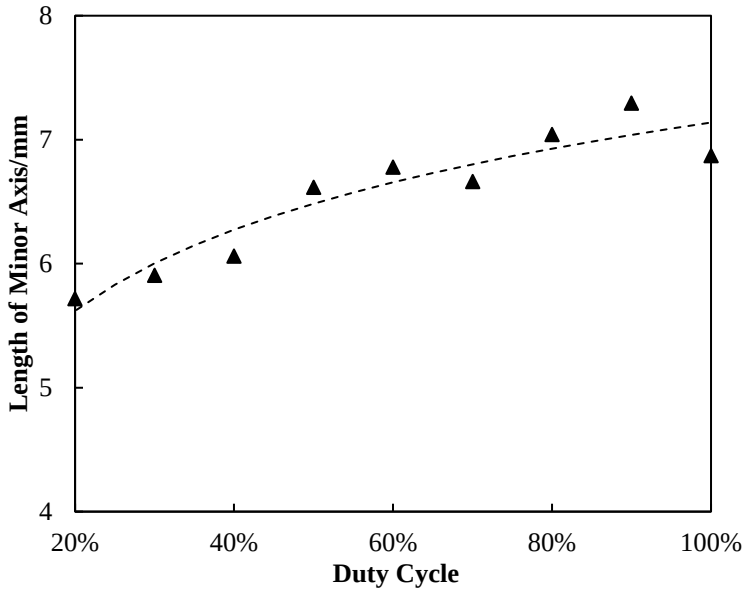

Fig. 2.7 The minor axis length of the green laser beam versus the modulation duty cycle. The dashed line is a fitting curve of these experiment results.

2.3.2 Discussion

The thermal effect usually plays an important role in a laser system, particularly in a compact intra-cavity frequency doubling laser [118]. There are two major heat sources in a running mGreen module-based laser within the Nd:YVO_4 crystal and the MgO:PPLN crystal respectively, which is due to the absorption within the crystals.

The Nd:YVO_4 and MgO:PPLN crystals are separated by air, and the top and bottom surfaces of the crystals are indirectly connected through the Al cover and Si substrate. According to our simulations, the heat generated in Nd:YVO_4 is quickly removed by the TEC underneath the mGreen module and cannot reach MgO:PPLN for the mGreen module used in the experiments. As a result, it is reasonable to suggest that the irradiated region of MgO:PPLN produces the most heat in the MgO:PPLN crystal. It is worth nothing that similar experimental results shown in Figs. 2.4 & 2.5 were obtained for a conventional DPSS laser configuration (i.e. without using the mGreen module), where Nd:YVO_4 crystal was completely separated from MgO:PPLN, implying that the heat transferred from Nd:YVO_4 crystal to MgO:PPLN is indeed negligible.

Obviously, at a fixed modulation frequency, a higher duty cycle leads to more heat generated in the MgO:PPLN crystal. Thus, the TEC temperature underneath the mGreen should be reduced to keep the MgO:PPLN cool for maintaining optimal SHG efficiency

when the duty cycle is increased. This is the origin of the shift in the QPM temperature of the mGreen module shown in Fig. 2.4.

Figure 2.5 indicates that the peak O-O efficiency rises in response to an increase in the duty cycle. To understand this experimental result, the thermal lens effect in Nd:YVO_4 was investigated.

The efficiency of the green laser depends mainly on two factors: the incident pump light intensity and MgO:PPLN temperature. Since the temperature of MgO:PPLN can be controlled by the TEC, the intensity of incident infrared light is the main factor affecting the O-O efficiency. As the dimensions of the mGreen module are fixed, cavity length change induced by thermal expansion is almost negligible. Therefore, it is the thermal lens effect in the Nd:YVO_4 crystal that mainly affects the output power of the laser.

From Fig. 2.7, one can see that the short axis of the beam profile nearly increases with the increase of duty cycle, this means that the minimum beam waist in the cavity also shrinks in respond to an increase in duty cycle. The decrease in the laser beam size (inside the cavity) corresponds to an increase in intensity of the fundamental laser beam, which results in an increase of SHG efficiency. This process is shown schematically in Fig. 2.8, in which the 532 nm-beam diameter increases as the duty cycle increases. This qualitatively explains the results shown in Fig. 2.5, in which the peak O-O efficiency increases as the duty cycle increases. Since the far-field beam size is inversely proportional to minimum beam waist, the results shown in Fig. 2.6 agree well with the above discussion.

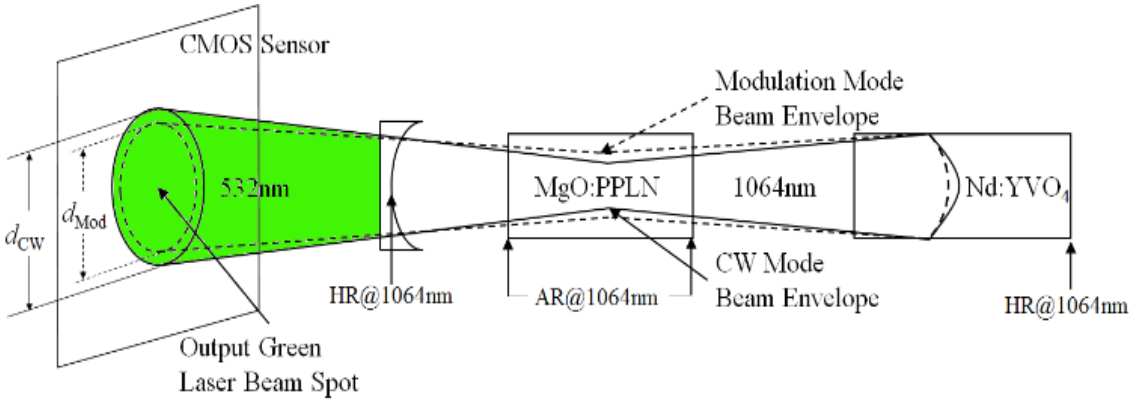

Fig. 2.8 Schematic diagram of thermal lens effect, beam waist, and green laser beam spot under a modulated and CW operation mode.

2.3.3 Theoretical estimation of minimum beam waist and divergence angle

In this paper, the 808 nm pump LD was modulated by a 1 kHz square waveform with different duty cycles. The thermal relaxation time (thermal response time) of the Nd:YVO_4 crystal is about 1.1 ms [116], which is longer than the modulation period used in this study. Therefore, the heat produced in the Nd:YVO_4 can gradually accumulate until it reaches a steady state.

To conduct further investigation, the COMSOL Multiphysics were employed to simulate the temperature gradient and thermal induced expansion of the Nd:YVO_4. In our simulations, the incident 808 nm laser was considered as a continuous heat source while incident on the Nd:YVO_4 crystal. The total power is linearly spread over a modulation period. (e.g., if the total absorbed pump power is 1 W, the total absorbed pump power at

50% duty cycle is 50%×1W=0.5W). In the simulations, the absorption coefficient was set at 31.4 cm^{-1} @810nm, thermal-optical coefficient 8.41×10^{-6}/K [119], and thermal expansion coefficient 8.2×10^{-6}/K [119]. The 3-D refractive index distribution of Nd:YVO_4 are shown in Fig. 2.9 (a). Fig. 2.9 (b) shows the thermal expansion effect on that crystal. (top view of the Nd:YVO_4 crystal). The black line is the original contour of the Nd:YVO_4 crystal, and the grey area means expanded crystal. We magnify the dimension by 500 times, so that the expansion effect can be seen clearly.

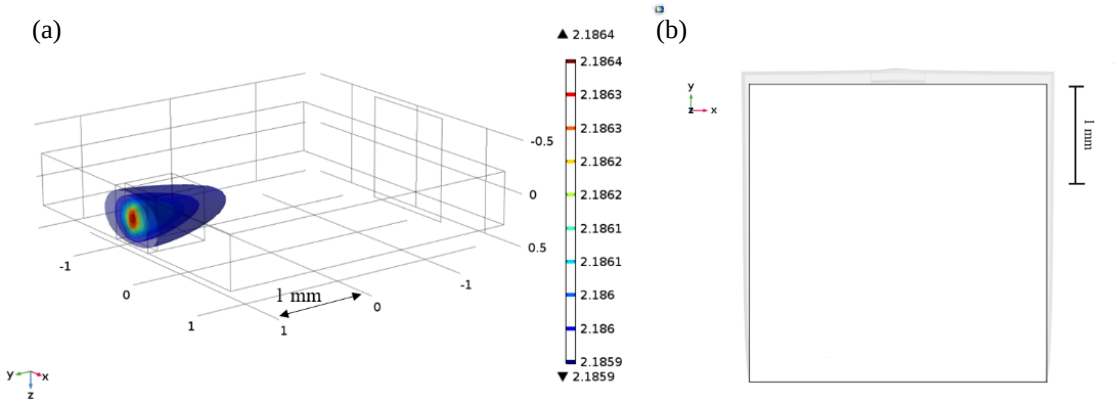

Fig. 2.9 (a). 3D refractive index distribution (b) Thermal induced surface distortion of the Nd:YVO_4 crystal in mGreen module. (taking a 50% duty cycle operation as an example.)

Although the captured beam spot is a multi-mode, most of the laser cavity theories are based on the Gaussian beam distribution. In this section, we theoretically study the laser beam propagation properties by assuming that the beam profile is a standard Gaussian beam.

To calculate the thermal lens effect of the Nd:YVO_4, a standard ABCD law method was used [102]. The gain medium was divided into many layers along the light propagation direction (Y-direction), a parabolic function, $n(r) = n_0(1 - \gamma r^2)$ was used to fit the refractive index distribution of each layer. Where n_0 is the index of the refraction at the center and r is the radial distance. The transfer matrix of each layer can be expressed as

$$M_{TL} = \begin{bmatrix} \cos\sqrt{2\gamma}l & \frac{1}{\sqrt{2\gamma}n_0}\sin\sqrt{2\gamma}l \\ -\sqrt{2\gamma}n_0\sin\sqrt{2\gamma}l & \cos\sqrt{2\gamma}l \end{bmatrix} \tag{2.1}$$

where l is the thickness of each layer.

The overall transfer matrix of the thermal lens generated in the Nd:YVO_4 crystal can be given by

$$M_{TL\,total} = M_{TL1}M_{TL2}M_{TL3}\cdots\cdots M_{TLn} = \begin{bmatrix} 1 - Dh & \frac{l}{n_0} \\ -D & 1 - Dh \end{bmatrix} \tag{2.2}$$

Where n is the number of layers, $h=l/2n_0$, $D= 2\gamma n_0 l$, which is also named as refractive power.

Then the divergence angle of a plan-concave cavity laser can be expressed as

$$\theta_{0i}^{*2} = \theta_{0i}^2 \frac{g_i\left(1+g_1^*g_2^*(n^2-1)\right)+n^2\left(g_j^*-2g_1^*g_2^*\right)}{|g_1^*+g_2^*-2g_1^*g_2^*|} \tag{2.3}$$

$$g_i^* = g_i - Dd_j\left(1 - \frac{d_i}{\rho_i}\right)$$

$$g_i = 1 - \frac{(d_1 + d_2)}{\rho_i}$$

$$\theta_{0i} = \frac{\lambda}{\pi \omega_{0i}} = \sqrt{\frac{\lambda L^*}{\pi} \frac{\sqrt{g_1^* g_2^* (1 - g_1^* g_2^*)}}{g_j^* \left(\frac{L^*}{\rho_i}\right)^2 + g_i^* (1 - g_1^* g_2^*)}} \tag{2.4}$$

$$L^* = d_1 + d_2 - D d_1 d_2$$

Where d_1 is the distance between the input mirror and the principle plane of the thermal lens, d_2 is the distance between the output mirror and the principle plane of the thermal lens, L^* is equivalent resonator length which is also equal to L_{eff}, effective length of the cavity. ω_{0i} is the minimum beam waist. Since the output coupler is a plano-concave mirror, the refraction effect of the mirror should be considered, the output beam divergence before the output mirror (inside the cavity) is represented by θ_{0i}^*, and the new divergence angle behind the output mirror is θ_{0i}.The calculated divergence angle (solid line) and minimum beam waist (dashed line) as a function of duty cycle are plotted in Fig. 2.10. The measured divergence (triangle) is also shown in Fig.2.10. As show in Fig.2.10, the simulated divergence angle shows an overall trend of increase with the increase of the duty cycle, which agrees well with the experimental data. In addition, the minimum beam waist within the cavity decreases with the increase of duty cycle, which also coincides with the discussion in the previous section.

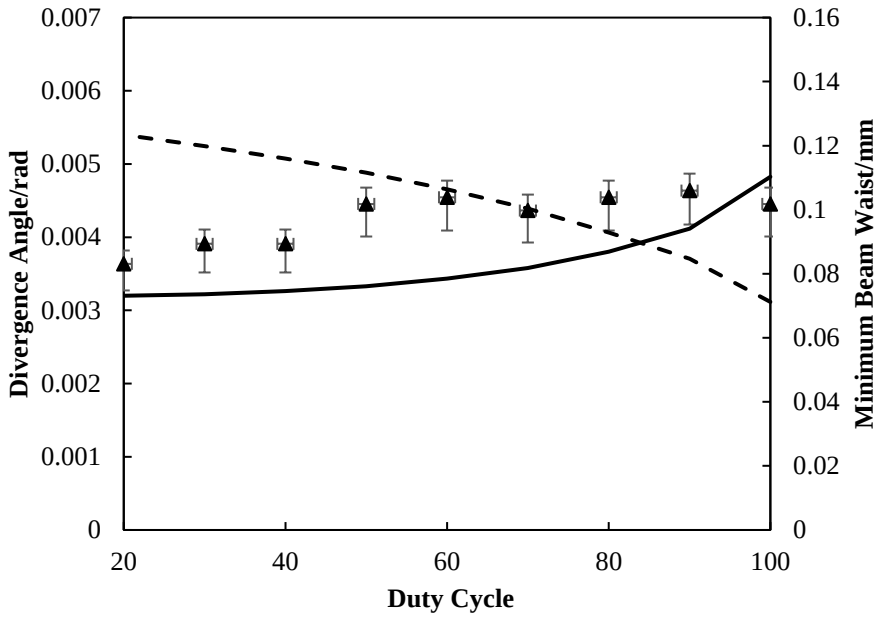

Fig. 2.10 Experimental (triangle), theoretical (solid line) divergence and minimum beam waist (dashed line) versus duty cycle.

The mismatch between the experimental results and theoretical estimation is due to the mode type of the experimental output spot, and the measurement apparatus. Since multimode beam spots were captured by the CMOS sensor, the multimode typically has larger divergence angle than fundamental mode, which makes the experimental beam spot a little larger than out theoretical results. Meantime, a CMOS detector was used to capture the beam spot image, this may bring some errors to our experimental results, which is due to the nonlinearity of the CMOS sensor.

2.4 Conclusion

For the first time, the field-sequential modulation (1 kHz frequency) properties of mGreen module based green lasers have been studied. It has been shown that by increasing the duty cycle, the QPM temperature of the mGreen module decreases, which is mainly due to the heat generated in the MgO:PPLN crystal. The peak efficiency of the temperature tuning curve of the mGreen module has been found to increase as the duty cycle increases, which is mostly due to the thermal lens effect in the Nd:YVO_4 crystal. It has also been found that the O-O efficiency of the mGreen module is almost independent on the duty cycle near 40℃, providing a guideline for selecting an operation temperature for applications where laser power needs to be maintained for different duty cycles. By simulating the thermal distribution in Nd:YVO_4 crystal and measurements of the 532 nm green laser beam spot size, it has been shown that the trend of the experimental results agrees well with the theoretical simulations, taking into account the thermal lens effect in Nd:YVO_4 crystal.

It is worth noting that the results presented in this paper can be applied to DPSS lasers with a conventional configuration and can be used as a guideline in designing and optimizing the DPSS lasers for variety applications with various modulation frequency and duty cycle.

Chapter 3 542/543 nm green lasers based on Nd:YVO_4 crystal[†]

Chapter Abstract

Efficient, compact and low cost 542/543 nm green DPSS lasers were proposed and demonstrated. Each laser was based on a Nd:YVO_4 crystal and a MgO:PPLN crystal. By aligning the z-axis of the MgO:PPLN crystal to σ- and π- direction of the Nd:YVO_4 crystal, the laser can emit green wavelengths at 542 nm and 543 nm, respectively. An optical-to-optical (O-O) efficiency as high as 22% was achieved for the 542 nm green laser, and the maximum O-O efficiency of the 543 nm laser was 35%. To the best of our knowledge, both results are the highest O-O efficiency achieved so far for Nd:YVO_4 542 nm and 543 nm.

[†] *This chapter is reproduced from a journal article "**Bin Zhang**, and Chang-qing Xu. "Compact, and efficient continues wave intra-cavity frequency doubling Nd:YVO_4/MgO:PPLN 542/543 nm green lasers. Optics & Laser Technology 122 (2020): 105885.", doi: https://doi.org/10.1016/j.optlastec.2019.105885. Reproduced with permission from Opt. Laser Technol., Copyright © 2019 Elsevier Ltd.*

The author of this thesis is the first author and the main contributor of this publication.

3.1 Introduction

Recently, projection systems based on laser light sources have attracted much attention due to the unique characteristics of lasers such as long lifetimes, high brightness, and vivid color. However, speckle noise is still an obstacle which limits the extensive commercialization of laser-based projection systems, especially for green lasers. One of the main methods for speckle reduction is to increase wavelength diversity [13, 120]. The wavelength blending technique, in which several laser beams with adjacent wavelengths are combined into a single light source, is considered an effective solution to increase the wavelength diversity of the laser sources for display applications.

Since human eyes are most sensitive to color green, the speckle noise from green lasers has been predominantly studied. It has been reported that speckle noise associated with the color green can be reduced by employing the wavelength blending technique, in which green laser diodes (center wavelength of 515-520 nm) were mixed with diode pumped solid state (DPSS) lasers with an emission wavelength of 532 nm [12]. Although this technique can provide significant speckle noise reduction, the resultant green light created by the mixing of these two lasers will be equivalent to a green light source with a wavelength shorter that 532 nm. Therefore, this wavelength does not fulfill the color gamut requirements for the Rec. 2020 color standard of a center wavelength of 532 nm. To achieve the correct wavelength of 532 nm and take advantage of the wavelength blending technique, the addition of a wavelength below 532 nm needs to be counteracted via the addition of wavelengths above 532 nm. Thus, the resulting total wavelength will be closer to 532 nm and provide a color gamut which better approaches the Rec. 2020 requirement.

Consequently, compact, efficient and sufficiently powerful (e.g. watt-level ~540 nm DPSS lasers) green lasers with a wavelength longer than 532 nm are needed.

Currently, neodymium-doped yttrium vanadate (Nd:YVO_4) crystals have been predominantly used as a gain medium in 532 nm DPSS green lasers, due to its high efficiency, low cost, and compact size. Furthermore, the spectroscopic study of Nd:YVO_4 shows two Stark components of the $^4F_{3/2}$—$^4I_{11/2}$ transition at 1084 nm and 1086 nm [72,121], respectively. To date, several studies [11,68-72,122] have demonstrated 542 nm and 543 nm green lasers by using an Nd:YVO_4 crystal and a nonlinear crystal. However, reported nonlinear crystals for 542 and 543 nm green light generation such as potassium titanyl phosphate (KTP) [68], barium borate (BBO) [69], and lithium triborate (LBO) [70-72, 122] have a lower nonlinear coefficient (d_{eff}) which limited the efficiency of the green laser system. The highest optical-to-optical (O-O) efficiency reported to date is 9% [68] at a pumping power of 14.5 W for a 542 nm green laser, and 25 % [70] at a pumping power of 17 W (with a pumping wavelength at 888 nm) for 543 nm green bulk lasers. In 2014, Shohda et al. used a planar waveguide of magnesium oxide-doped periodically poled lithium niobate (MgO:PPLN) to convert the fundamental light from a Nd:YVO_4 planar waveguide and achieved an O-O efficiency of ~28% at 543 nm [11]. However, the planar waveguide cavity configuration significantly increased manufacturing cost and complexity. Therefore, cost effective, efficient, and compact Nd:YVO_4 542/543 nm green lasers based on bulk crystals are desired.

In this paper, Nd:YVO_4/MgO:PPLN intra-cavity frequency doubling 542/543 nm green lasers are proposed and demonstrated. The proposed green lasers have advantageous features of small-size, low-cost, and high-efficiency. The output power and power stability of the green laser were studied, which demonstrated the highest O-O efficiency achieved so far.

3.2 Configuration of 542/543 nm green DPSS lasers

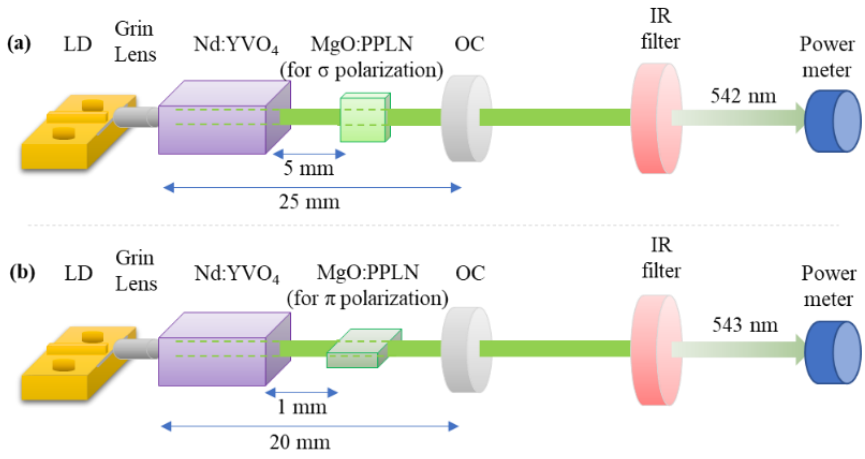

Fig. 3.1 A schematic diagram of experimental setup for the proposed 542/543 nm green lasers. (a) The z-axis of MgO:PPLN was aligned along σ-polarization; (b) The z-axis of MgO:PPLN was aligned along π-polarization.

Figure 3.1 shows a schematic diagram of the proposed intra-cavity frequency doubling Nd:YVO_4/MgO:PPLN green lasers. An 808 nm TM mode F-mount laser diode (LD) with

a fast axis collimator (FAC) was used as a pumping source (Focuslight, Inc. FL-CM01-5-808-Y, fast/slow axis divergence (FWHM) is around 7°). A Ø1.8 mm 0.25 pitch anti-reflection (AR) coated Grin lens (Edmund Optics, # 64543) was used to further converge the pump beam, and the distance between the Grin lens and the LD was less than 1 mm. A 3 mm (H) ×3 mm (W)×5 mm (L) a-cut Nd:YVO_4 crystal with a doping concentration of 0.5% was used as a gain medium. A high transmittance (HT) coating at 808 nm and a high reflection (HR) coating at 532 and 1064 nm were applied to the input facet of the Nd:YVO_4 crystal, while an AR coating for 532 and 1064 nm was applied to its output facet. To achieve the optimal quasi-phase-matching (QPM) condition for different fundamental wavelengths, a normal period MgO:PPLN crystal with dimension of 0.5 mm (H) × 2 mm (W) ×2 mm (L) was used as a frequency doubling element for the 542 nm laser, while a 0.5 mm (H) × 2 mm (W) × 4.1 mm (L) chirped period MgO:PPLN crystal was used for generation of 543 nm. The input and output facets of the MgO:PPLN crystals were also coated with an AR coating at 532 nm and 1064 nm. It is worth noting that the proposed lasers are potentially low cost since Nd:YVO_4 is widely used in laser pointers and cost effective MgO:PPLN is available on the market now.

The nonlinear crystal was placed on a customized copper jig, and a thermal electronic cooler (TEC) was attached to the jig to control the temperature of the MgO:PPLN crystal to meet its QPM condition. To achieve the optimal conversion efficiency, the polarization axis of the fundamental light must be aligned with the z-axis of the MgO:PPLN crystal. According to Ref. [121], the 1084 nm and 1086 nm transition lines of the Nd:YVO_4 crystal are in σ-polarization and π-polarization, respectively. Therefore, as shown in Fig. 3.1 (a) &

(b), the z-axis of the MgO:PPLN was aligned along σ-polarization for 542 nm emission, and π-polarization for 543 nm emission, respectively. A R = -50 mm plano-concave mirror was used as the output coupler (OC), and the overall cavity length was approximately 20-25 mm, which means a very compact green laser can be made by using the proposed configuration. The 1084 nm and 1086 nm are two weak transition lines in the Nd:YVO_4 crystal [72], and in order for the OC to suppress the lasing of other transition lines, a specialized coating is needed. The transmittance curve of the OC is shown in Fig. 3.2. It demonstrated an HR coating at 1084 nm and 1086 nm, as well as an HT coating at 542 nm, 543 nm, 914 nm, 1064 nm, and 1342 nm. It is worth noting that the measured transmittance of the OC at 542 and 543 nm is only about 90%, due to difficulties within the coating design and fabrication. An infrared (IR) filter was placed after the OC, which was used to eliminate the fundamental light from the output laser beam. Finally, a power meter (Thorlabs, S302C) was used to measure the output power of the green laser.

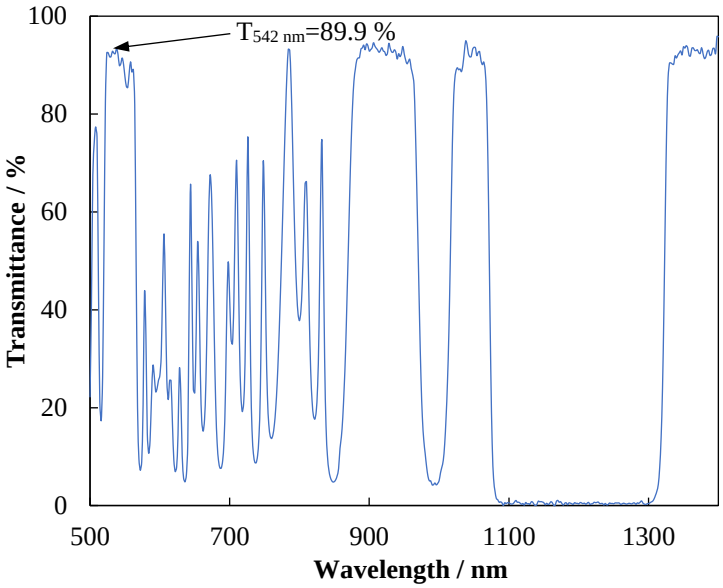

Fig. 3.2 The transmittance curve of the OC.

3.3 Experimental results and discussion

In our experiments, the z-axis of a normal period MgO:PPLN crystal was aligned with σ-polarization direction of the Nd:YVO_4 crystal for obtaining the 542 nm emission. Then a chirped period MgO:PPLN crystal was inserted with its z-axis aligned with π-polarization direction of the Nd:YVO_4 crystal to generate the 543 nm green light. In 2011, Florent Pallas et. al. [123] reported that two orthogonally polarized emission wavelengths from a single gain medium (neodymium-doped gadolinium vanadate (Nd:$GdVO_4$)) can be controlled by tilting the output mirror. Thus, in our experiments, the OC was carefully adjusted along x- and y- direction to achieve the optimal output performance for each green wavelength. The output spectrum of the proposed green lasers was measured by an optical spectrum analyzer

(Ando, AQ6315E) with a resolution of 0.1 nm, and are shown in Fig. 3.3 (a) & (b), respectively.

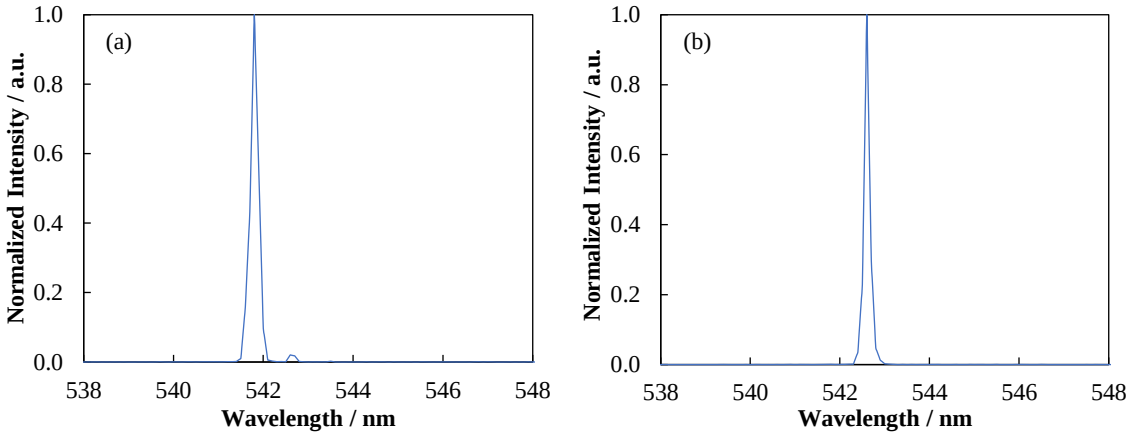

Fig. 3.3 Output spectrum of the green laser. (a) spectrum of 542 nm green laser (center wavelength at 541.8 nm); (b) spectrum of 543 nm green laser (center wavelength at 542.6 nm).

Figure 3.4 shows the output power and O-O efficiency (O-O efficiency = Output power of green light / Output power of pump light × 100 %) of the 542 and 543 nm green lasers. The maximum output power for the 542 and 543 nm green lasers was 1 and 1.63 W, respectively. This was obtained with a pumping power of ~5.15 W from the 808 nm LD. After considering the green loss from the OC, the maximum O-O efficiency of the 542 nm green laser was 22%, while the maximum O-O efficiency of the 543 nm green laser was 35%. To the best of our knowledge, both are the highest O-O efficiency achieved to date.

Due to the emission cross section at 1086 nm being slightly larger than at 1084 nm, the maximum O-O efficiency of the 543 nm green laser demonstrated a higher O-O efficiency and lower lasing threshold compared to the 542 nm green laser. It is worth mentioning that after comparing the O-O efficiencies reported in previous works [11,68-72,122] for 542 or 543 nm green lasers, the maximum O-O efficiencies of our green lasers were obtained under a notably low pump power level (~5.15 W). This allows for advantages such as improved thermal dissipation and compact. Also, the output power did not show saturation at the maximum pumping power (~5.15 W) available in the experiments, implying that green lasers with higher output power could be achieved by using a higher pumping power.

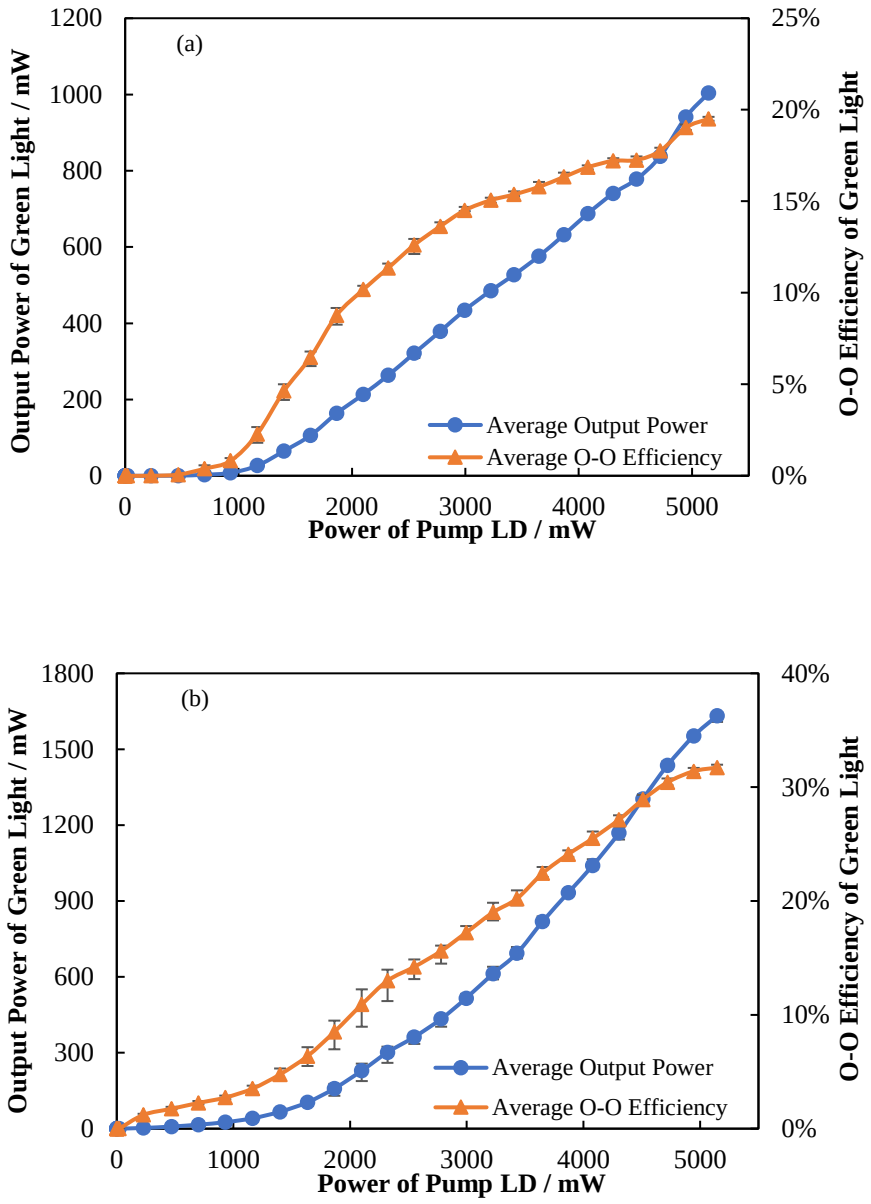

Fig. 3.4 Output power and O-O efficiency of the green lasers. (a) 542 nm green laser; (b) 543 nm green laser. The filled triangle in the figures represent the O-O efficiency, and the sold circles represent the output power.

For applications such as laser display and confocal laser microscopy, a stable output power is required. Therefore, the power stabilities of the 542 and 543 nm lasers were also studied. The collected data was analyzed according to Ref. [124], and the power instability ($Power\ Instability = \frac{2\sqrt{\frac{\sum_{i=1}^{n}(P_i-\bar{P})^2}{(n-1)}}}{\bar{P}} \times 100\ \%$) was found to be 0.46 % for 542 nm laser and 0.19 % for 543 nm laser and was measured using a thermal power meter (Thorlabs-S302C) with an integration time of 1 second. Note that the power instability measured by the thermal power meter reflects the long-term stability of the laser, which is of greater interest with regards to laser display applications. The power instabilities of 542 and 543 nm lasers were also inspected by using a fast response CCD sensor (Ocean Optics USB-2000 spectrometer, integration time was 0.01 s). The power instability was 5.2% for 542 nm laser and 2.3% for 543 nm. The power stability obtained in our experiments is comparable with the values presented in other literature about Nd:YVO_4 green lasers [72, 125, 126], further validating the suitability of our lasers for many applications. One can notice that the power stability of 543 nm is better than that of the 542 nm, which can be explained as follows: first, a chirped MgO:PPLN crystal was used for 543 nm generation, which is more resistant to the mode hoping effect on the fundamental frequency and environmental temperature fluctuations; second, to achieve the σ-polarization 542 nm emission, the OC needs to be adjusted for the suppression of lasing of the stronger π-polarization component (543 nm), this requires the OC to be slightly mis-aligned [123] from its optimal position, which has a negative effect on the power stability.

3.4 Conclusion

In this paper, watt-level efficient intra-cavity frequency doubling 542 and 543 nm DPSS lasers have been proposed and demonstrated. The lasers only consist of a Nd:YVO_4 crystal and a MgO:PPLN crystal, with the advantageous features of compact size, simple structure and low cost. The pump power dependence and the power stability at each wavelength have been studied. An O-O efficiency of 22% has been achieved for the 542 nm green laser, while an O-O efficiency of 35% was obtained for 543 nm green laser. The long-term power instability of 542 nm and 543 nm green lasers are 0.19% and 0.46%, respectively. The proposed green laser has several features including low cost, small size, high efficiency, and high stability, making them quite attractive for use in many practical applications.

Chapter 4 A 531.5 nm green laser based on Nd:$GdVO_4$ crystal[‡]

Chapter Abstract

A 531.5 nm intra-cavity frequency doubling green laser was built and tested. The laser consisted of a Nd:$GdVO_4$ crystal and a MgO:PPLN crystal. An output power as high as 1.9 W was achieved under 5 W pumping power, and the O-O efficiency was 37%. Its speckle performance was also examined by blending with a conventional 532 nm laser. Lower SCR value was achieved when the two wavelengths were blended.

[‡] *This chapter is reproduced from a poster presentation, "Bin Zhang, Qianli Ma, and Chang-qing Xu. High Efficiency Nd:$GdVO_4$/MgO:PPLNs 531.5 nm green laser.", disseminated in Photonics North Conference (May 21-23, 2019), Québec City, Québec, Canada.*

The author of this thesis is the first author and the main contributor of this publication.

4.1 Introduction

Laser speckle is still an obstacle for the commercialization of laser-based display systems. One practical solution for speckle reduction is the wavelength blending technique, in which several close wavelengths are blended together [12]. However, the Rec.2020 recommends 532 nm as the optimal green wavelength for achieving the optimal color gamut in a display system. Currently, a wavelength of 532 nm can be achieved by Nd:YVO_4 based DPSS laser through frequency doubling technique. Therefore, a green laser with an emission wavelength differ from 532 nm is needed.

Neodymium doped gadolinium vanadate (Nd:$GdVO_4$) has a lasing line at 1063 nm [84], which can be used for 531.5 nm lasing by frequency doubling techniques. The Nd:$GdVO_4$ crystal has larger absorption and emission cross section compared to neodymium-doped yttrium aluminum garnet (Nd:YAG), which is similar to neodymium doped yttrium vanadate (Nd:YVO_4). Moreover, the Nd:$GdVO_4$ also poses higher thermal conductivity than Nd:YVO_4, which decreases the thermal lensing effect within the Nd:$GdVO_4$ laser and improve the beam quality of the emitting laser beam.

To the best of our knowledge, the highest optical to optical (O-O) efficiency of a 531.5 nm Nd:$GdVO_4$ laser has been reported to be approximately 26 % [86]. It was achieved by a z-type intra-cavity configuration, and a lithium triborate (LBO) crystal which was placed inside the cavity for second harmonic generation (SHG). It should also be noted that magnesium oxide doped periodically poled lithium niobate (MgO:PPLN) has a larger

nonlinear coefficient compare to LBO. Thus, the DPSS green laser based on MgO:PPLN crystal promises smaller size and higher efficiency.

4.2 Laser configuration and performance

The configuration of an Nd:$GdVO_4$/MgO:PPLN green laser is shown in Figure 4.1. An F-mount 5 W 808 nm LD with fast axis collimate (FAC) lens was used as a pump source. An a-cut 0.5 % Nd:$GdVO_4$ crystal with dimensions of 3×3×4 mm^3 was employed as a gain medium. The input facet of the crystal has an anti-reflective coating at 808 nm and high-reflective coating at 1064 nm, while its output facet has an anti-reflective coating at 1064 nm and high reflective coating at 532 nm. A 2×2×0.5 mm^3 MgO:PPLN was used as a nonlinear crystal for converting the 1063 nm fundamental light to 531.5 nm green light, and both of its facets were coated by anti-reflective film for 532/1064 nm. A plano-concave output coupler was used to form an intra-cavity configuration with the input facet of the Nd:$GdVO_4$ crystal. The OC has radius of curvature of 100 mm and its input facet has an AR coating at 532 nm and HR coating at 1064 nm, and its output facet has an AR coating at 1064 nm.

The LD, Nd:$GdVO_4$ crystal and MgO:PPLN crystal were attached on the cold side of thermo-electric coolers (TECs) for temperature management. A power meter (Thorlabs, S302C) was used to measure the output power of the 540nm green laser. A notch filter (@1064 nm) was placed between the power meter and OC, which was used to remove the fundamental light from the output green laser. The output spectrum was collected by an

optical spectrum analyzer (OSA) (Ando, AQ6315E) and is shown in Figure 4.2. The setting resolution of the OSA is 0.1 nm and the measured linewidth of the green laser is 0.13 nm. The beam profile was also investigated by a beam profile analyzer (), several natural density (ND) filters were employed to reduce the laser power to fit the measurement limit of the beam profiler. The temperature tuning characteristics of the MgO:PPLN crystal are shown in Figure 4.3. Figure 4.4 shows the output power performance of the 531.5 nm laser and the corresponding O-O efficiency. As high as 1.9 W output green power was achieved with the O-O efficiency of 37 %, those results are comparable with the results we got from the conventional Nd:YVO_4/MgO:PPLN 532 nm green laser. It is worth noting that this is the highest O-O efficiency achieved so far for 531.5 nm Nd:$GdVO_4$ based green laser by using bulk laser materials.

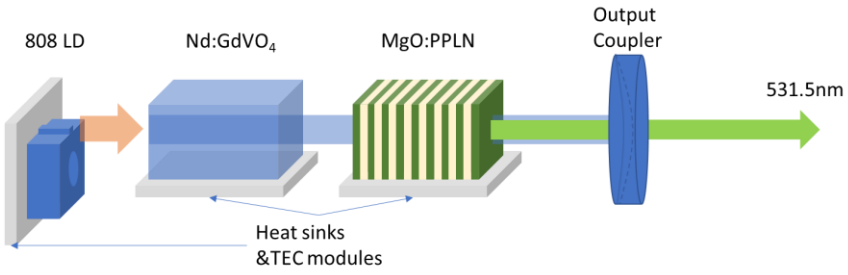

Fig. 4.1 Schematic diagram of the Nd:YAP/LBO green laser.

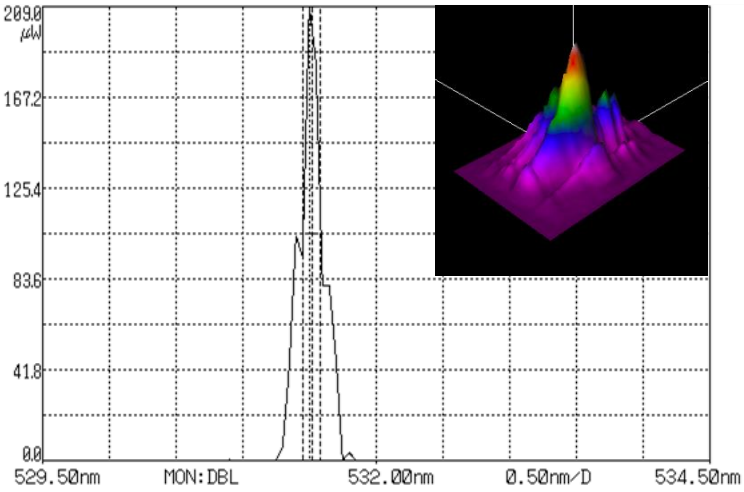

Fig. 4.2 Output spectrum of Nd:$GdVO_4$/MgO:PPLN green laser versus pump power of LD. (up-right: beam profile of 531.5 nm laser)

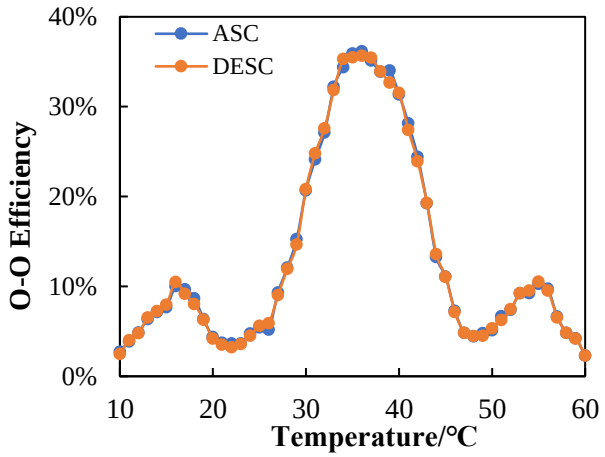

Fig. 4.3 temperature tuning curve of MgO:PPLN crystal. (The temperature tuning curves were measured by ascending and descending direction for collecting accurate temperature performance)

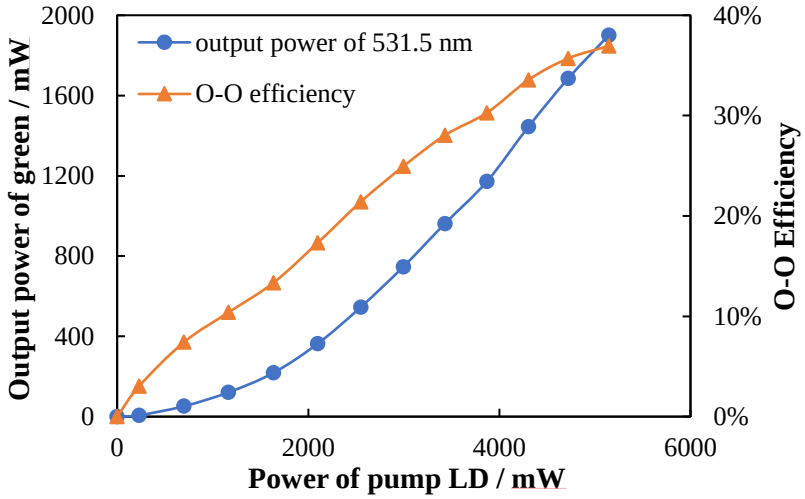

Fig. 4.4 Output power and O-O efficiency of Nd:$GdVO_4$/MgO:PPLN 531.5 nm laser.

4.3 Speckle measurement via wavelength blending technique

A schematic diagram of our proposed system for SCR measurement is shown in Figure 4.5. A 531.5 nm Nd:$GdVO_4$/MgO:PPLN laser with a linewidth of around 0.2 nm and a 532 nm Nd:YVO4/MgO:PPLN DPSS laser with a linewidth of 0.2nm were used in our system as light sources. Both lasers were coupled into a 2-in-1 multimode fiber with a length of 2 m (core diameter = 800 um). A diffuser with 24° divergence angle was fixed on the top of a voice coil motor (VCM) which was placed after the exit port of multimode fiber bundle. The VCM was driven by a function generator to vibrate the diffuser with a frequency of 60 Hz. The light passed through the diffuser and entered an 18cm hexagonal light pipe with a 1 cm aperture. Then the output green light from the light pipe was cast upon a depolarized

screen by a projection lens. A scientific camera was used to capture images which displayed laser speckle. The frame rate of the camera was set to 15 fps. The camera lens on the scientific camera had a focal length of 50 mm and F/16, which makes the aperture of the camera lens have an almost identical diameter to the human iris in a real projection environment. Figure 4.6 shows the captured speckle images which were projected on the screen. The results show that the combination of 531.5 nm and 532 nm has the lower SCR value than single wavelength cases, which prove the feasibility of the wavelength blending technique.

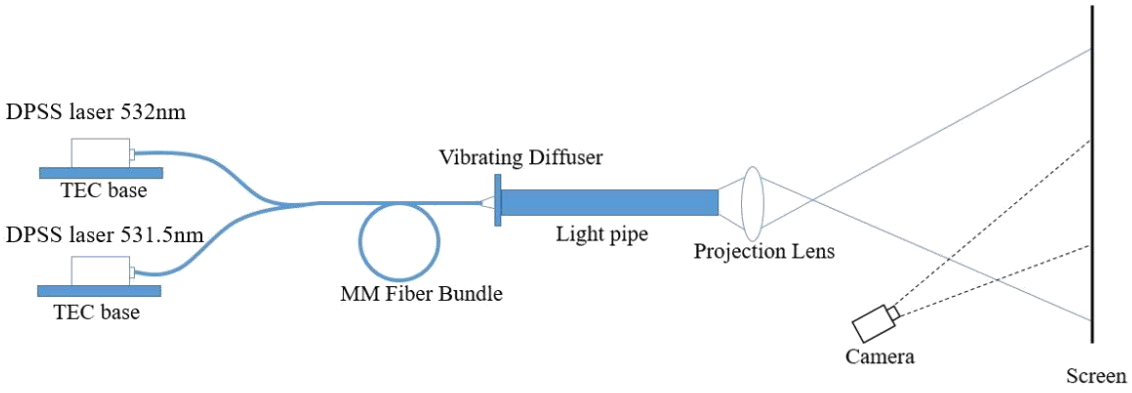

Fig. 4.5 Schematic diagram of the SCR measurement system

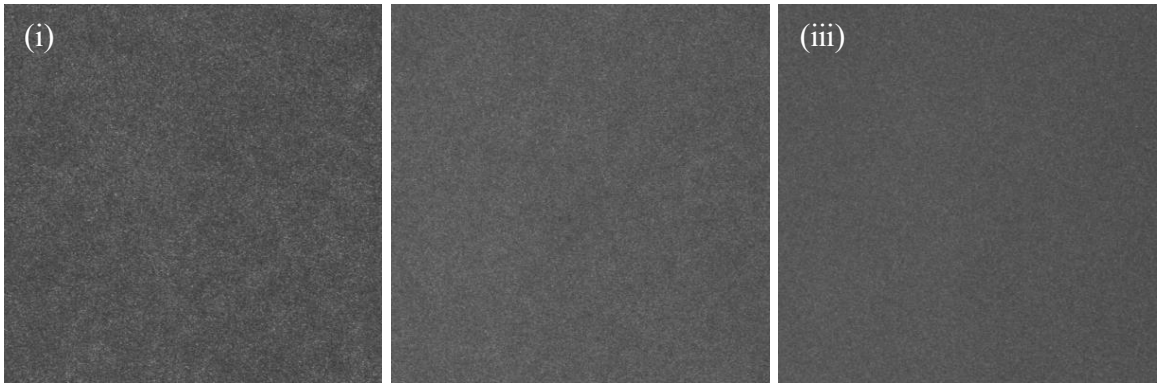

Fig. 4.6 Captured speckle patterns of different light sources. (i) 532 nm, SCR=7.85%; (ii) 531.5 nm, SCR=6.69%; (iii) 531.5 nm + 532 nm, SCR=5.94%.

4.4 Conclusion

A compact and efficient Nd:$GdVO_4$/MgO:PPLN intra-cavity frequency doubling 531.5 nm green laser was proposed and demonstrated. An O-O efficiency of 37% was achieved with 5 W pump power, which is the highest O-O efficiency achieved so far for a 531.5 nm laser which are based on bulk crystals. Speckle performance of the green laser has also been studied by our own speckle measurement system, it was found that a lower SCR value was achieved by blending 531.5 nm and 532 nm lasers together.

Chapter 5 A 540 nm green laser based on Nd:YAP crystal[§]

Chapter Abstract

A 540 nm intra-cavity frequency doubling green laser was built and tested. The laser consisted of a Nd:YAP crystal and a LBO crystal. An output power of 0.8 W was achieved under 4 W pumping power, and the O-O efficiency was 20 %. Its speckle performance was also inspected by blending with the conventional 532 nm laser. Lower SCR value was achieved in the case of two wavelengths blended together.

[§] *This chapter is reproduced from a poster presentation, "Bin Zhang, Qianli Ma, and Chang-qing Xu. Intra-cavity frequency doubling Nd:YAP/LBO 540 nm green laser for laser display", disseminated in Photonics North Conference (May 21-23, 2019), Québec City, Québec, Canada.*

The author of this thesis is the first author and the main contributor of this publication

5.1 Introduction

Lasers are considered as the most promising light sources for projection applications due to their long lifetime, high brightness and vivid color. However, speckle problem is still an obstacle for extensive commercialization of laser-based displays. So far, a lot of efforts have been made to reduce the speckle contrast ratio (SCR) [5-9], and those de-speckle methods are based on increasing the spatial and wavelength diversity. On the other hand, there is a limit for speckle reduction by only improving the spatial diversity in an optical system [6]. Therefore, the improvement of wavelength diversity is necessary for further SCR reduction [9, 13, 14], and wavelength blending is a popular technique for increasing the wavelength diversity.

At present, the 532 nm diode pumped solid state (DPSS) lasers and ~520 nm GaN based laser diodes (LDs) are widely used in laser projection systems to provide green color. From a color gamut and wavelength diversity point of view, a green laser with longer wavelength (~540nm) is needed to achieve the optimal green color. The Nd^{3+} doped yttrium aluminium perovskite (Nd:YAP) crystal has spectral lines at 1073nm, 1079nm and 1084nm [58], so it is a suitable gain medium for generating ~540nm green laser via frequency doubling process. Currently, only a few of articles studied the characteristics of an Nd:YAP based frequency doubling laser [79,80,130].

For laser projection applications, the laser sources must be efficient and compact, but the reported Nd:YAP green lasers [79,80] cannot meet those requirements. For example, Ref [80] reported a high power Nd:YAP based green laser with 23% O-O efficiency, but

its cavity length is ~ 70 cm. Therefore, it is necessary to develop a compact and efficient Nd:YAP based green laser which is suitable for laser projectors.

In this chapter, a compact Nd:YAP/LBO based intra-cavity frequency doubling laser was proposed and demonstrated. The speckle reduction performance was also measured and analyzed by our proposed speckle reduction system.

5.2 Laser configuration and experiments

5.2.1 Structure of Nd:YAP/LBO intracavity green laser

The configuration of the green laser is shown in Figure 5.1. A 5W 803 nm LD (Focuslight, Inc) was used as the pump source. A focusing lens was employed to converge the pump beam for increased power density of the pump light. A plano-parallel input mirror and a plano-parallel output mirror were used to form a resonator. The input side of the output mirror (M2) had a radius of curvature of -100 mm and was coated HR @ 1064 nm and high transmissive (HT) @ 532 nm, while the output side of M2 is a Plano surface with HT coating @ 532 nm. A b-cut Nd:YAP crystal with dimensions 3×3×20 mm^3 was used as the gain material. Both facets of the Nd:YAP crystal were coated with AR coating at 1080 nm. The laser crystals and the input mirror (M1) are same as used in above section. An LBO crystal was inserted between the Nd:YAP crystal and output mirror (M2) for frequency doubling purposes. The dimensions of the LBO crystal were 2×2×10mm, and both sides were coated with AR @ 540nm. The temperature of the LBO crystal was finely adjusted and the crystal itself was finely tilted to meet the phase matching condition for achieving

the optimal conversion efficiency. For temperature management, the LD, Nd:YAP crystal and LBO crystal were attached on the cold side of thermo-electric coolers (TECs), respectively. A power meter (Thorlabs Inc, S302C) was used to measure the output power of 540 nm green laser. A notch filter (@1064 nm) was placed between power meter and M2, which was used to remove the fundamental light from the output green laser.

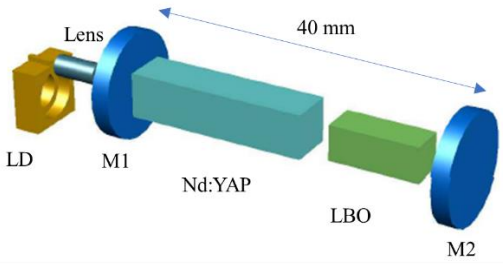

Fig. 5.1 Schematic configuration of Nd:YAP/LBO green Laser

5.2.2 Experimental Results of Nd:YAP/LBO Green Laser

To achieve the best performance of the green laser, the operation temperature of LBO was kept at 13℃ to meet the phase matching condition. In the meantime, the temperature of Nd:YAP and LD were kept at 19℃ and 26℃, respectively. Figure 5.2 shows the green output power as a function of pump power. The maximum output power is 0.8 W which corresponds to an O-O efficiency of 20%. The output spectrum of green laser is shown in Fig. 5.3 with center wavelength of 539.8 nm and 0.2 nm linewidth. One can see that there

is a small peak (538.1 nm) on the left side of the 540 nm, this is due to the sum-frequency generation (SFM) process of 1073 nm and 1080 nm.

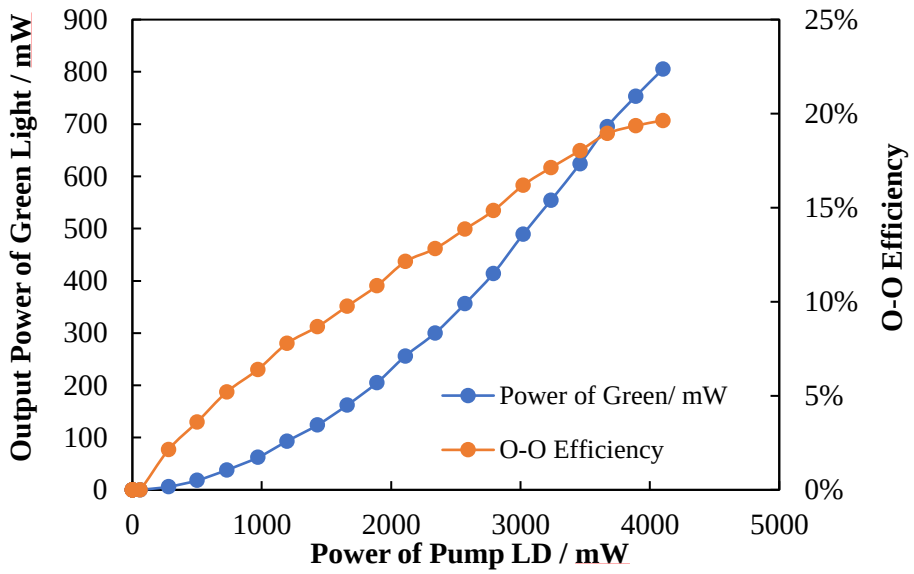

Fig. 5.2 Output power of green laser versus pump power of LD.

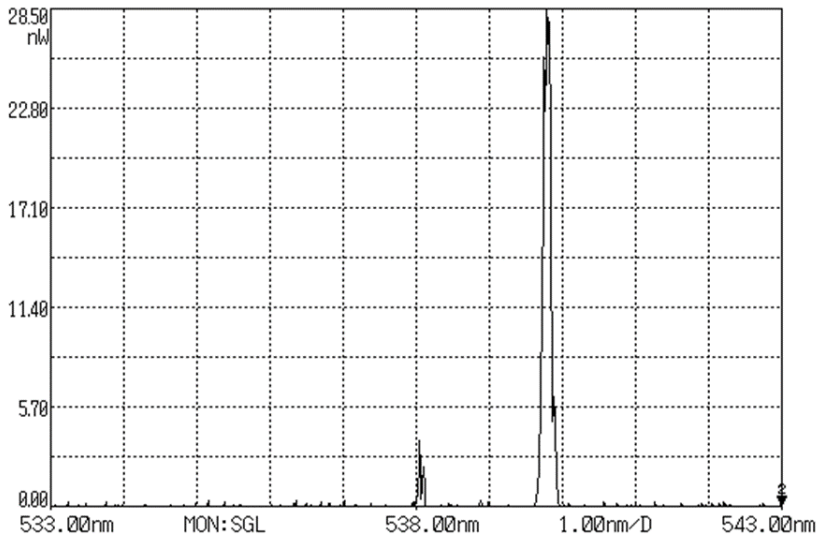

Fig. 5.3 Output spectrum of Nd:YAP/LBO green Laser

5.3 Speckle reduction measurement

A schematic diagram of our proposed system for SCR measurement was shown in Figure 5.4. Two different types of green lasers with different wavelengths were used in our system as light sources, i.e., a 540 nm Nd:YAP/LBO Laser with a linewidth of around 0.2 nm, and a 532 nm Nd:YVO_4/MgO:PPLN DPSS Laser (CQ Laser Technologies Co., Ltd.) with a linewidth of 0.2 nm. Those two laser beams were coupled into a 2-in-1 multimode fiber with a length of 2 m. A diffuser (divergence angle = 24 °) fixed on the top of a voice coil motor (VCM) was placed after the exit port of multimode fiber bundle. Then the VCM was connected to a function generator, and a 10 V-1 kHz sinusoidal signal was applied on the VCM to quickly move the diffuser up and down. The green lasers passed through the diffuser then entered into an 18cm hexagonal light pipe with 1 cm aperture. Then the output green light from the light pipe was casted on a depolarized screen by a projection lens. A scientific camera (Thorlabs, DCU-224M-GL) was used to capture speckle images, and all the speckle images were transmitted to a computer for calculation and analysis.

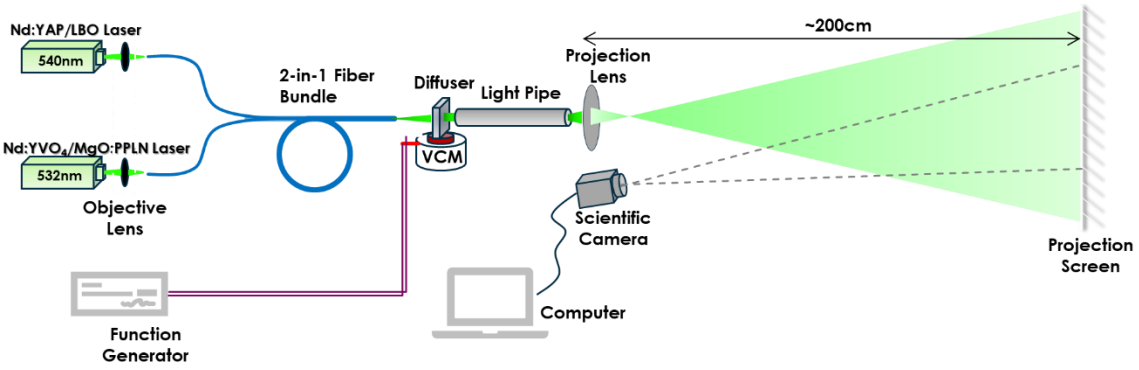

Fig. 5.4 Experimental setup for SCR measurement.

The speckle images with single wavelength and dual-wavelength (532 nm & 540 nm) are shown in Figure 5.5. An SCR value as low as 3.93% was achieved by combining the 532 nm and 540 nm laser together. Since there is a small wavelength peak beside the 540 nm of the Nd:YAP laser, the SCR value of the 540 nm laser was lower than 532 nm laser.

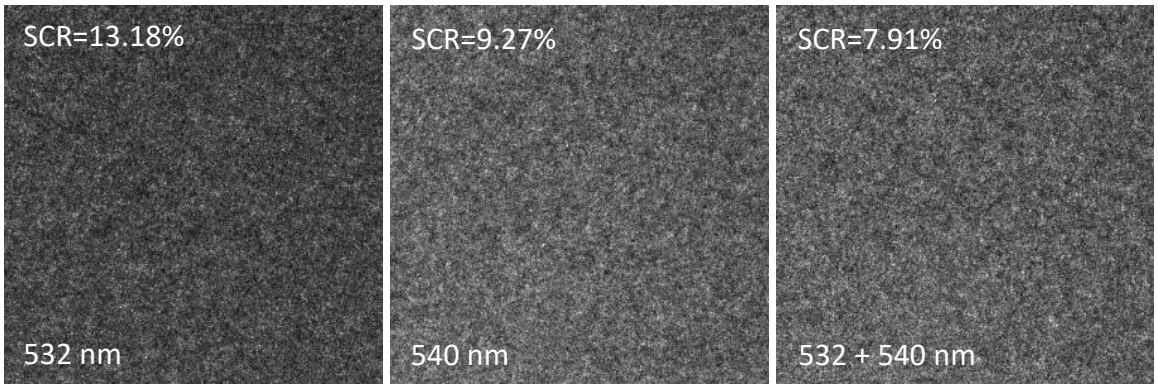

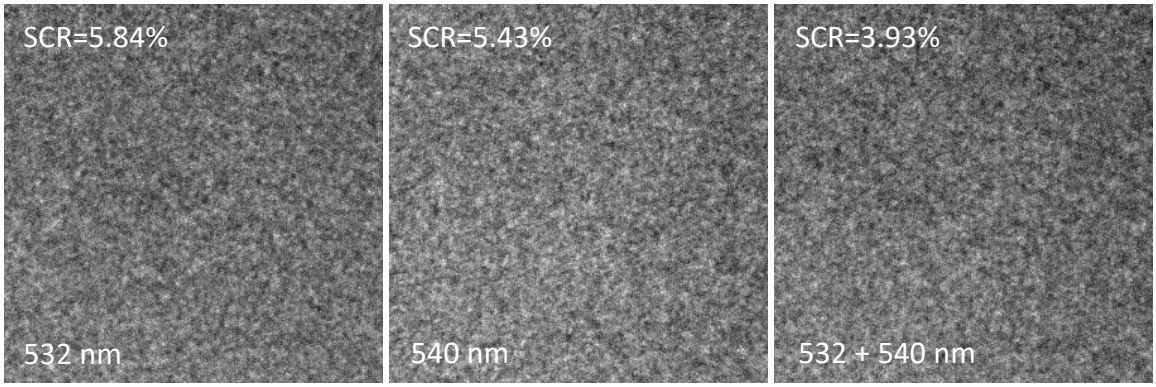

Fig. 5.5 The captured speckle images and theirs corresponding SCR value. (upper sub-figures: captured speckle images without vibration of diffuser; lower sub-figures: captured speckle images with vibration of diffuser.)

5.4 Conclusion

An Nd:YAP based DPSS infrared laser was demonstrated and tested. Its wavelength tuning properties were studied by adjusting the angle of the etalon inside the cavity. Furthermore, a compact and efficient Nd:YAP/LBO intra-cavity frequency doubling 540 nm green laser was built and tested. 800 mW output power was achieved under 4 W pump power with an O-O efficiency of 20%. Speckle performance of the green laser had also been studied. The SCR of 532 nm, 540 nm, and 532 nm+540 nm was measured by our speckle testing system. Lower SCR value was achieved by blending 532 nm and 540 nm lasers together.

Chapter 6 Dual-wavelength Nd:YVO_4/MgO:PPLN green laser for speckle reduction[**]

Chapter Abstract

An orthogonally polarized dual-wavelength laser emitting at 542 nm and 543 nm was proposed and demonstrated. The laser was based on a single Nd:YVO_4 crystal and two MgO:PPLN crystals. An optical-to-optical (O-O) efficiency as high as 15.3% was achieved when the powers of the two emission wavelengths were equal. The long-term power stability was 4.5% for 542 nm and 3.5% for 543 nm, respectively. The Laser speckle contrast ratio (SCR) was also measured as a function of power ratio of the two emission wavelengths. The measured SCR values agreed with theoretical simulations with a difference less than 5 %.

[**] *This chapter is reproduced from a journal article "**Bin Zhang**, Qianli Ma, and Chang-Qing Xu. Orthogonally polarized dual-wavelength Nd:YVO_4/MgO:PPLN intra-cavity frequency doubling green laser. Optics & Laser Technology 125 (2020): 106005", doi: https://doi.org/10.1016/j.optlastec.2019.106005. Reproduced with permission from Opt. Laser Technol., Copyright © 2019 Elsevier Ltd.*

The author of this thesis is the first author and the main contributor of this publication.

6.1 Introduction

Orthogonally polarized dual-wavelength lasers have attracted much attention in past years due to their many applications, such as speckle reduction [6], terahertz generation via type-II difference frequency generation (DFG) [131], and heterodyne interferometry [98]. There are two main methods used to create dual-wavelength lasers. One is to use two gain media with each gain medium generating one wavelength [132]; another method is to utilize the multiple transition lines from a single gain medium [91]. The first method demonstrates better power stability as there is no mode competition between the transition lines. However, the use of two laser gain media requires more space than a single laser crystal configuration and presents challenges when attempting to achieve optimal alignment. On the other hand, in the second method, the two transition lines typically share the same upper energy state, which causes serious mode competition between the two emission wavelengths. Thus, customized output couplers [90], a wavelength selection element [89] (e.g. etalon), and the birefringent effect [91] are typically used to balance the gain and losses of the two wavelengths in the single gain medium configuration. However, the additional components may result in unnecessary losses and increases the size and complexity of the overall laser system.

To date, most of the reported dual-wavelength lasers emit infrared light [88-91,132,133], but only a few of the reports [14, 92, 134] discussed dual-wavelength lasers in the visible regime. The optical-to-optical (O-O) efficiencies reported in those papers were low. So far, to the best of our knowledge, the highest reported O-O efficiency of a dual-wavelength visible laser at the balanced point (when the power ratio between two wavelengths is 1:1)

was about 6 % [134] and it was achieved under pulsed mode operation. The costs of the reported dual-wavelength lasers are high as a result of immature laser materials [14], low-efficiency frequency doubling crystals, Q-switch elements [134] and pulsed pumping lasers [92] being used in those lasers.

For many applications, orthogonally polarized dual-wavelength green lasers with high efficiency, small size, and low cost are in high demand. For example, it is necessary to reduce the cost, size and power consumption of green lasers used in display systems. It is expected that dual-wavelength emission can also reduce the laser speckle noise [6], which is crucial to display, laser ranging, and biomedical applications. Furthermore, for applications such as heterodyne interferometry, a compact dual-wavelength visible laser with orthogonal polarization and large wavelength difference is needed [135] [136]. At present, the most practical orthogonally polarized dual-wavelength visible laser is a helium neon (He-Ne) Zeman laser [136]. However, the power of the He-Ne Zeman laser is too low, and the frequency difference is too small. Therefore, an orthogonally polarized dual-wavelength visible laser with high output power, compact size, larger wavelength difference and low cost is needed. Neodymium-doped yttrium vanadate (Nd:YVO_4) is a competitive candidate to achieve orthogonally polarized dual-wavelength lasing. Due to its high efficiency and low cost, the Nd:YVO_4 crystal has been widely used in laser systems to generate infrared light or visible light via the frequency doubling technique. The spectroscopic study of Nd:YVO_4 shows that it has two adjacent transition lines with orthogonal polarization [89][121]: 1084nm in σ-polarization and 1086nm in π-polarization.

Those two transition lines have close emission cross sections, which makes the Nd:YVO_4 crystal suitable for achieving simultaneous dual-wavelength emission.

In this paper a compact, efficient, low cost and stable orthogonally polarized dual-wavelength solid state green laser is proposed and demonstrated. This laser was built on a single Nd:YVO_4 crystal and two magnesium doped periodically poled lithium niobate (MgO:PPLN) crystals. The output power and power stability of the dual-wavelength laser were studied. The speckle noise of the dual-wavelength laser was also investigated.

6.2 Configuration of the orthogonally polarized dual-wavelength green laser

Fig. 6.1 shows a schematic diagram of the proposed intra-cavity frequency doubling Nd:YVO_4/MgO:PPLNs green laser. A 5 W 808 nm F-mount laser diode (LD) with a fast axis collimator (FAC) was used as a pump source. A 0.25 Pitch Grin lens was used to further converge the pump beam. An a-cut 0.5 at%, 3×3×5 mm^3 Nd:YVO_4 crystal was used as a gain medium. The input facet of the Nd:YVO_4 crystal had a high reflection (HR) coating centered at 532 nm and 1064 nm and a high transmittance (HT) coating at 808 nm, while its output facet had an anti-reflection (AR) coating at 532 nm and 1064 nm. Both Nd:YVO_4 crystal and LD were placed in specialized copper holders, and the two holders were attached on the cold sides of two thermal electronic coolers (TECs). Two 0.5×2×2 mm^3 MgO:PPLN crystals were used as frequency doubling elements with AR coatings on all of the facets at 532 nm and 1064 nm. The two MgO:PPLN crystals were placed orthogonally with respect to each other. The first MgO:PPLN crystal converted the 1084

nm fundamental light to 542 nm, while the second MgO:PPLN crystal was used to generate 543nm green light from the 1086 nm fundamental light. These two nonlinear crystals were placed on two separate copper jigs. Two TECs were attached on those jigs to control the temperature of the MgO:PPLN crystals to meet their quasi-phase matching conditions. An $R_{\text{(radius of the concave surface)}}$ = -50 mm plano-concave mirror was used as the output coupler (OC). Since 1084 nm and 1086 nm are two weak transition lines in the Nd:YVO_4 crystal, a special customized coating is needed to suppress the lasing of other transition lines, and the transmittance curve of the OC is shown in Fig. 6.2. The input facet of the OC had an HR coating at 1084/1086 nm, and an HT coating at 542/543 nm, 914 nm, 1064 nm and 1342 nm. It is worth noting that the measured transmittance of the OC at 542/543 nm is approximately 90%, due to the difficulties of coating design and fabrication. The output facet of the OC had a typical AR coating designed for green light. The green laser beam emitted from the OC was then passed through a polarization beam splitter (PBS), in which the AR coating on its facets was designed for 670-1064nm. Therefore, the power loss at the PBS will be considered in our calculation of the O-O efficiency as well. An IR filter was placed after the OC, which was used to remove the leaking fundamental light from the green laser. Two power meters were placed after the PBS to collect the refracted power. Power meter 1 was used to collect the power of the 543 nm π-polarization light, while power meter 2 measured the power of the 542nm σ-polarization green beam.

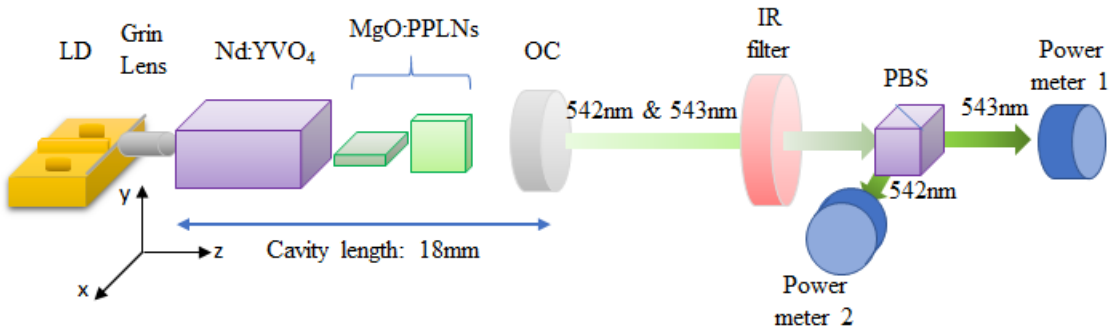

Fig. 6.1 A schematic experimental setup for testing the proposed orthogonally polarized dual-wavelength green laser.

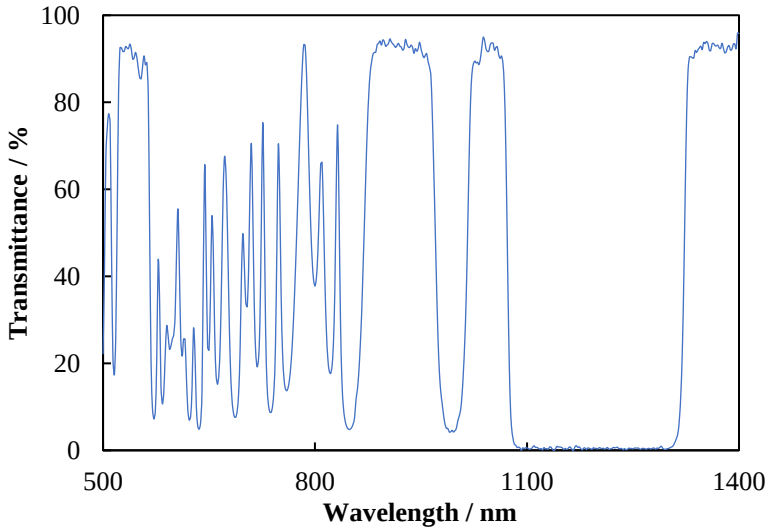

Fig. 6.2 The transmittance curve of the OC.

6.3 Experimental results and discussion

In 2002, Ram Oron et. al. studied orthogonally polarized emission in a single gain medium by manipulating the transverse modes [137]. In 2011, Florent Pallas et. al. [123] reported that dual-wavelength emission was achieved by tilting the output mirror for an a-cut neodymium: gadolinium vanadate (Nd:$GdVO_4$) laser. M. T. Chang et. al. had explored the transverse modes in a monolithic Yb:KGW laser [138], in which different polarization components had different transverse modes. We also found it is possible to maintain stable and efficient dual-wavelength lasing by carefully controlling the modes inside the cavity via our experiments. If the two polarization (or) wavelength components have different (higher order) transverse modes and the two modes have less spatial overlap, the mode competition between 1084 nm and 1086 nm transition lines would not be critical which is beneficial for simultaneous dual-wavelength emission. In our experiment, the OC was carefully adjusted along the x and y direction to achieve a specific cavity condition in which it is favourable for two orthogonally polarized transverse/longitudinal modes to oscillate for both fundamental wavelengths and green wavelengths. The output spectrum (normalization factor = 0.5189) of the orthogonally polarized dual-wavelength green laser is shown in Fig. 6.3. An optical spectrum analyzer (Ando, AQ6315E) was used to measure the spectrum with a resolution of 0.1 nm.

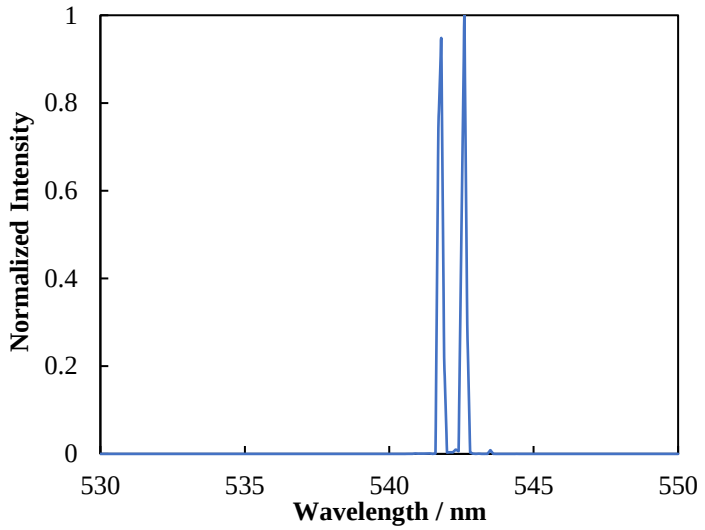

Fig. 6.3 Normalized output spectrum of the orthogonally polarized dual-wavelength green laser. The inset shows details of the 542 nm and 543 nm.

The output power of the green laser is shown in Fig. 6.4. The output power at 542 nm and 543 nm increased with increasing pump power up to the pump power exceeded 3.65 W. Afterwards, the output power of the 542 nm wavelength began to saturate while the power at 543 nm continued to increase. This is mainly due to the fact that the emission cross section of 543 nm is slightly higher than that of 542 nm [89], thus the 543 nm wavelength dominated lasing in the high pump power region.

Since most of the previously discussed applications need a dual-wavelength laser that can emit stable and equal power at both wavelengths, the output performance of a laser at the balanced point is more interesting. The output powers of 542 nm (σ-polarization) and 543 nm (π-polarization) of the developed green laser at the balance point (pump power =

3.65W) were 220 mW and 228 mW, respectively. After compensating for the losses from the OC and PBS, the overall O-O efficiency was 15.3% at the balance point.

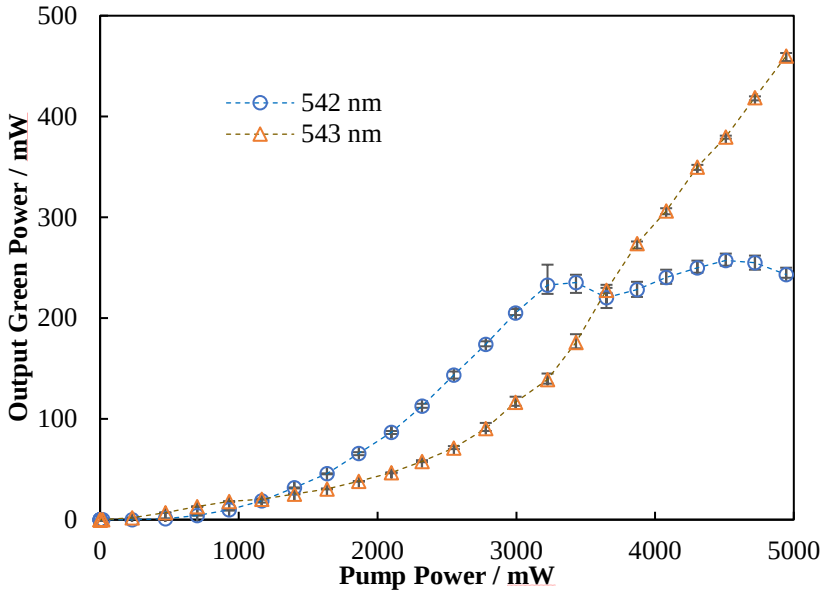

Fig. 6.4 Output power of the orthogonally polarized dual-wavelength green laser.

For applications such as heterodyne interferometry, laser displays, and terahertz generation, a stable output power is needed. Therefore, the power stability of each wavelength at the balance point was measured. Fig. 6.5 shows the measured power fluctuation at 542 nm and 543 nm for 1 hour. The power stabilities of the 542 and 543 nm lasers were inspected using a fast response CCD sensor (Ocean Optics USB-2000 spectrometer, integration time was 0.01 s, time interval was 1 s). The collected data was

analyzed according to literature [124], and the power stability ($Power\ stability = \frac{2\sqrt{\frac{\sum_{i=1}^{n}(P_i-\bar{P})^2}{(n-1)}}}{\bar{P}} \times 100\ \%$) was 4.5% for 542nm and 3.5% for 543nm.

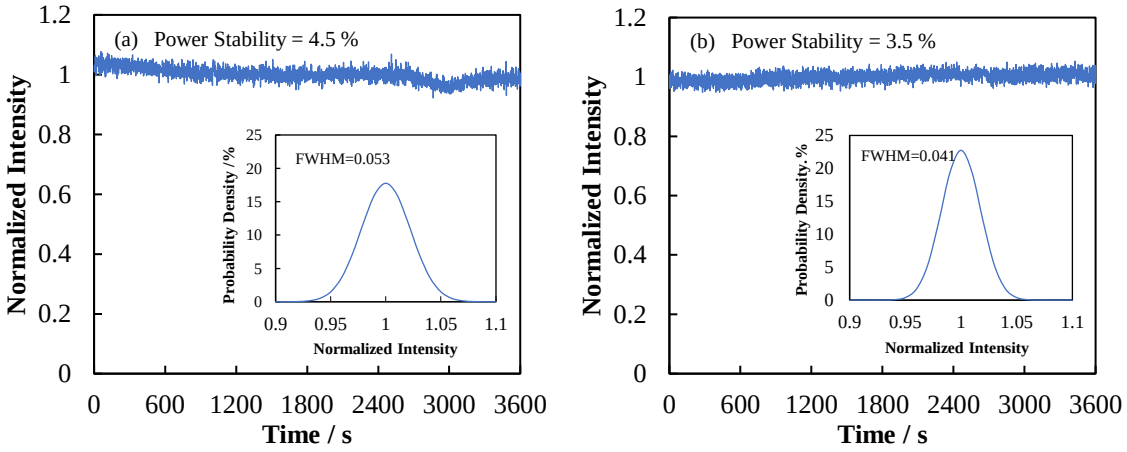

Fig. 6.5 Intensity (power) fluctuations of the542 nm and 543 nm components of the orthogonally polarized dual-wavelength green laser. (a) The intensity fluctuations of 542 nm, and the insert shows the normal distribution of the intensity; (b) the intensity fluctuations of 543 nm, and the insert shows the normal distribution of the intensity.

6.4 Speckle contrast ratio (SCR) measurement of the green laser

One important motivation for developing dual-wavelength green lasers is to reduce the laser speckle for display systems. Laser speckle is still an obstacle for the commercialization of laser-based display systems. One practical solution for speckle reduction is the wavelength blending technique, in which several close wavelengths are

blended together. This is due to the fact that emissions at different wavelengths could potentially generate different speckle patterns, meaning they could overlap with each other and provide a low speckle light field. In terms of simplicity and cost, a single dual (multi) -wavelength laser has more advantages than blending wavelengths from separate lasers.

In this paper, the SCR value of the green laser was measured by experimental setup shown in Fig. 6.6. The output laser beam was coupled into a 600 nm core diameter multimode fiber with a length of 2 m. A diffuser with a divergence angle of 24° which was fixed on the top of a voice coil motor (VCM) which was placed after the exit port of the fiber. The VCM was connected to a function generator, and a 5 V-60 Hz sinusoidal signal was applied on the VCM to vibrate the diffuser. The green laser passed through the diffuser then entered an 18 cm hexagonal light pipe with 1 cm aperture. The output green light from the light pipe was projected onto a depolarized screen via a projection lens. A camera (Thorlabs, DCU-224M-GL) was used to capture the speckle images. The frame rate of the camera was set to 15 fps. The lens on the camera had a focal length of 50 mm and F/16, which makes the diameter of the camera lens aperture nearly identical to that of the human iris in a real projection environment [139].

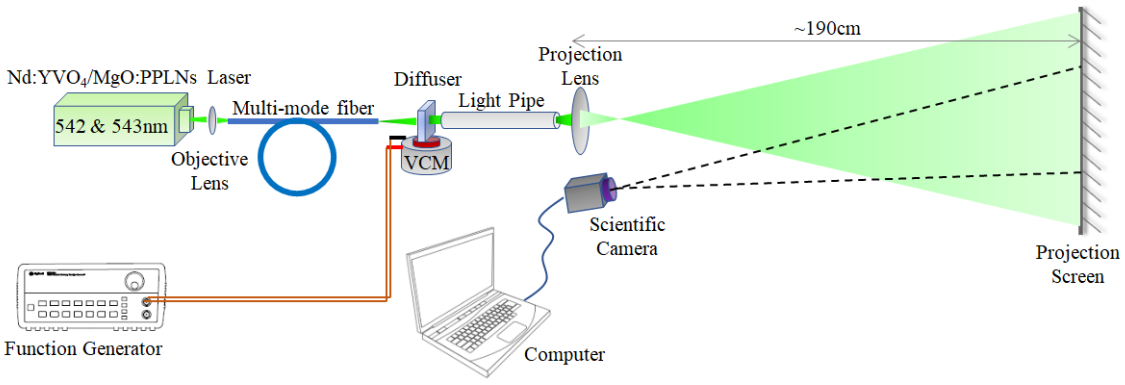

Fig. 6.6 Schematic diagram of the SCR measurement system.

By slightly varying the x-y position of the OC, different power ratios between the two green wavelengths can be achieved. In the speckle test, the speckle contrast ratio (SCR) with varying power ratios was studied. The SCR was sampled at five different power ratio points, 1:0, 2:1, 1:1, 1:2, and 0:1. The experimental results at those five power ratio points are depicted by dots in Fig. 6. In Fig. 6, the x-axis represents the power ratio between two green wavelengths, “0” means pure 542 nm, while “1” means pure 543 nm; “0.5” means their power ratio is 1:1; “1/3” and “2/3” means their power ratio is 1:2 and 2:1, respectively. Fig. 6 shows that the lowest value of SCR was achieved when the power ratio is 1:1, while pure single wavelength green light had the highest SCR value. The dashed line shows the simulation values which were derived from a theoretical model [12]. The right end of the simulation curve was set equal to the measured SCR value for offsetting the speckle reduction effect caused by all other techniques (vibrating diffuser, multi-mode fiber, light pipe and de-polarized screen). Thus, the changing of the simulated SCR value as a function

of the power ratio is only related to the wavelength diversity. One can see that the experimental results agree with the theoretical values as shown in Fig. 6.7.

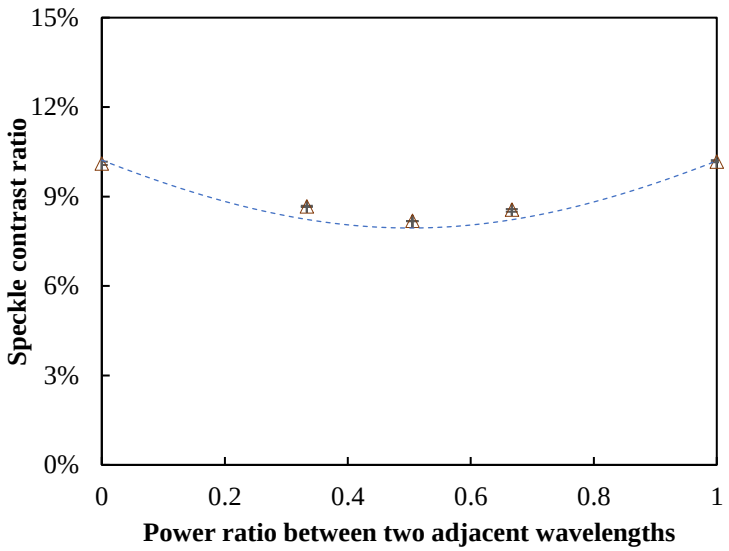

Fig. 6.7 Experimental and theoretical SCR variation with the changing of the power ratio between the two wavelengths of the green laser.

6.5 Conclusion

In this paper, an orthogonally polarized dual-wavelength diode pumped solid state (DPSS) green laser has been proposed and demonstrated. The laser consisted of an Nd:YVO_4 crystal and two MgO:PPLN crystals, which featured small size and low cost. The laser can emit two green wavelengths at 542 nm (σ-polarization) and 543 nm (π-polarization) simultaneously. The pump power dependence and the power stability of each wavelength was also studied. An O-O efficiency of 15.3% has been achieved for the green

laser at the balance point. The power stability of 542 nm and 543 nm were 3.5% and 4.5%, respectively. The speckle reduction of the dual-wavelength green laser was studied as well. It has been shown that the lowest SCR value was achieved when the output powers of 542 nm and 543 nm were equal, which agrees with theoretical simulations. It is worth noting that the proposed green laser is based on mature laser components and a simple laser structure, and no additional elements are used to balance the lasing wavelengths. These principles ensure that the proposed green laser maintains low cost, small size, high efficiency, and high stability, which makes it attractive for use in many applications.

Chapter 7 Multi-wavelength blending for speckle reduction and color improvement[††]

Chapter abstract

A novel three wavelength blending speckle reduction method was studied. The 543 nm laser was added into the wavelength blending method described in Chapter 1 for further speckle reduction and color improvement. The green laser source includes wavelengths of 523 nm, 532 nm and 543 nm. As low as 3.3% speckle contrast ratio was achieved where the power ratio of 523 nm, 532 nm and 543 nm are equal to 4:1:1. The affect on the color gamut after the use of tri-wavelength blending method was investigated. The simulation results show that the use of three wavelength blending method can offer better color gamut than those using a single and two green lasers.

[††] *This chapter is reproduced from an original paper pending for submission "**Bin Zhang**, Qianli Ma, and Chang-Qing Xu. Study of multi-wavelength blending for speckle reduction and color improvement."*

The author of this thesis is the main contributor of this work and will be the first author of this article.

7.1 Introduction

Based on the outstanding features of the lasers, such as high brightness, long lifetime, higher energy efficiency and vivid color, laser-based display systems had attracted a lot of attentions from researchers and industrial community. Currently, one of the main obstacles which prevents the further commercialization of laser projections systems is the obvious speckle noise caused by the high coherence of the laser light sources. However, a lot of efforts had been made to reduce the speckle noise in a laser display system [3-9, 11-13]. Among them, the spatial (angle and polarization) diversification and wavelength (spectral) diversification are two popular methods which had been widely used. But the theoretical limitation of the spatial diversification method prevents it to be the sufficient de-speckle solution [6]. Consequently, the wavelength blending method (an important sub-discipline of wavelength diversification method) start to get more attention recently [9, 11-13]. The wavelength blending method is a type of wavelength hybrid in which several distinct wavelengths are combined into a single laser source, so the wavelength diversity could be increased.

In a laser display system, three primary color sources (red, green and blue) are essential for generating full color images. Some conventional laser projectors use the R/G/B laser diodes as the light sources instead of the diode pumped solid state (DPSS) lasers, since the LDs typically have larger spectral linewidth (multiple longitude modes) and posses more homogenous beam profile than DPSS lasers. However, the popular Rec. 2020 standard

requires that the center wavelength for a display system should be at 630 nm, 532 nm and 467 nm for R/G/B color, respectively. Though current commercial LDs already cover the red and blue wavelengths which are recommended by the Rec. 2020, the wavelength of conventional green LDs is still in the range of 510-520 nm, which is shorter than the green wavelength recommended by Rec. 2020. Shorter green wavelength could deteriorate the overall color performance of a display system, especially yellow color area may not be covered if the wavelength of green laser is too short.

In addition, though the green LDs have better speckle performance than the conventional green DPSS lasers, its SCR value is not low enough since green is the most sensitive color to human eyes. A lot of efforts had been made to further reduce the speckle contrast ratio (SCR) of green LDs, but color problem has not been touched until 2017 [12]. Ma. et all first discussed the wavelength blending method by combining a 532 nm DPSS laser and a green LD for color improvement, and it is also demonstrated that lower SCR was achieved. However, the center wavelength of the proposed wavelength blending method was still shorter than 532 nm, which implies that a green laser with longer wavelength (> 532 nm) is needed to pull the overall color gamut to the yellow regime. In 2020, we firstly demonstrated an efficient and compact watt-level 543 nm laser based on conventional Nd:YVO_4/MgO:PPLN crystals [140]. That wavelength is an ideal candidate which could be used in three green wavelengths blending for reducing the speckle and improving the color. Ideally, with the utilization of three uniformly distributed green wavelengths, better coverage of Rec. 2020 should be expected, and low SCR value can be achieved.

In this paper, a novel tri-wavelength blending method for speckle reduction and color improvement is studied. Three green lasers with distinct wavelengths are going to be used, the speckle performance will be evaluated by our own speckle test platform, and its color performance is studied as well.

7.2 Experiment and Analysis

7.2.1 Tri-wavelength blending speckle measurement

Three different green lasers are used in our experiment. An ~520 nm green LD (NDG7475, Nichia Corp.), a 532 nm DPSS green laser and 543 nm DPSS laser. The spectrums of each laser system are shown in Fig. 7.1.

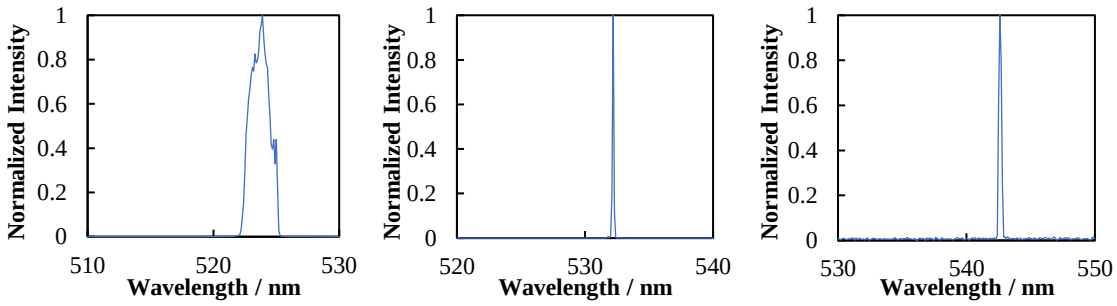

Fig. 7.1 Output spectrum of a green laser diode, 532 nm DPSS laser, and a 543 nm lab made DPSS laser.

Fig. 7.2 shows our speckle test setup. All the lasers are coupled into a 3 in 1 multi-mode fiber with a core diameter of 200 um. The length of fiber is 1.5 m, and the its output side was pointed at a diffuser with a divergence angle of 24°. The diffuser was fixed on a voice coil motor (VCM), and a square wave signal was applied on the VCM to vibrate the diffuser up and down. The frequency of input signal is 60 Hz and the applied voltage is 7 V (peak to peak), further increasing on voltage and frequency did not have obvious effect on speckle reduction according to our test. Afterward, the mixed light entered an 18 cm hexagonal light pipe which has an aperture size of 1 cm. A projection lens was used to project the mixed light from the light pipe to the depolarized screen. The projection lens was finely adjusted so a clear image can be displayed on the screen. The distance between the projection lens and the screen is in approximate of 1.8 m. A camera (Thorlabs, DCU-224M-GL) was used to capture the speckle images, and the exposure time of the camera was set to 40 ms. The lens on the camera had a focal length of 50 mm and F/16, which makes the diameter of the camera lens aperture nearly identical to that of the human iris in a real projection environment.

The power of each wavelength component was calibrated by monitoring the average intensity of the captured images flow, since the actual emitted power may vary by the coupling efficiency of each wavelength. In our measurement, the power of each wavelength component was divided into 6 power levels, i.e. 1 (full power), 5/6, 2/3, 1/2, 1/3, 1/6, and 0, so there are 21 combinations for our wavelength blending experiments. Each combination we captured 5 speckle images and calculated their average SCR value.

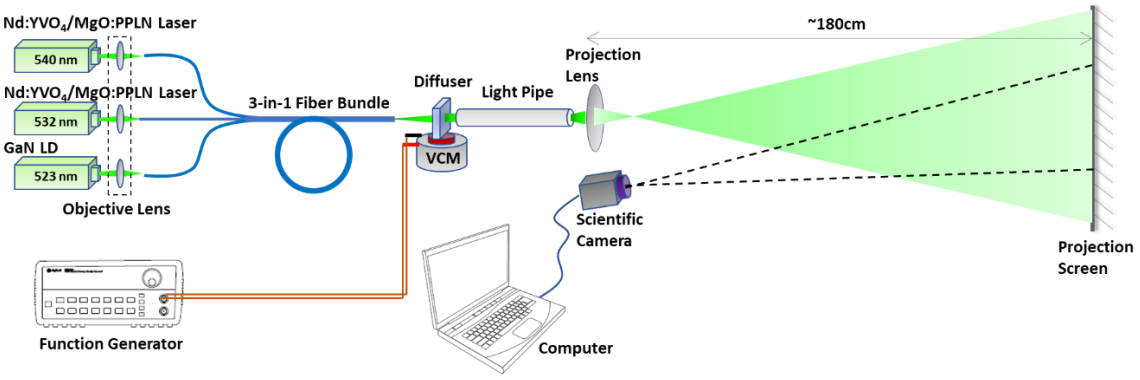

Fig. 7.2 Testbench of SCR value of tri-wavelength laser sources

7.2.2 Speckle measurement results and analysis

Figure 7.3 shows several captured speckle images with different wavelength combinations. It can be found that the LD has the lowest SCR value (3.81%) comparing to other single wavelength sources, since it has much larger linewidth than other DPSS green laser. However, we also notice that a further lower SCR value (3.31%) was achieved by blending the 523 nm, 532 nm and 543 nm together with power ratio of 4:1:1, which are shown in Fig. 7.3 (e). The lower-left triangle in figure 6.4 shows the mapping of SCR values of all measured combinations. The color shows the strength of the corresponding SCR values of different wavelength combinations, and the red color means higher SCR value while blue color represents lower SCR value. The x axis represents the power ratio of the 543 nm in the case of tri-wavelength blending and y axis represents the power ratio of the 532 nm in the case of tri-wavelength blending. The end of the x and y axis represents the SCR value of pure 543 nm or 532 nm light source, so the color in those region moves red.

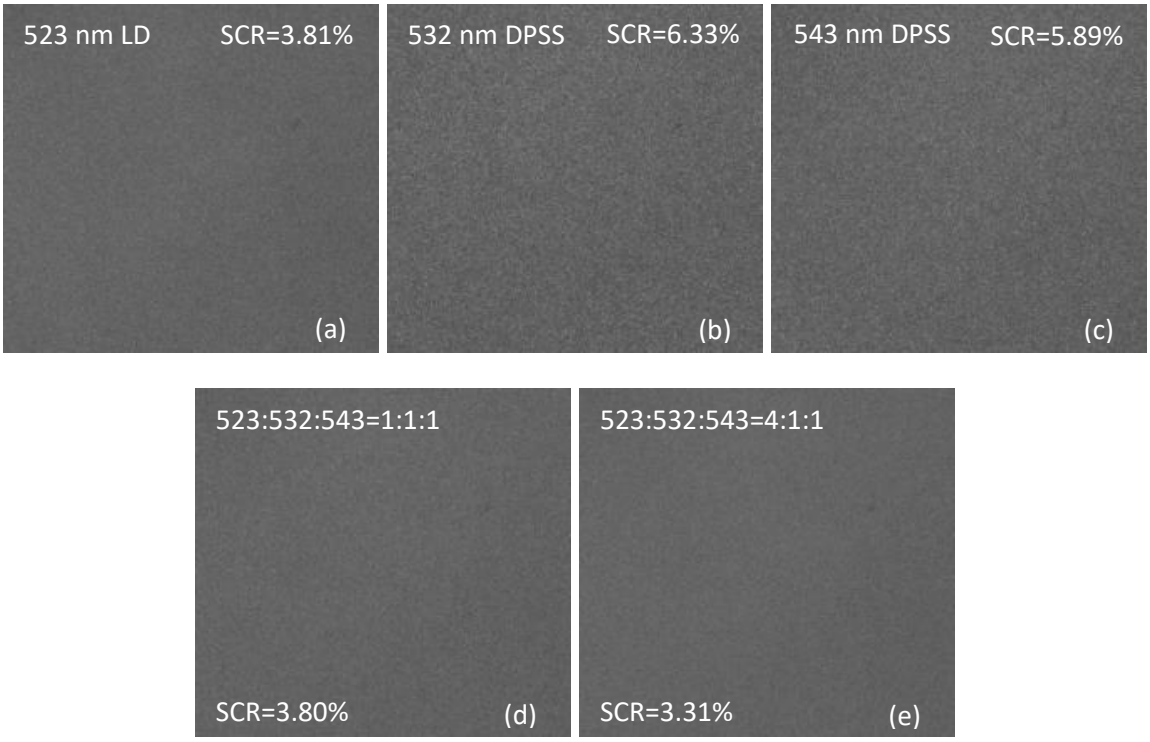

Fig. 7.3 Captured speckle images from single wavelength green laser sources and tri-wavelength green laser sources. (a) captured speckle image of pure 523 nm emission; (b) capture speckle image of pure 532 nm emission; (c) capture speckle image of pure 543 nm emission; (d) capture speckle image when power ratio between 523, 532 and 543 nm is 1:1:1; (e) capture speckle image when power ratio between 523, 532 and 543 nm is 4:1:1.

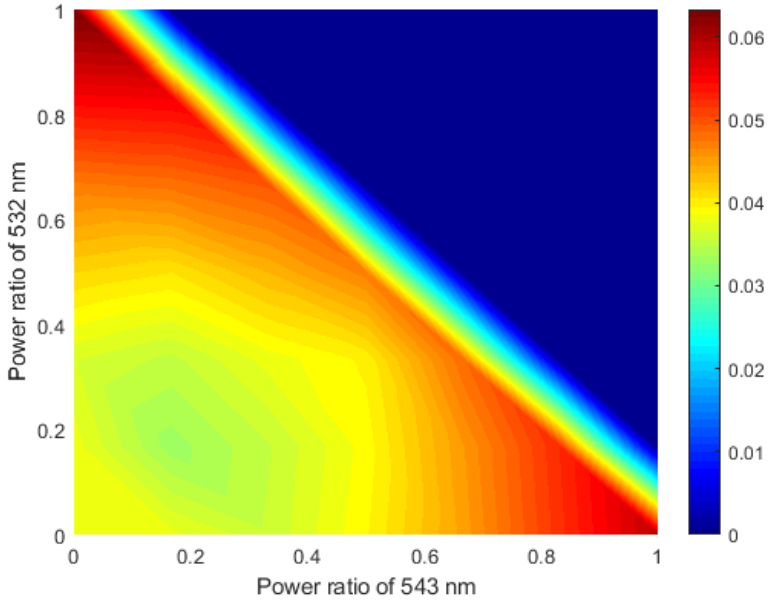

Fig. 7.4 2-D mapping of the measured SCR value of different tri-wavelength cases. x-axis represents the power percentage of the 543 nm laser over the total power of blended laser sources; y-axis represents the power percentage of the 532 nm laser over the total power of blended laser sources.

There were some theoretical models had been proposed for simulating the speckle reduction performance of wavelength diversification method. In 2017, Ma, et. al put forward a detail theoretical model for analyzing the speckle reduction effect of multiple wavelengths blending. According to literature [141], the wavelength diversity speckle reduction factor R_λ can be expressed as:

$$\frac{1}{R_\lambda} = \sqrt{\int_{-\infty}^{+\infty} \left[\int_0^{+\infty} \sum_{i=1}^{n} C_i \, \hat{g}_i(\xi) \sum_{i=1}^{n} C_i \, \hat{g}_i(\xi) \hat{g}(\xi - \Delta\nu) d\xi \right] [M_h(\Delta q_z)]^2 \, d\Delta\nu} \quad (7.1)$$

C_i is the power ratio of the i^{th} laser over the total mixed power;

$\hat{g}_i$ is the normalized power spectrum density function of the i^{th} laser and it can be represented by $\frac{g_i(\xi)}{\int_0^\infty g_i(\xi) d\xi}$, the $g_i(\xi)$ is the power density function of the i^{th} laser in which ξ represents the frequency. In our simulation, we simplified the power spectrum density function into a typical gaussian function.

M_h is the first order characteristic function of the surface height fluctuations and Δq_z can be represented by $2\pi|\xi| \cdot \frac{(\cos\theta_i + \cos\theta_o)}{c}$, where θ_i is the incident angle of the laser beam and θ_o is the observation angle of the monitoring camera (or audience).

Figure 7.5 shows the simulating SCR results of our three wavelengths blending test. It can be found that the results shown in Fig. 6.5 matches well with our experiment results draw in Fig. 7.4. Specifically, for pure DPSS laser cases (532 nm or 543 nm), both SCR value are distributed around 6%, and the SCR is close to 4% for a single 523 nm LD. Both figures show that the lowest SCR value is achieved where the power ratios of 532 nm and 543 nm are in approximate of 20%.

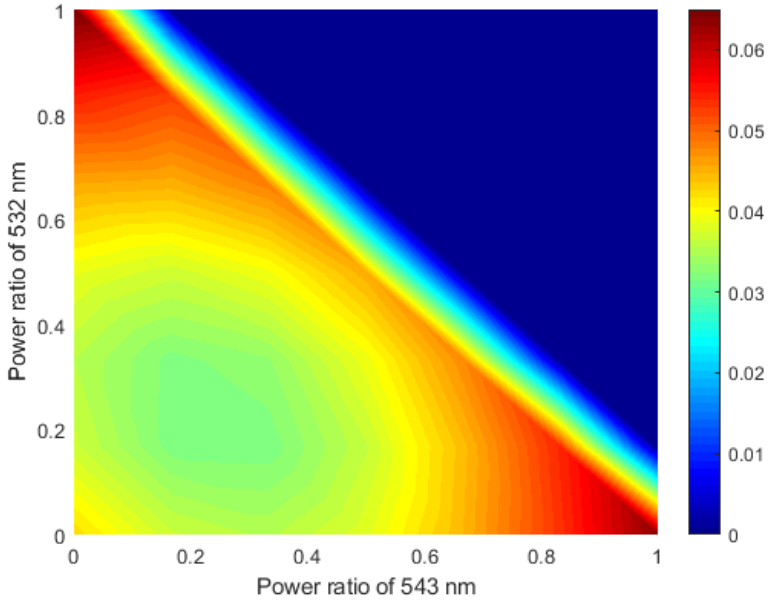

Fig. 7.5 2-D mapping of the measured SCR value of different tri-wavelength cases. x-axis represents the power percentage of the 543 nm laser over the total power of blended laser sources; y-axis represents the power percentage of the 532 nm laser over the total power of blended laser sources.

7.3 Color gamut analysis for three wavelengths blending

One important reason for employing the 543 nm green laser in wavelength blending method is for improving the color gamut of the display devices. The use of 543 nm laser could pull the mixed green light to longer wavelength region so more yellow color region can be covered. Currently, the sRGB and Rec. 709 standards are widely adopted by most video displays, but the Rec. 2020 standard is designated for ultra high definition (4K and 8K) displays. The color gamut of a display system is determined by a triangle connected

by 3 sets of x,y-coordinates corresponding to the R/G/B primaries of the display system. The chromaticity coordinates can be calculated by using the following equations:

$$X = \int_{380}^{780} I(\lambda)\bar{x}(\lambda)d\lambda\,,\; Y = \int_{380}^{780} I(\lambda)\bar{y}(\lambda)d\lambda\,,\; Z = \int_{380}^{780} I(\lambda)\bar{z}(\lambda)d\lambda \qquad (7.2)$$

$$x = \frac{X}{X+Y+Z}\,, y = \frac{Y}{X+Y+Z}\,, z = \frac{Z}{X+Y+Z}$$

Where $I(\lambda)$ is normalized line-shape function of the equivalent monochromatic light (in nanometers), $\bar{x}(\lambda)$ is the color matching functions of CIE 1931 color space. For the case where two or more colors are additively mixed, the following formulas can be used to calculate the x and y chromaticity coordinates of the resulting color (x_{mix}, y_{mix}) from the chromaticity coordinates of the blended wavelength components (x_1,y_1; x_2,y_2; … x_n,y_n), and L_n is luminance value of the n^{th} wavelength component.

$$x_{mix} = \frac{\frac{x_1}{y_1}L_1 + \frac{x_2}{y_2}L_2 + \cdots + \frac{x_n}{y_n}L_n}{\frac{L_1}{y_1} + \frac{L_2}{y_2} + \cdots \frac{L_n}{y_n}}, y_{mix} = \frac{L_1 + L_2 + \cdots + L_n}{\frac{L_1}{y_1} + \frac{L_2}{y_2} + \cdots \frac{L_n}{y_n}} \qquad (7.3)$$

The color gamut of Rec. 2020 standard is plotted in Figure 6.6 with solid line triangle by employing eq. (7.2), in which the R/G/B primary colors for Rec. 2020 is 630 nm, 532 nm and 467 nm.

From theoretical study point of view, to compare the Rec. 2020 color gamut with the color gamut which the green wavelength blending is employed, we set up a virtual laser projector where a red and blue laser diode are employed as well. The wavelengths of red

and blue lasers used for calculating the color gamut are according to the listed wavelength of popular commercial red and blue laser diodes. In detail, we assume the wavelength of red color is 635 nm and the wavelength of blue is 465 nm. The triangles plotted by white continuous line in Fig. 7.6 represent the color gamut of the virtual laser. It can be found that the chromaticity coordinates of the green color are pulled to the longer wavelength region (more yellow wavelength is covered) after employing the 543 nm green laser, and the color gamut coverage (overlap between Rec. 2020 color gamut and the color gamut of the proposed laser projector) is also improved. For example, in Fig. 7.6 (b) where the power ratio between the three green wavelength components are equal, the theoretical color gamut of the virtual projector is nearly identical to the Rec. 2020 standard, since the 523 nm and 543 nm are distributed symmetrically around 532 nm. For the power ratio where the lowest green SCR value was achieved, the color gamut coverage is also better than the case where only a 523 nm green laser diode is used, especially more yellow color area is covered which is important for image color quality improvement.

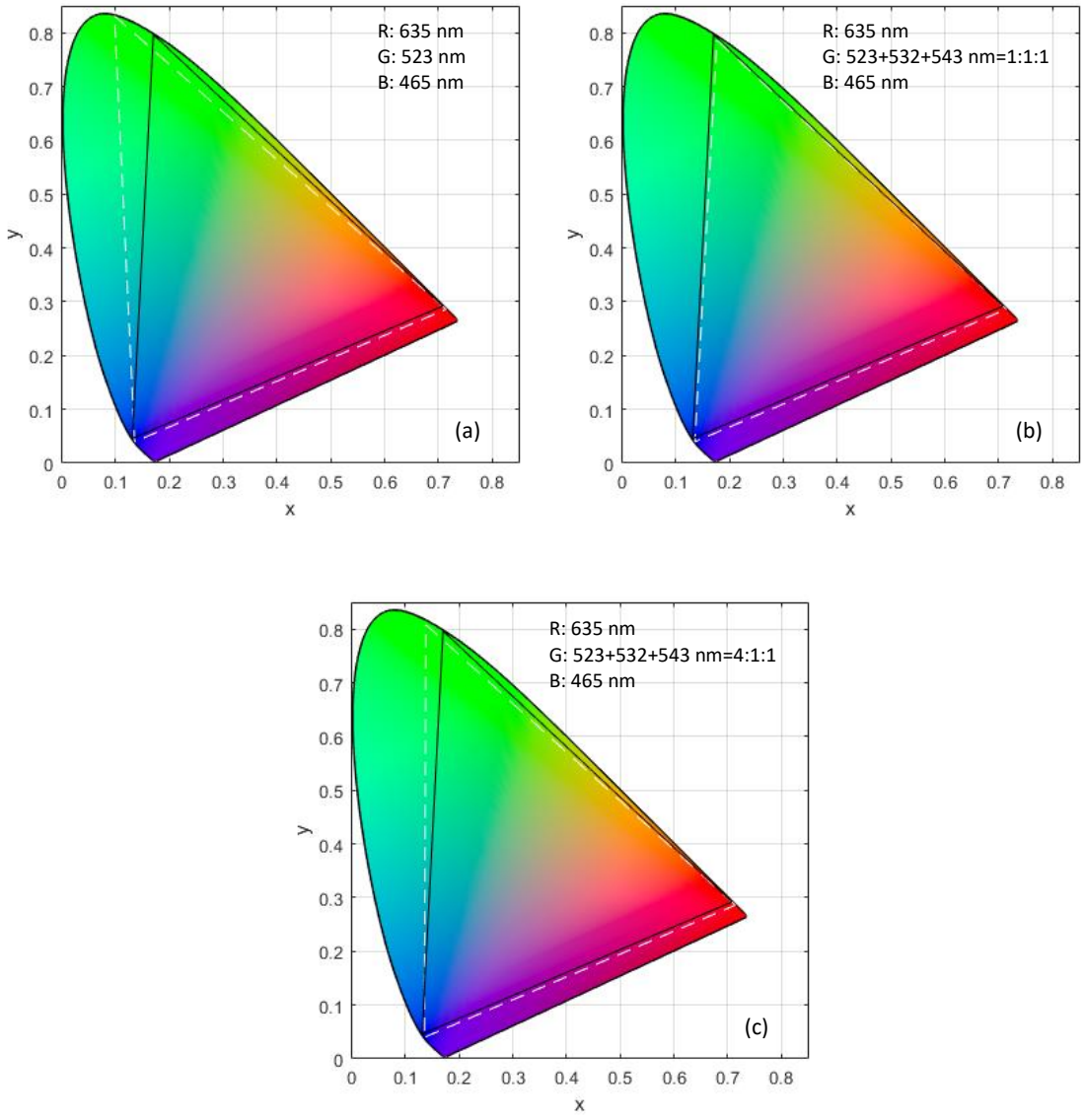

Fig. 7.6 Color gamut comparison between the Rec. 2020 standard and the virtual colorful display system in which the multiple green wavelengths are employed. The triangle with solid line is the color gamut recommended by Rec. 2020 standard. The triangles with white continuous lines are color gamut where the blended green wavelengths are used. (a) Color gamut comparison where only 523 nm green laser

are used in the virtual projector; (b) Color gamut comparison where the power ratio of 523 nm, 532 nm and 543 nm are 1:1:1; (c) Color gamut comparison where the power ratio of 523 nm, 532 nm and 543 nm are 4:1:1.

In the meantime, we also evaluated the color gamut coverages of other green power ratios, which is shown in Figure 7.7. The lower-left triangle filled by red color is the mapping of the coverage with different green power ratio, and the depth of the red color shows the strength of the coverage. Since the blue and red wavelengths are not identical to the wavelength recommended by Rec. 2020, it is impractical to obtain 100 % coverage ratio even when single 532 nm laser is used. However, it is still can be found that by employing more green wavelengths, better color gamut coverage (>97%) can be achieved, which is comparable with the color gamut coverage (99.2%) where pure 532 nm are used. In detail, for the case where the power ratio of 523 nm, 532 nm and 543 nm is 1:1:1, the gamut coverage is 97.4%, and it is 97.6 when the power ratio is 4:1:1 (It is also the power ratio where we achieve the lowest experimental SCR value).

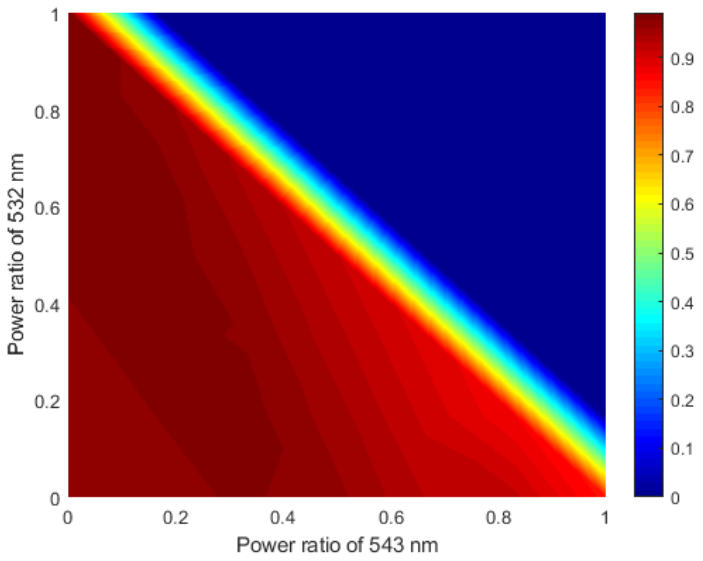

Fig. 7.7 Gamut coverage ratio mapping with different green power ratio. x axis represents the power ratio of 543 nm and y axis represents the power ratio of 532 nm.

7.4 Conclusion

Current wavelength blending technology has prove its ability to effectively reduce the SCR value in display system. And the main difficulty for wavelength blending method is about how to lower the speckle noise with maintaining good color gamut. In this paper, we introduce a novel longer wavelength (543 nm) green DPSS laser into our wavelength blending method, which further lower the SCR value to 3.3 % with good color gamut. The wavelength blending method in this paper uses three green lasers with distinct wavelengths (523 nm, 532 nm and 543 nm), and the SCR value of the three wavelengths blending method are evaluated experimentally and theoretically. Both experimental results and

theoretical simulation shows that the lowest SCR value can be achieved where the power ratios of the 532 nm and 543 nm are in approximate of 20%. In the meantime, outstanding color gamut coverage was also achieved after employing the 543 nm laser into the wavelength blending method. It is worth noting that the multi-wavelength blending method discussed in this paper offer a competitive solution for speckle reduction and color improvement in laser projectors.

8. Conclusion

8.1 Thesis summary

Laser-based displays have a number of advantages over other display technologies, such as high brightness, better color performance, and low maintenance cost. However, speckle noise caused by high coherent lasers limits further commercialization of laser displays. Moreover, the speckle problem is more critical in green color, and a lot of effort have been made to reduce the speckle noise of green lasers. In the meantime, due to the short radiation wavelength of commercial green LD, efficient and compact >530 nm green DPSS lasers are still needed for speckle reduction, color improvement and pico-projectors application.

In this thesis, a number of intra-cavity frequency doubling DPSS green lasers are proposed and demonstrated. Those lasers designed for speckle reduction and color improvement in laser display application, and they have features of compact, efficient, and low cost. Moreover, the modulation characteristics of a compact green laser module (mGreen) is studied for the purpose of pico-projector application.

Chapter 2 studied the field-sequential properties of a Nd:YVO_4/MgO:PPLN based intra-cavity frequency doubling green laser module. The field sequential modulation is need for LCoS and DLP based pico-projection system, and the modulation properties of that mGreen module was poorly studied. In this chapter, by experimental demonstrations and theoretical analysis, we find the thermal lens effect has a significant impact on the output performance

(O-O efficiency and QPM temperature) of the mGreen module which is caused by different heat accumulation as different duty cycle of the applied modulation signal. We found that the increase of duty cycle could result in the increase of O-O efficiency and decrease of QPM temperature. The results concluded in this chapter can be used as a guideline in operating, optimizing, and designing the DPSS lasers for variety applications with various modulation frequency and duty cycle.

Chapter 3, 4, and 5 proposed and demonstrated three types of single wavelength green lasers with radiation wavelength of 531.5 nm, 540 nm, and 542/543 nm. Those lasers were based on intra-cavity frequency doubling configuration, in which Nd:$GdVO_4$/MgO:PPLN, Nd:YAP/LBO, and Nd:YVO_4/MgO:PPLN were used, respectively. For 531.5 nm green laser, 1.9 W output green power was achieved with an O-O efficiency of 37%. For 540 nm green laser, its output power was 0.8 W and the O-O efficiency was ~20%. The speckle performance of both lasers was tested, which show lower SCR value can be achieved after blending with other green wavelength.

In the case of 542 nm and 543 nm Nd:YVO_4/MgO:PPLN green laser, since the 1084 and 1086 transition line are not the strongest fluorescence peak of Nd:YVO_4, an OC with customized coating was used to suppress the radiation of 1064 nm. Different green radiation can be achieved by rotating the orientation of the MgO:PPLN crystal and adjusting the OC. As high as 22% and 35% O-O efficiency were achieved for 542 nm and 543 nm, respectively. It is worth noting that they are the highest efficiency achieved so far to the best of out knowledge. Moreover, those lasers have an advantage of better heat

dissipation capability over other reported 542/543 nm lasers, because the use of low power pump 808 nm LD.

It is the simplest way to blend several single wavelength lasers together for increasing the overall wavelength diversity. However, the size of the overall illuminating laser systems is always an issue plaguing the researchers. Therefore, multi-wavelength lasers attracted a lot of attention recently. In chapter 6, a novel orthogonally polarized dual-wavelength green laser is proposed and demonstrated. That laser is not only suitable to be used in speckle reduction application but also can be employed in heterodyne interferometry and THz generation. That laser was consisted of cost-effective Nd:YVO_4 crystal and MgO:PPLN crystals, and it has emitting wavelengths at 542 nm and 543 nm. It is the first time that orthogonally polarized dual-wavelength radiation is achieved in a visible solid state laser. Moreover, an O-O efficiency of 15.3% has been achieved for the green laser at the balance point (where the powers of the two emission wavelengths were equal), and that is the highest efficiency achieved so far for dual-wavelength visible lasers. Its speckle performance was successfully demonstrated by our speckle test bench which shows the lowest SCR value was achieved at the balance point.

The main application scenario for our proposed green lasers is display application. Speckle reduction and color improvement are their main tasks in laser displays. In chapter 7, the speckle and color performance of a tri-wavelength green laser source was studied. The laser source is blended by a commercial 523 nm LD, a 532 nm DPSS laser, and a 543 nm DPSS laser developed in chapter 3. Both experimental results and theoretical simulation shows that lower SCR value can be achieved where three wavelengths are blended over

single or two wavelength blending. Moreover, due to the use of longer wavelength green laser (543 nm), the chromaticity coordinates of the green primary in the CIE 1931 color space was significantly improved. Better color gamut coverage with Rec. 2020 standard was achieved with the employment of the tri-wavelength green laser source. The results concluded in this chapter demonstrates the practicability of the longer wavelength green lasers developed in chapter 4, 5, and 6 in the laser display application for speckle reduction and color improvement.

8.2 Directions for future work

This work has made a lot of efforts towards the ultimate goal of ideal green laser for display application. But there still exist a few issues to be solved in the near future.

First, the green lasers described in this thesis were built in lab, so packaging is needed for those lasers to be applied in practical applications. Second, the efficiency of the 540 nm green laser described in chapter 4 was not high enough, which are mainly limited by inappropriate coatings and low doping concentration of the Nd:YAP crystals. It is expected that the O-O efficiency will increase if new improved Nd:YAP crystal is used. Third, the detail physical mechanism of simultaneous multi-wavelength emission from single laser host material is still not clear, and the theoretical modal of single laser crystal based multi-wavelength laser is poorly developed. Forth, there is still lack of precise numerical modal for simulation the intra-cavity green generation in which the weaker transition lines of the gain media are used to provide the fundamental wave.

Publications

Journal Articles:

1. **Zhang, Bin**, Yi Gan, and Chang-Qing Xu. "Study of the field-sequential modulation of Nd:YVO_4/MgO: PPLN based intra-cavity frequency doubling green laser." Optics & Laser Technology 102 (2018): 174-179.
2. **Zhang, Bin**, and Chang-qing Xu. "Compact, and efficient continues wave intra-cavity frequency doubling Nd:YVO_4/MgO: PPLN 542/543 nm green lasers." Optics & Laser Technology 122 (2020): 105885.
3. **Zhang, Bin**, Qianli Ma, and Chang-Qing Xu. "Orthogonally polarized dual-wavelength Nd:YVO_4/MgO: PPLN intra-cavity frequency doubling green laser." Optics & Laser Technology 125 (2020): 106005.
4. Mohamed, Mahmoud, **Bin Zhang**, Qianli Ma, Josh Kneller, and Chang-Qing Xu. "Efficient Dual-Wavelengths Continuous Mode Lasers by End-Pumping of Series Nd:YVO_4 and Nd:$GdVO_4$ Crystals and Speckle Reduction Study." Photonics. Vol. 6. No. 2. Multidisciplinary Digital Publishing Institute, 2019.

Conferences:

1. **Bin Zhang**, Qianli Ma, and Chang-Qing Xu. “High Efficiency Nd:$GdVO_4$/MgO:PPLNs 531.5 nm green laser." Photonic North, May 2019, Québec City, QC, Canada. (Poster Presentation by Bin Zhang)
2. **Bin Zhang**, Qianli Ma, and Chang-Qing Xu. “Intra-cavity frequency doubling Nd:YAP/LBO 540 nm green laser for laser display." Photonic North, May 2019, Québec City, QC, Canada. (Poster Presentation by Bin Zhang)
3. Mohamed, Mahmoud, **Bin Zhang**, Qianli Ma, Josh Kneller, and Chang-Qing Xu. "Efficient and low speckle dual-wavelengths laser based on end-pumping of series crystals." Photonic North, May 2019, Québec City, QC, Canada. (Oral Presentation by Bin Zhang)

Reference

[1]. Baker, Charles E., and Anthony D. Rugari. "A large-screen real-time display technique." Information Display 3 (1966): 37-46.

[2]. Online source: http://www.ipgphotonics.com/laser?id=327.

[3]. Ma, Qianli. STUDY OF LASER SPECKLE REDUCTION FOR LASER DISPLAY APPLICATIONS. Diss. 2018.

[4]. Roelandt, Stijn, et al. "Human speckle perception threshold for still images from a laser projection system." Optics express 22.20 (2014): 23965-23979.

[5]. Chen, Hsuan-An, Jui-Wen Pan, and Zu-Po Yang. "Speckle reduction using deformable mirrors with diffusers in a laser pico-projector." Optics express 25.15 (2017): 18140-18151.

[6]. Trisnadi, Jahja I. "Speckle contrast reduction in laser projection displays." Projection Displays VIII. Vol. 4657. International Society for Optics and Photonics, 2002.

[7]. Ma, Qianli, et al. "Speckle reduction by optimized multimode fiber combined with dielectric elastomer actuator and light-pipe homogenizer." Journal of Display Technology 12.10 (2016): 1162-1167.

[8]. Lee, Jae-Yong, et al. "Speckle reduction using twin green laser diodes and oscillation of MEMS scanning mirror for pico-projector." 2015 20th Microoptics Conference (MOC). IEEE, 2015.

[9]. Yu, Nan Ei, et al. "Speckle noise reduction on a laser projection display via a broadband green light source." Optics express 22.3 (2014): 3547-3556.

[10]. Gan, Yi, et al. "38.5% optical-to-optical efficiency neodymium-doped yttrium vanadate/magnesium-oxide-doped periodically poled lithium niobate integrat ed green module with watt-level output power for laser display applications." Optical review 19.6 (2012): 409-411.

[11]. Yanagisawa, Takayuki, et al. " De-speckle effects resulted by wavelength multiplexing of intra-cavity solid-state green lasers " The 4th Laser Display and Lighting Conference (LDC'15), 2015.

[12]. Ma, Qianli, and Chang-Qing Xu. "Wavelength blending with reduced speckle and improved color for laser projection." Optics and Lasers in Engineering 97 (2017): 27-33.

[13]. Kuksenkov, Dmitri V., et al. "Multiple-wavelength synthetic green laser source for speckle reduction." Nonlinear Frequency Generation and Conversion: Materials, Devices, and Applications X. Vol. 7917. International Society for Optics and Photonics, 2011.

[14]. Wang, Dong Zhou, et al. "Three-wavelength green laser using intracavity frequency conversion of Nd:Mg:$LiTaO_3$ with a MgO:PPLN crystal." Applied Physics B 117.4 (2014): 1117-1121.

[15]. Maiman, Theodore H. "Stimulated optical radiation in ruby." nature 187.4736 (1960): 493-494.

[16]. Bridges, William B. "Laser oscillation in singly ionized argon in the visible spectrum." Applied Physics Letters 4.7 (1964): 128-130.

[17]. Willett, Colin S. "Introduction to gas lasers: population inversion mechanisms." (1974).

[18]. Geusic, J. E., et al. "CONTINUOUS 0.532-μ SOLID-STATE SOURCE USING $Ba_2NaNb_5O_{15}$." Applied Physics Letters 12.9 (1968): 306-308.

[19]. Koechner, Walter. Solid-state laser engineering. Vol. 1. Springer, 2013.

[20]. Hartman, R. L., N. E. Schumaker, and R. W. Dixon. "Continuously operated (Al, Ga) As double-heterostructure lasers with 70° C lifetimes as long as two years." Applied Physics Letters 31.11 (1977): 756-759.

[21]. Botez, Dan, and Donald E. Ackley. "Phase-locked arrays of semiconductor diode lasers." IEEE Circuits and Devices Magazine 2.1 (1986): 8-17.

[22]. Luft, Johann, and Martin Behringer. "Diode Lasers–Small devices with great performance." Laser Technik Journal 2.2 (2005): 57-63.

[23]. https://www.laserfocusworld.com/lasers-sources/article/16551659/photonic-frontiers-laser-diodes-looking-backlooking-forward-laser-diodes-have-come-a-long-way-and-brought-five-nobel-prizes

[24]. Dimmick, Timothy E. "Semiconductor-laser-pumped, mode-locked, and frequency-doubled Nd:YAG laser." Optics letters 14.13 (1989): 677-679.

[25]. Fields, R. A., M. Birnbaum, and C. L. Fincher. "Highly efficient Nd:YVO_4 diode-laser end-pumped laser." Applied physics letters 51.23 (1987): 1885-1886.

[26]. Cheng, L. K., W. R. Bosenberg, and C. L. Tang. "Growth and characterization of nonlinear optical crystals suitable for frequency conversion." Progress in Crystal Growth and Characterization of Materials 20.1-2 (1990): 9-57.

[27]. Zhou, M., et al. "52% optical-to-optical conversion efficiency in a compact 1.5 W 532 nm second harmonic generation laser with intracavity periodically-poled MgO:$LiNbO_3$." Laser physics 20.7 (2010): 1568-1571.

[28]. Miyoshi, Takashi, et al. "510–515 nm InGaN-based green laser diodes on c-plane GaN substrate." Applied Physics Express 2.6 (2009): 062201.

[29]. Hecht, Jeff. "A short history of laser development." Applied optics 49.25 (2010): F99-F122.

[30]. Nathan, Marshall I., et al. "Stimulated emission of radiation from GaAs p‐n junctions." Applied Physics Letters 1.3 (1962): 62-64.

[31]. Quist, Ted M., et al. "Semiconductor maser of GaAs." Applied Physics Letters 1.4 (1962): 91-92.

[32]. Hall, Robert N., et al. "Coherent light emission from GaAs junctions." Physical Review Letters 9.9 (1962): 366.

[33]. Alferov, Zh I. "AlAs-GaAs heterojunction injection lasers with a low room-temperature threshold." Fiz, Tekh. Poluprov 3 (1969): 1328-1332.

[34]. Holonyak Jr, Nick, and S. F. Bevacqua. "Coherent (visible) light emission from Ga (As1− x P x) junctions." Applied Physics Letters 1.4 (1962): 82-83.

[35]. Ikeda, Masao, et al. "Room-temperature continuous-wave operation of an AlGaInP double heterostructure laser grown by atmospheric pressure metalorganic chemical vapor deposition." Applied physics letters 47.10 (1985): 1027-1028.

[36]. Gaines, J. M., et al. "Blue-green injection lasers containing pseudomorphic Zn1− x Mg x S y Se1− y cladding layers and operating up to 394 K." Applied physics letters 62.20 (1993): 2462-2464.

[37]. Haase, MICHAEL A., et al. "Blue-green laser diodes." Applied Physics Letters 59.11 (1991): 1272-1274.

[38]. Schwarz, Ulrich T., and Wolfgang G. Scheibenzuber. "The green laser diode: completing the rainbow." Optics and Photonics News 22.9 (2011): 38-44.

[39]. Sizov, Dmitry, Rajaram Bhat, and Chung-En Zah. "Gallium indium nitride-based green lasers." Journal of lightwave technology 30.5 (2011): 679-699.

[40]. Monavarian, Morteza, Arman Rashidi, and Daniel Feezell. "A Decade of Nonpolar and Semipolar III-Nitrides: A Review of Successes and Challenges." physica status solidi (a) 216.1 (2019): 1800628.

[41]. Khan, Asif. "Semiconductor photonics: Laser diodes go green." Nature Photonics 3.8 (2009): 432.

[42]. Murayama, Masahiro, et al. "Watt-class green (530 nm) and blue (465 nm) laser diodes." physica status solidi (a) 215.10 (2018): 1700513.

[43]. Franken, eg PA, et al. "Generation of optical harmonics." Physical Review Letters 7.4 (1961): 118.

[44]. Deserno, U., F. Kappeler, and C. Hanke. "Coherent 440-nm light source by optical frequency doubling of the radiation of a phase-locked high power laser array using $LiIO_3$." Applied optics 26.8 (1987): 1367-1368.

[45]. Goldberg, L., and D. Mehuys. "21 W broad area near - diffraction - limited semiconductor amplifier." Applied physics letters 61.6 (1992): 633-635.

[46]. Ross, Graeme W., et al. "Generation of high-power blue light in periodically poled $LiNbO_3$." Optics letters 23.3 (1998): 171-173.

[47]. Wright, J. K. "Enhancement of second harmonic power generated by a dielectric crystal inside a laser cavity." Proceedings of the IEEE 51.11 (1963): 1663-1663.

[48]. Baer, T., and M. S. Keirstead. "Intracavity Frequency Doubling of a Nd:YAG Laser Pumped by a Laser Diode Array." Conference on lasers and electro-optics. Optical Society of America, 1985.

[49]. Shen, Deyuan, et al. "Efficient operation of an intracavity-doubled Nd:YVO_4/KTP laser end pumped by a high-brightness laser diode." Applied optics 37.33 (1998): 7785-7788.

[50]. Essaian, Stepan, et al. "73.4 L: Late - News Paper: Miniature, Highly Efficient, and Low Cost Green Laser Source for Pico - Projectors." SID Symposium Digest of Technical Papers. Vol. 42. No. 1. Oxford, UK: Blackwell Publishing Ltd, 2011.

[51]. Shchegrov, Andrei V., et al. "532-nm laser sources based on intracavity frequency doubling of extended-cavity surface-emitting diode lasers." Solid State Lasers XIII: Technology and Devices. Vol. 5332. International Society for Optics and Photonics, 2004.

[52]. Lin, Zhi, et al. "Diode-pumped simultaneous multi-wavelength linearly polarized Nd:YVO_4 laser at 1062, 1064 and 1066 nm." Laser Physics 26.1 (2015): 015801.

[53]. Fields, R. A., M. Birnbaum, and C. L. Fincher. "Highly efficient Nd:YVO_4 diode-laser end-pumped laser." Applied physics letters 51.23 (1987): 1885-1886.

[54]. Pang, Q. S., et al. "1073 nm continuous-wave Nd:YVO_4 laser with Type I phase-matching LiB_3O_5." Optics letters 36.7 (2011): 1266-1268.

[55]. Lü, Yanfei, et al. "Simultaneous triple 914 nm, 1084 nm, and 1086 nm operation of a diode-pumped Nd: YVO_4 laser." Journal of Applied Physics 116.16 (2014): 163107.

[56]. Wu, Bo, et al. "Compact dual-wavelength Nd:$GdVO_4$ laser working at 1063 and 1065 nm." Optics express 17.8 (2009): 6004-6009.

[57]. Chen, Y. F., M. L. Ku, and K. W. Su. "High-power efficient tunable Nd:$GdVO_4$ laser at 1083 nm." Optics letters 30.16 (2005): 2107-2109.

[58]. Tzeng, Y. S., et al. "High-power tunable single-and multi-wavelength diode-pumped Nd:YAP laser in the $^4F_{3/2} \rightarrow {}^4I_{11/2}$ transition." Optics express 21.22 (2013): 26261-26268.

[59]. Yaney, Perry Pappas, and L. G. DeShazer. "Spectroscopic studies and analysis of the laser states of Nd^{3+}:YVO_4." JOSA 66.12 (1976): 1405-1414.

[60]. Zeller, P., and P. Peuser. "Efficient, multiwatt, continuous-wave laser operation on the $^4F_{3/2}$–$^4I_{9/2}$ transitions of Nd:YVO_4 and Nd:YAG." Optics Letters 25.1 (2000): 34-36.

[61]. Chen, F., et al. "Efficient generation of 914 nm laser with high beam quality in Nd:YVO_4 crystal pumped by π-polarized 808 nm diode-laser." Laser Physics Letters 5.9 (2008): 655-658.

[62]. Chen, F., et al. "8.9-W continuous-wave, diode-end-pumped all-solid-state Nd:YVO_4 laser operating at 914 nm." Laser physics 19.3 (2009): 389-391.

[63]. Bowkett, G. C., et al. "Single-mode 1.34-μm Nd:YVO_4 microchip laser with cw Ti:sapphire and diode-laser pumping." Optics letters 19.13 (1994): 957-959.

[64]. Sennaroglu, Alphan. "Efficient continuous-wave operation of a diode-pumped Nd:YVO_4 laser at 1342 nm." Optics communications 164.4-6 (1999): 191-197.

[65]. Liang, H. C., et al. "High-power, diode-end-pumped, multi-gigahertz self-mode-locked Nd:YVO_4 laser at 1342 nm." Optics letters 35.1 (2010): 4-6.

[66]. Lü, Y. F., et al. "1085 nm Nd:YVO_4 laser intracavity pumped at 914 nm and sum-frequency mixing to reach cyan laser at 496 nm." Laser Physics Letters 7.1 (2009): 11.

[67]. Wang, Xiao-Zhong, et al. "A 1064 nm, 1085 nm Dual-Wavelength Nd:YVO_4 Laser Using Fabry–Perot Filters as Output Couplers." IEEE Photonics Technology Letters 26.19 (2014): 1983-1985.

[68]. Liu, J. H. "Continuous-wave Nd:YVO_4/$KTiOPO_4$ green laser at 542 nm under diode pumping into the emitting level." Laser Physics 22.10 (2012): 1463-1465.

[69]. Zhang, Z., et al. "Intra-cavity second harmonic generation with Nd:YVO_4/BIBO laser at 542 nm." Optics communications 267.2 (2006): 487-490.

[70]. Fu, S. C., X. Wang, and H. Chu. "The generation of a continuous-wave Nd:YVO_4/LBO laser at 543 nm by direct in-band diode pumping at 888 nm." Laser Physics 23.2 (2013): 025002.

[71]. Yao, Y., et al. "Laser diode and pumped Cr:Yag passively Q-switched yellow-green laser at 543 nm." Optics and Spectroscopy 114.3 (2013): 459-462.

[72]. Yao, Yi, et al. "All-solid-state continuous-wave frequency-doubling Nd:YVO_4/LBO laser with 2.35 W output power at 543 nm." Optics letters 34.23 (2009): 3758-3760.

[73]. Sulc, Jan, et al. "Comparison of diode-side-pumped triangular Nd:YAG and Nd:YAP laser." Solid State Lasers XIV: Technology and Devices. Vol. 5707. International Society for Optics and Photonics, 2005.

[74]. Hanson, F., and P. Poirier. "Multiple-wavelength operation of a diode-pumped Nd:$YAlO_3$ laser." JOSA B 12.7 (1995): 1311-1315.

[75]. Yu, X., et al. "Diode-pumped continuous-wave Nd:YAP laser emitting at 1073 nm based on the $^4F_{3/2}$-$^4I_{11/2}$ transition." Laser Physics 21.5 (2011): 880-882.

[76]. Blum, Jean-Yves, and Marc JM Abadie. "Study of the Nd:YAP laser. Effect on canal cleanliness." Journal of endodontics 23.11 (1997): 669-675.

[77]. Schearer, L. D., and Padetha Tin. "Tunable lasers at 1080 nm for helium optical pumping." Journal of Applied Physics 68.3 (1990): 943-949.

[78]. Nie, Weijie, et al. "Dual-wavelength waveguide lasers at 1064 and 1079 nm in Nd:YAP crystal by direct femtosecond laser writing." Optics letters 40.10 (2015): 2437-2440.

[79]. Wang, Yajun, et al. "High-power low-noise Nd:YAP/LBO laser with dual wavelength outputs." IEEE Journal of Quantum Electronics 47.7 (2011): 1006-1013.

[80]. Yao-Hui, Zheng, Wang Ya-Jun, and Peng Kun-Chi. "A high-power single-frequency 540 nm laser obtained by intracavity frequency doubling of an Nd:YAP laser." Chinese Physics Letters 29.4 (2012): 044208.

[81]. Jensen, T., et al. "Spectroscopic characterization and laser performance of diode-laser-pumped Nd:$GdVO_4$." Applied Physics B 58.5 (1994): 373-379.

[82]. Sato, Yoichi, and Takunori Taira. "Comparative study on the spectroscopic properties of Nd:$GdVO_4$ and Nd:YVO_4 with hybrid process." IEEE Journal of selected topics in quantum electronics 11.3 (2005): 613-620.

[83]. Zagumennyĭ, A. I., et al. "The Nd:$GdVO_4$ crystal: a new material for diode-pumped lasers." Soviet journal of quantum electronics 22.12 (1992): 1071.

[84]. Wang, C. Q., et al. "A comparative study of the laser performance of diode-laser-pumped Nd:$GdVO_4$ and Nd:YVO_4 crystals." Applied Physics B 70.6 (2000): 769-772.

[85]. Shen, D. Y., et al. "Efficient and compact intracavity-frequency-doubled Nd: $GdVO_4$/KTP laser end-pumped by a fiber-coupled laser diode." Applied Physics B 72.3 (2001): 263-266.

[86]. Pavel, Nicolaie, and Takunori Taira. "High-power continuous-wave intracavity frequency-doubled Nd:$GdVO_4$/LBO laser under diode pumping into the emitting level." IEEE Journal of selected topics in quantum electronics 11.3 (2005): 631-637.

[87]. Cheng, Hui-Chuan, Linghui Rao, and Shin-Tson Wu. "Color breakup suppression in field-sequential five-primary-color LCDs." Journal of display technology 6.6 (2010): 229-234.

[88]. Liu, Yang, et al. "Compact and flexible dual-wavelength laser generation in coaxial diode-end-pumped configuration." IEEE Photonics Journal 9.1 (2016): 1-10.

[89]. Huang, Y. P., et al. "Orthogonally polarized dual-wavelength Nd:$LuVO_4$ laser at 1086 nm and 1089 nm." Optics Express 20.5 (2012): 5644-5651.

[90]. Chen, Y-F. "cw dual-wavelength operation of a diode-end-pumped Nd:YVO_4 laser." Applied Physics B 70.4 (2000): 475-478.

[91]. Cheng, Hao Ping, et al. "Orthogonally polarized single-longitudinal-mode operation in a dual-wavelength monolithic Nd:YAG laser at 1319 nm and 1338 nm." Photonics Research 6.8 (2018): 815-820.

[92]. Maestre, H., et al. "Dual-wavelength green laser with a 4.5 THz frequency difference based on self-frequency-doubling in Nd^{3+}-doped aperiodically poled lithium niobate." Optics letters 33.9 (2008): 1008-1010.

[93]. Wang, Zhichao, et al. "Multiwavelength green-yellow laser based on a Nd:YAG laser with nonlinear frequency conversion in a LBO crystal." Applied optics 51.18 (2012): 4196-4200.

[94]. Ye P, Zhu S, Li Z, Yin H, Zhang P, Fu S, Chen Z. Passively Q-switched dual-wavelength green laser with an Yb:YAG/Cr^{4+}:YAG/YAG composite crystal. Opt Express 2017; 25(5):5179-85.

[95]. Jin, Yu-Ye, et al. "Zeeman-birefringence He-Ne dual frequency lasers." Chinese Physics Letters 18.4 (2001): 533-536.

[96]. https://en.wikipedia.org/wiki/Laser_Doppler_vibrometer

[97]. Zhang, Shulian, and Thierry Bosch. "Orthogonally polarized lasers and their applications." Optics and photonics news 18.5 (2007): 38-43.

[98]. Dändliker, René, R. Thalmann, and D. Prongué. "Two-wavelength laser interferometry using superheterodyne detection." Optics letters 13.5 (1988): 339-341.

[99]. Lü, Yanfei, et al. "Diode-Pumped Quasi-Three-Level Nd:YVO_4 Laser With Orthogonally Polarized Emission." IEEE Photonics Technology Letters 26.7 (2014): 656-659.

[100]. Xu, Bin, et al. "Efficient and compact orthogonally polarized dual-wavelength Nd:YVO_4 laser at 1342 and 1345 nm." Applied optics 55.1 (2016): 42-46.

[101]. Boyd, Robert W. Nonlinear optics. Elsevier, 2003.

[102]. X. Li, Optoelectronic Devices: Design, Modeling, and Simulation,1st ed. Cambridge, U.K.: Cambridge Univ. Press, Jul. 2009.

[103]. Hodgson, Norman, and Horst Weber. Laser Resonators and Beam Propagation: Fundamentals, Advanced Concepts, Applications. Vol. 108. Springer, 2005.

[104]. Li, Tao, et al. "Pulse-width reduction in a diode-pumped doubly Q-switched YVO_4/Nd:YVO_4 laser with electro-optic modulator and GaAs saturable absorber." JOSA B 26.5 (2009): 1146-1150.

[105]. Kuhn, Kelin J. Laser Engineering,1st ed. United States. Prentice Hall (Higher Education Division, Pearson Education). Dec. 1997.

[106]. Hadley, G. Ronald, et al. "Numerical simulation and experimental studies of longitudinally excited miniature solid-state lasers." Applied optics 27.5 (1988): 819-827.

[107]. Sileo, Leonardo, et al. "Optical fiber technologies for in-vivo light delivery and optogenetics." 2015 17th International Conference on Transparent Optical Networks (ICTON). IEEE, 2015.

[108]. Della Patria, Andrea, et al. "Influence of laser beam quality on modal selection in tapered optical fibers for multipoint optogenetic control of neural activity." Transparent Optical Networks (ICTON), 2016 18th International Conference on. IEEE, 2016.

[109]. Wang, Dong Zhou, et al. "Periodically poled self-frequency-doubling green laser fabricated from Nd:Mg:$LiNbO_3$ single crystal." Optics express 23.14 (2015): 17727-17738.

[110]. Madhukar, Yuvraj K., et al. "Effect of laser operating mode in paint removal with a fiber laser." Applied surface science 264 (2013): 892-901.

[111]. Guttag, Karl M., Shawn Hurley, and Bill Mei. "39.1: Distinguished Paper: Laser+ LCoS Technology Revolution." SID Symposium digest of technical papers. Vol. 42. No. 1. Blackwell Publishing Ltd, 2011.

[112]. Janssens, Peter, and Koen Malfait. "Future prospects of high-end laser projectors." SPIE OPTO: Integrated Optoelectronic Devices. International Society for Optics and Photonics, 2009.

[113]. Khaydarov, John, et al. "Modulation and efficiency characteristics of miniature microchip green laser sources based on PPMgOLN nonlinear material." SPIE LASE. International Society for Optics and Photonics, 2011.

[114]. Ssaian, Stepan, et al. "Microchip green laser sources: broad range of possibilities." SPIE LASE. International Society for Optics and Photonics, 2012.

[115]. Wang, B., et al. "Effect of duty cycles and repetition rates of QCW pumped LD on Nd: YVO_4 blue laser efficiency." Laser Physics 21.4 (2011): 656-658.

[116]. Lu, Yang, et al. "Field-Sequential Operation of Laser Diode Pumped Nd:YVO_4/PPMgLN Microchip Green Laser." Photonics Technology Letters, IEEE 22.13 (2010): 990-992.

[117]. D. Armitage, I. Underwood, and S. T. Wu, Introduction to Microdisplays (Wiley, New York, 2006).

[118]. Mukhopadhyay, P. K. "Diode-Pumped Solid-State Lasers and Intracavity Frequency Conversion." Laser Physics and Technology. Springer India, 2015. 85-113.

[119]. Sato, Yoichi, and Takunori Taira. "Highly accurate interferometric evaluation of thermal expansion and dn/dT of optical materials." Optical Materials Express 4.5 (2014): 876-888.

[120]. Yılmazlar I, Sabuncu M. Speckle noise reduction based on induced mode hopping in a semiconductor laser diode by drive current modulation. Optics & Laser Technology. 2015 Oct 1; 73:19-22.

[121]. Peterson R, Jenssen HP, Cassanho A. Investigation of the spectroscopic properties of Nd:YVO_4. In Advanced Solid State Lasers 2002 Feb 3 (p. TuB17). Optical Society of America.

[122]. Yao Y, Zheng Q, Qu DP, Zhou K, Liu Y, Guo JX, Zhao L. All-solid-state 543 nm green laser generated by frequency doubling of a diode pumped Nd:YVO_4 laser at 1086 nm. Laser Physics. 2010 Apr 1;20(4):773-6.

[123]. Pallas, Florent, et al. "Stable dual-wavelength microlaser controlled by the output mirror tilt angle." Applied Physics Letters 99.24 (2011): 241113.

[124]. ISO 11554:2017 Optics and photonics - Lasers and laser-related equipment - Test methods for laser beam power, energy and temporal characteristics, 2017.

[125]. Harimoto, T., and J. Watanabe. "Efficient and stable 532 nm microchip laser pumped by single-longitudinal-mode laser-diode." Electronics Letters 41.12 (2005): 702-704.

[126]. Zheng, Yaohui, et al. "High-stability single-frequency green laser with a wedge Nd:YVO_4 as a polarizing beam splitter." Optics Communications 283.2 (2010): 309-312.

[127]. Pauwels, Jaël, and Guy Verschaffelt. "Speckle reduction in laser projection using microlens-array screens." Optics express 25.4 (2017): 3180-3195.

[128]. Yusheng, Duan, et al. "Laser-Diode-Pumped Nd:YAP Single Crystal Fiber Laser." Chinese Physics Letters 8.12 (1991): 622.

[129]. Boucher, M., et al. "Multiwatt CW diode end-pumped Nd:YAP laser at 1.08 and 1.34 μm: influence of Nd doping level." Optics communications 212.1-3 (2002): 139-148.

[130]. Guo, Ruixiang, et al. "Application of an all-solid-state, frequency-doubled Nd:YAP laser to the generation of twin beams at 1080 nm." Applied optics 41.12 (2002): 2304-2307.

[131]. Akiba, Takuya, et al. "Terahertz wave generation using type II phase matching polarization combination via difference frequency generation with $LiNbO_3$." Japanese Journal of Applied Physics 54.6 (2015): 062202.

[132]. Huang, Y. J., et al. "Efficient high-power terahertz beating in a dual-wavelength synchronously mode-locked laser with dual gain media." Optics letters 39.6 (2014): 1477-1480.

[133]. Liu, Yang, et al. "Compact and stable high-repetition-rate terahertz generation based on an efficient coaxially pumped dual-wavelength laser." Optics express 25.25 (2017): 31988-31996.

[134]. Ye, Pingping, et al. "Passively Q-switched dual-wavelength green laser with an Yb:YAG/Cr^{4+}:YAG/YAG composite crystal." Optics express 25.5 (2017): 5179-5185.

[135]. Hou, Wenmei, and Günter Wilkening. "Investigation and compensation of the nonlinearity of heterodyne interferometers." Precision engineering 14.2 (1992): 91-98.

[136]. Zhang, Shulian, Yidong Tan, and Yan Li. "Orthogonally polarized dual frequency lasers and applications in self-sensing metrology." Measurement Science and Technology 21.5 (2010): 054016.

[137]. Oron, Ram, et al. "Laser operation with two orthogonally polarized transverse modes." Applied optics 41.18 (2002): 3634-3637.

[138]. Chang, M. T., et al. "Exploring transverse pattern formation in a dual-polarization self-mode-locked monolithic Yb:KGW laser and generating a 25-GHz sub-picosecond vortex beam via gain competition." Optics express 24.8 (2016): 8754-8762.

[139]. Cui, Zhe, et al. "Analysis of the speckle properties in a laser projection system based on a human eye model." JOSA A 31.3 (2014): 616-620.

[140]. Zhang, Bin, and Chang-qing Xu. "Compact, and efficient continues wave intra-cavity frequency doubling Nd:YVO_4/MgO: PPLN 542/543 nm green lasers." Optics & Laser Technology 122 (2020): 105885.

[141]. Ma, Qianli, and Chang-Qing Xu. "Speckle reduced laser projection with color gamut optimization." U.S. Patent Application No. 16/423,087.